UNIVERSITAT ROVIRA I VIRGILI

THEORETICAL STUDIES OF HETEROGENEOUS CATALYSIS FOR HALOGEN CHEMISTRY

Michael David Higham

UNIVERSITAT ROVIRA i VIRGILI

Theoretical Studies of Heterogeneous Catalysis for Halogen Chemistry

MICHAEL DAVID HIGHAM

DOCTORAL THESIS
2017

UNIVERSITAT ROVIRA I VIRGILI
THEORETICAL STUDIES OF HETEROGENEOUS CATALYSIS FOR HALOGEN CHEMISTRY
Michael David Higham

UNIVERSITAT ROVIRA I VIRGILI
THEORETICAL STUDIES OF HETEROGENEOUS CATALYSIS FOR HALOGEN CHEMISTRY
Michael David Higham

UNIVERSITAT ROVIRA I VIRGILI
THEORETICAL STUDIES OF HETEROGENEOUS CATALYSIS FOR HALOGEN CHEMISTRY
Michael David Higham

Theoretical Studies of Heterogeneous Catalysis for Halogen Chemistry

Michael David Higham

Doctoral Thesis supervised by:

Prof. Núria López Alonso

Institut Català d'Investigació Química

UNIVERSITAT ROVIRA i VIRGILI

ICIQ
Institut
Català
d'Investigació
Química

Tarragona
2017

UNIVERSITAT ROVIRA I VIRGILI
THEORETICAL STUDIES OF HETEROGENEOUS CATALYSIS FOR HALOGEN CHEMISTRY
Michael David Higham

Institut Català d'Investigació Química
Avgda. Països Catalans 16
43007, Tarragona

I STATE that the present study, entitled "Theoretical Studies of Heterogeneous Catalysis for Halogen Chemistry", presented by Michael David Higham for the award of the degree of Doctor, has been carried out under my supervision at the Institute of Chemical Research of Catalonia (ICIQ).

Tarragona, September 2017

Prof. Núria López Alonso

UNIVERSITAT ROVIRA I VIRGILI
THEORETICAL STUDIES OF HETEROGENEOUS CATALYSIS FOR HALOGEN CHEMISTRY
Michael David Higham

Acknowledgements

The work presented in this thesis represents the cumulation of nearly three years of research. During this time, I have had the pleasure of working with many outstanding scientists, all of whom having contributed, directly or indirectly, to my experiences as a doctoral student, and thus to the presentation of this thesis, which would be incomplete without dedicating a few words to their honour.

First and foremost, I would like to thank my supervisor, Prof. Núria López, whose support and guidance was vital to the progression of the research. Throughout my doctoral studies, Prof. López has provided valuable insights into a myriad of subjects, and I am pleased to say that I have learned a great deal from her tuition, not only in Chemistry, but on the topic of human behaviour. Every moment spent in her group has become a treasured memory, never to be forgotten. I am sure I will fondly recall my time working with her for many years to come.

I would also like to thank ICIQ for providing financial support in the form of the ICIQ PhD Fellowship, and for granting me the opportunity to undertake my doctoral research at the institute. I am most appreciative of all of the administrative staff at the institute who support the PhD programme.

In addition to the support I received from my supervisor, my group colleagues contributed immensely to my development as a researcher, offering help and assistance without hesitation when requested, as well as solidarity and cameraderie. I would especially like to thank Dr. Marçal Capdevila-Cortada; at every stage of my doctoral research, he was ready to provide useful scientific contributions, and I am extremely grateful for his patience and the privilege of being able to benefit from his deep knowledge of theoretical chemistry. I would also like to individually acknowledge every member of Prof. López's group, both past and present, who have made a positive contribution to my time working in the office: Dr. Luca Bellarosa, Dr. Neyvis Almora-Barrios, Dr. Sergey Pogodin, Dr. Guillem Revilla-López, Dr. Giuliano Carchini, Dr. Rodrigo García-Muelas, Qiang Li (who should probably be correctly referred to as Dr. Li by the time this thesis reaches

vi

the examiners), Dr. Miquel García-Ratés, Marcos Rellán-Piñeiro, Dr. Jesús Jover, Franziska Hegner, Dr. Masoud Shahrokhi, Dr. Damien Cornu, Edvin Fako, Nathan Daelman, Dr. Bob Nguyën, Dr. Javier Navarro, and Konstantin Karajovic. If I may address the aforementioned scientists directly, I hope that you find this thesis to be detailed and informative. All of you have my deepest gratitude for your support.

In addition to members of Prof. López's group, I would also like to acknowledge the other residents of the theory office for their support and contributions. Firstly, I would like to thank all of the scientists, both past and present, from the groups of Prof. Maseras and Prof. Bo, who contributed to the productive atmosphere of the office. I am immensely grateful to Martin Gumbau; without his technical expertise, dedication and perserverance, none of the calculations presented in this thesis would be possible (lest we do them all by hand, which might have taken a while). I would also like to thank Moisés Àlvarez, whose technical capabilities have been beneficial to all of the scientists at the theory office. Additionally, I would like to thank Núria Vendrell for her tireless efforts to ensure the smooth-running of the theory office, and for her indispensable assistance in bureaucratic matters.

Much of the theoretical work presented in this thesis is accompanied by complementary experimental studies. To all of my experimental counterparts, I offer my most sincere gratitude; the quality of this thesis, and the rigour of our scientific results, would have been greatly compromised if it were not for your valuable contributions. I would like to thank Prof. Javier Peréz-Ramírez, Dr. Max Moser, Dr. Zhen Guo, Vladimir Paunović, Dr. László Szentmiklósi, Dr. Detre Teschner, Dr. Miguel Hevia, and Matthias Scharfe; it has been a pleasure to work with all of you, and I have been most fortunate to have had the privilege of your experimental expertise.

I am truly indebted to all of my good friends in Tarragona who have supported me and provided much appreciated companionship over the past three years. These individuals have brought great joy to my life in Tarragona, as well as being present to offer their support in darker times. I will miss all of them greatly when it is time for us to part ways. I will not engage in the tedium of listing each of these people by name, for they will know for themselves how important their support has been to me.

I would also like to thank all of the acquaintances I have made in Tarragona, both at ICIQ and around the city. The past three years have been a time to develop not only as a scientist, but as a person, and I feel greatly enriched by the culture of the region and by those acquaintances with whom I have enjoyed it. Indeed, as I write these words, politicians in both my home country and here in Catalonia are contemplating a more divided world, albeit

viii

Contents

CONTENTS   1

Thesis Summary

Computational techniques are applied to investigate the utility of rutile transition metal oxide based systems as catalysts for halogen chemistry. The studies explore the interplay between surface structure and composition, catalytic activity and product selectivity.

The work focuses on ruthenium dioxide and titanium dioxide based systems as catalysts for hydrogen halide oxidation and ethylene oxychlorination reactions. DFT calculations show that under hydrogen halide oxidation conditions, replacement of surface oxygen atoms in the rutile catalyst can occur. In particular, significant bromine uptake was found to occur in ruthenium dioxide, with bromine replacement extending beyond the surface to the subsurface layers and inducing a major structural rearrangement at the surface. It is thus proposed that the reaction mechanism is closely linked to the extent of surface replacement. The investigations also examine doped titanium dioxide based systems. The relationship between dopant-induced electronic structure defect states, and the catalyst activity towards elementary processes associated with hydrogen halide oxidation, is explored. In particular, it was found that a judicious choice of dopant atom can be made to optimise the number of defect states, and their associated energies, in order to fine-tune the electronic structure of the system for optimal activity. Finally, ruthenium dioxide is investigated as a potential catalyst for ethylene oxychlorination. It was found that competition between combustion and oxychlorination processes is enhanced by dimensional confinement of adsorbates on the catalyst surface, and that surface coverage is an essential factor in determining the feasibility of certain elementary processes, and thus product selectivity.

The thesis provides a clear overview of rutile catalysts for halogen chemistry and provides detailed insights which can inform the future development of superior catalysts.

Part I

Introduction and Methodology

UNIVERSITAT ROVIRA I VIRGILI
THEORETICAL STUDIES OF HETEROGENEOUS CATALYSIS FOR HALOGEN CHEMISTRY
Michael David Higham

Chapter 1

Introduction

1.1 History of Catalysis

1.1.1 Early History

The earliest recorded use of the term "catalysis" most closely resembling its modern usage is attributed to Jöns Jacob Berzelius (1778-1848), who described a phenomenon whereby substances can "promote the conversion of the component parts of the body they influence into other states, without necessarily participating in the process with their own component parts", referring to this ability of a substance as "catalytic power" and the process induced by these substances as "catalysis".[1] Berzelius' formulation was based on observations made by many scientists in the preceding years. Perhaps the earliest writings on the subject are those of Valerius Cordus (1515-1544), who described the conversion of alcohol to ether when heated in the presence of sulphuric acid.[2] In the late 18th and early 19th centuries, the first systematic studies investigating catalytic phenomena were conducted. In 1796, Johann Rudolph Deiman (1743-1808), Adrien Paets von Trootswijk (1752-1837), Anthoni Lauwerenberg (1758-1820), Nicolas Bondt (1765-1796) and Pieter Nieuwland (1764-1794) reported the production of ethylene from alcohol using a variety of methods, including by treating the alcohol with concentrated sulphuric acid, passing alcohol vapours through a glass tube containing silica or alumina, or an empty clay tube.[3] Later, in 1817, Sir Humphrey Davy (1778-1829) found that a hot metal wire could facilitate the combustion of coal gas at temperatures well below ignition, with no changes being observed to the metal itself. Davy repeated the experiment for several different combustible gases and obtained similar results. Additional experiments testing different metals found that whilst platinum and pallidium exhibited this phenomenon, other metals such as copper, silver, gold, iron and zinc did not.[4] Similar experiments were conducted by Louis-

7

Jacques Thenard (1777-1857), investigating the role of finely divided metal in hydrogen peroxide decomposition, noting how even very diverse materials were able to facilitate the decomposition, and it was supposed that this could be attributed to a common force.[5] Further work by Edmund Davy (1785-1851) showed that a finely-divided form of platinum powder, known as platinum black, was able to spontaneously react with ethanol vapour upon contact, becoming white hot and remaining so until all of the alcohol vapour was consumed, leaving the powder unchanged.[6] Johann Wolfgang Döbereiner (1780-1849) repeated Edmund Davy's experiments on platinum black successfully, and extended the studies to performing the catalytic combustion of hydrogen.[7] Remarkably, this process was able to take place at room temperature or even temperatures as low as -10 ℃.[8] This led to Döbereiner's famous invention, his *Platinfeuerzeug*, or lighter, a pneumatic device which ignited hydrogen (produced from the reaction of zinc with sulphuric acid) by passing the gas through a platinum sponge at a narrow opening, producing a flame which may be used to conveniently light candles. This invention caused a sensation, bringing international recognition to Döbereiner's work, and attracting the attention of many scientists to the phenomenon of catalysis. Crucially, Döbereiner recognised that the phenomenon was a result of the activity of the platinum, rather than the action of the gas or vapour on the platinum, since the metal remained unchanged after the reaction.[9] Thenard was intrigued by Döbereiner's results, since it was now evident that the same material, platinum black, appeared to facilitate not only hydrogen peroxide decomposition, but also the combustion of hydrogen to water, and was inspired to conduct further investigations, supporting the notion of the generality of catalysis that he had observed earlier, an idea reiterated by Davy's later writings.[10] An early attempt by Ambrogio Fusinieri (1775-1852) to rationalise the observations of Döbereiner and Davy described the formation of "concrete laminae" of reactant gases on the surface of the metal, being continually replenished as the reaction proceeds and the products are evolved, foreshadowing ideas that today would be associated with the adsorption and desorption of gases on solids.[11] Having read Fusinieri's work, Michael Faraday (1791-1867) then turned his attention to the subject, suggesting a physical force associated with the platina induces the combination of the gaseous components (maintaining that metal surface remains chemically inert throughout the reaction, in contrast to modern theories of catalysis), and that this force would appear to be a general property of all solids, to a lesser or greater extent, with platinum exhibiting this property to a highly significant degree, in contrast with less active substances.[12] Faraday also made key observation on catalyst poisoning, noting how the presence of *Olefiant Gas* (ethylene) was able to inhibit the combination of hydrogen and oxygen over platina. Berzelius'

1836 review unified these ideas, suggesting a link to observed electrochemical phenomena in additional to the physical aspects of origin of catalysis identified by Faraday, and of course famously naming the process catalysis.[1]
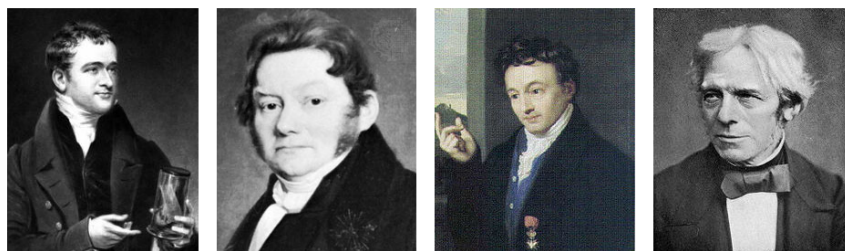
Figure 1.1: Some important figures in the early history of catalysis. From left to right: Sir Humphrey Davy, Jöns Jacob Berzelius, Johann Wolfgang Döbereiner, and Michael Faraday.

1.1.2 First Applications to Industry and Development of Theory

Throughout the 19th century, new industrial processes began to utilise catalysts, especially the well-studied Pt catalysts, with processes being developed for the oxidation of CO, SO_2 and NH_3, to CO_2, SO_3 and NO, respectively.[13] However, progress was slow and inconsistent, and consequently scientists of the day made further efforts to develop a more formal and complete theory of this newly identified phenomenon. Developments in the fundamental understanding of chemical processes precipitated a paradigm shift which permitted a more abstract consideration of catalytic phenomena by later researchers. Work by Ludwig Wilhelmy (1812-1864) established the dependence of the rate of a chemical reaction on the concentration of the reactants.[14] These observations were formalised by Jacobus van't Hoff (1852-1911), who identified some of the most important quantitative relationships governing chemical kinetics.[15] At the same time, advances were made in the establishment of chemical thermodynamics, replacing older theories based on the hypothetical substance caloric with more rigourous theories describing the relationship between heat and chemical equilibrium. Some of the most important contributions were those of Rudolph Clausius (1822-1888),[16] Josiah Willard Gibbs (1839-1903),[17] and Hermann von Helmholtz (1821-1894),[18] whose successive works led to the establishment of a clear framework for understanding chemical thermodynamics in terms of heat (enthalpy) and disorder (entropy), and their contribution to free en-

ergy associated with a chemical process, terms which are familiar to modern scientists. Using this new theoretical perspective, investigations by Georges Lemoine (1841-1922) led to a slight restatement of the definition of a catalyst: that a catalyst may not alter the positions of the thermodynamic equilibrium of a reaction, but can alter the rate at which that equilibrium is achieved.[19] Developing on this notion, Wilhelm Ostwald (1853-1932) proposed that the true role of the catalyst was not so much to initiate or induce a reaction, but merely accelerate a reaction that under non-catalytic conditions would occur at an infinitely slow rate.[20] Ostwald also introduced the notion of a chemical aspect of the association of a catalyst with reactant molecules; previous work, following the ideas presented by Faraday, supposed an entirely physical interaction, with Henri Moissan (1852-1907) and Jacques Duclaux (1877-1978) concluding from their studies that the activity of certain finely divided metals as catalysts originated from their porous nature, allowing sufficent absorption of reactant molcules in structural cavities to permit a reaction to take place when a sufficiently high degree of compression had been achieved.[3] Paul Sabatier (1854-1941), opposing this purely physical view, noted the differences in selectivity of apparently similar catalysts, and extended Ostwald's proposed chemical origin of catalysis,[21, 22] unifying the physical and chemical aspects of the phenomenon. Sabatier proposed that during the catalytic cycle, unstable intermediate compounds are formed between the catalyst and reactant, facilitating certain processes in the overall reaction, and regenerating the catalyst at the end of the cycle. This work foreshadowed the notion of chemisorption. Hence, in this view, the catalyst is not seen as being inert, as earlier researchers might have supposed, but is nonetheless preserved at the end of the catalytic cycle.[23] The work of Ostwald and Sabatier provided a clear chemical picture of the possible mechanisms of catalysis, and accordingly the two scientists recieved recognition in the form of Nobel prizes, in the years 1909 and 1912, respectively.

1.1.3   Expansion and Ubiquity in Industry

With the basic theoretical framework of catalysis now firmly established, the early 20th century saw an explosive increase in the industrial application of catalysis. One of the most important catalytic processes discovered at this time was the elemental synthesis of ammonia. Walther Nernst (1864-1941) and Fritz Haber (1868-1934) realised that high temperature and pressure were key to obtaining industrially viable activity.[24–26] Carl Bosch (1874-1940) adapted Haber's process for large-scale industrial use, switching from the expensive osmium catalyst used in Haber's original demonstration to cheaper iron-based catalysts.[13] Whilst originally devised as a method to

1.1. HISTORY OF CATALYSIS 11

produce fertiliser for agricultural use, in reality the process was quickly utilised as a means to obtain ammonia to produce nitrogen-based explosive to support the German effort in the ongoing Great War (1914-1919). During this time period, further theoretical developments also emerged, such as the theory of chemisorption proposed by Irving Langmuir (1881-1957). Building on Sabatier's work, Langmuir introduced the idea of unsaturated valences providing a means for the formation of intermediates between reactants and a catalyst during a reaction.[27] This notion was especially important for heterogeneous catalysis, as Langmuir's theory allowed one to approximate the surface of a catalyst as consisting of an array of identical non-interacting active sites, on which reactants may be adsorbed. Despite its obvious limitations (which Langmuir readily recognised), this model allowed for some of the first quantitative analyses of adsorption phenomena.[28] After the Great War, the use of catalysts was widely applied to the petrochemicals industry, with one of the most important discoveries being the synthesis of hydrocarbons from CO and H_2. This discovery in 1923, by Franz Fischer (1887-1947) and Hans Tropsch (1889-1935),[29] represents a second time where catalytic technologies have been of great importance for the German war effort, this time as a means of producing synthetic *ersatz* oil to power vehicles and industry in the Second World War (1939-1945), since Germany lacked native oil reserves.[13] Likewise, Allied forces relied on catalytic technology in the form of catalytic cracking of hydrocarbons with high molecular weight using acid-treated clays as a catalyst, as devised by Eugène Houdry (1892-1962) in 1928, in order to produce short-chain alkanes suitable for use in aviation fuel.[30] The conflict of the early 20th century not only provided a context for catalytic processes discovered earlier, but also catalysed the discovery of new technologies.

In the aftermath of the Second World War, developments in the petrochemicals industry continued to be relevant due to the increase in demand for fuel for civilian automobiles. Processes such as naptha reforming and hydrocracking were developed during the 1950s, contributing to the fuel industry, whilst other oil fractions were utilised to produce plastics, which were also in demand due to their use in cheap consumer goods.[30] A major breakthrough in polymerisation was the discovery that titanium salts in combination with organoaluminium compounds are able to catalyse the polymerisation of ethylene to polyethylene, by Karl Ziegler (1898-1973) in 1954. Giulio Natta (1903-1979) extended on this work by producing highly steroregular polypropylene using the new catalysts. Within a few years, the new catalysts had been adopted by industry, producing high-quality plastics for the market. Both chemists were recognised with the 1963 Nobel prize.[15]

1.1.4   Specialist and Environmental Catalysis

Since the middle of the last century, catalysis has expanded in its application, with catalysts being developed for the highly selective, small-scale production of fine chemicals, rather than being restricted only to bulk industrial products in large quantities. The development of zeolite catalysts in the 1960s represented one of the earliest examples of highly selective catalysts, having easily manipulated properties to direct selectivity. The porous nature of zeolite catalysts affords a high degree of size and shape selectivity, since only appropriately proportioned molecules can enter the porous channels of the catalyst and undergo reaction. Similarly, the steric confinement afforded by porous channels in zeolite catalysts also enhances selectivity, preventing certain potential products from being formed if their dimensions are not commensurate with that of the catalyst pores.[31]

Additionally, the increase in the use of petroleum-based fuels and polymer materials created a new demand for catalysts for environmental purposes.[30] Political action against automotive pollution resulted in the introduction of strict regulations on emissions in many countries, spurring industry on to develop catalysts to alleviate pollution. Hydrodesulphurisation catalysts based on molybdenum sulphide, typically promoted with cobalt, were developed to remove sulphur from fuels, limiting the amount of harmful sulphur oxides emitted to the environment.[32] Whilst these catalysts were identified in the 1940s as being ideal for removing sulphur from petroleum fuels,[33] the focus of these studies was more based on improving engine performance than on protecting the environment; as sulphur has a low ignition temperature, it causes knocking in internal combustion engines, hampering performance. Until the late 20th century, tetraethyllead was used to prevent knocking, primarily for economic reasons; whilst ethanol was found to be a suitable anti-knocking additive, it could not be patented, hence companies resorted to continuing the use of tetraethyllead (which could be patented) in order to realise short-term gains, in spite of the environmental cost.[34] It was not until the impact the of toxic compound on public health and the environment was fully realised and efforts were made to limit or prohibit the use of tetraethyllead that the compound was phased out, prompting industry to find alternatives. Hence modern unleaded fuels fell back to ethanol as a suitable anti-knock additive.[30] Perhaps one of the most famous applications of environmental catalysis known to the general public is the use of catalytic converters in automobile exhausts. Precious metals such as platinum, palladium, and rhodium are used as catalysts to facilitate the combination of CO and NO to form CO_2 and N_2, which are considerably less harmful to the environment.[35] The implementation of catalytic converters, enforced by environmental laws passed in many countries, resulting in automobile

emissions being reduced by over 90%, compared to 1965 levels, by 1990.[36] Clearly, the importance of catalysis for the wellbeing of the environment cannot be overstated, with catalytic processes developed during the 20th century both contributing to environmental pollution, and helping to limit or ameliorate the effects of pollution.

As of the present, catalysis continues to be an essential component of industrial chemistry, with an estimated 90% of all industrial processes utilising catalysis in some form.[37] However, the drive for improved catalyts with better activity, selectivity, cost and stability continues to the present day, as researchers aim to design catalysts on a rational basis, tailoring catalysts to be optimal for particular processes. This requires an accurate, detailed model, in order to clearly establish the factors which can affect catalytic behaviour, and how these factors can be manipulated to obtain the desired properties. Hence, a clear theoretical perspective on catalysis is essential to the design of the next generation of catalysts in industry.

1.2 Principles of Heterogeneous Catalysis

As the early pioneers of catalysis observed, catalysts may exist in the same phase as the reactants (such as the action of sulphuric acid in the conversion of alcohol to ether), or in a different phase from the reactants (as in the combustion of ethanol vapour facilitated by metallic platinum). This distinction leads to the division of the study of catalysis into two broad categories; reactions where the catalyst is in the same phase as the reactants is termed *homogeneous catalysis*, whilst *heterogeneous catalysis* refers to catalysts which are in a different phase from the reactants. Heterogeneous catalysis is the primary focus of this thesis.

The modern definition of a heterogeneous catalyst refers to a substance possessing an active site on the surface of a solid, which facilitates a reaction taking place in a liquid or gas phase in such a way that alters the kinetics of the reaction, but not the overall thermodynamics, in line with Ostwald's definition;[38] that is to say, the catalyst is not consumed during the reaction, and is regenerated by the end of the catalytic cycle.[30] Langmuir's highly simplified, but nonetheless successful, model involved considering the surface of a heterogeneous catalyst as a regular array of active sites, whereby atoms or molecules can be accomodated by adsorption.[27] Such active sites are sometimes referred to as coordinatively unsaturated sites, since atoms at the surface termination are necessarily deprived of some of the chemical bonds which are present for that atom in the bulk solid, hence giving rise to the phenomenon of chemisorption. This character renders the site active

14   1.2.   PRINCIPLES OF HETEROGENEOUS CATALYSIS

towards the adsorption of species from the gas phase. Additionally, a condition of monolayer chemisorption for heterogeneous catalysis is imposed as a consequence; whilst multilayer physisorption is possible, direct chemical bond formation between the adsorbate and substrate is necessarily confined only to the monolayer.
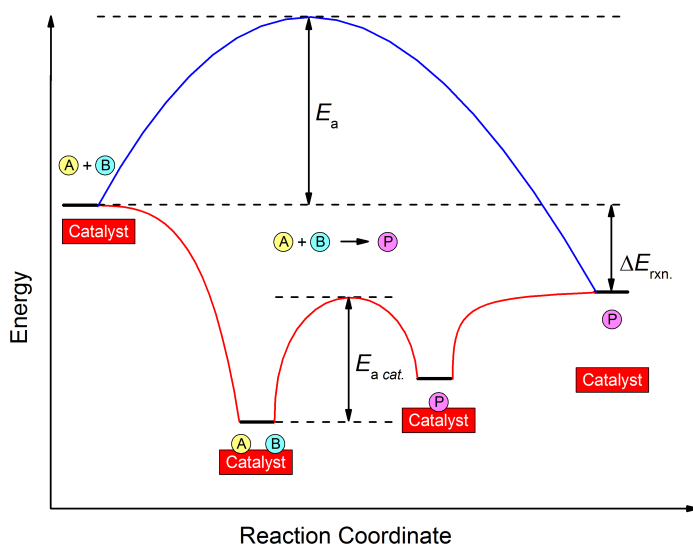
Figure 1.2: A schematic diagram comparing non-catalytic (blue line) versus catalytic (red line) reaction profiles for a generic gas phase reaction. In the gas phase, combination of reactants A and B involves breaching a large activation barrier, making the reaction kinetically unfeasible. The catalytic route, however, offers a more kinetically accessible alternative. Reactants A and B are exothermically adsorbed onto the catalyst surface, forming reactive intermediates with the catalyst. These intermediates can then combine on the catalyst surface with a much smaller kinetic barrier (i.e. $E_{\text{a } cat.} < E_{\text{a}}$), forming the product, P. The product P is then endothermically desorbed to the gas phase. Notice how $\Delta E_{\text{rxn.}}$ is the same in both reaction profiles; the catalyst only affects the kinetics of the reaction, and not the overall thermodynamics.

The nature of adsorption is key to understanding heterogeneous catalysis. In order for a reaction to take place, adsorption must be strong enough to ensure that gaseous reactants are attracted to the surface, but at the same time, adsorption cannot be so strong as to ensure that only one reactant dominates on the surface, for example. Similarly, product species cannot be too strongly adsorbed on the surface, otherwise the product will essentially poison the catalyst, preventing further catalytic cycles from taking place,

1.2. PRINCIPLES OF HETEROGENEOUS CATALYSIS 15

since fewer active sites will be available for reactants. The Sabatier principle states this more succinctly by proposing that an unstable intermediate between the reactant and catalyst surface must exist which is sufficiently stable to be generated in high quantities on the catalyst surface, yet is also sufficiently unstable so as to readily decompose to form the products.[39] The interpretation of this is that there exists an optimal stability of the intermediate that corresponds to maximal catalytic activity. The stability of the intermediate can be judged by considering a related thermodynamic quantity, such as the heat of adsorption of a reactant, for example. Considering how the rate of reaction (usually determined from an appropriate descriptor) varies as a function of the quantity correlated to the stability of the intermediate for different potential catalysts leads to so-called volcano plots, which aim to establish the best existing catalysts for a given reaction, and identify the optimal value for the quantity describing the stability of the intermediate.[13]

In heterogeneous catalysis, the nature of the adsorption site is strongly affected by the surface composition under a given set of conditions. The main issue with the Langmuir model is the uniformity it imposes on the surface; real catalysts are typically polycrystalline solids, possessing several different surface morphologies, and additionally, the terraces, kinks and nanoparticle edges present in real catalyst samples may very well have important adsorption properties of their own. Moreover, it is know that surface segregation phenomena mean that the composition and structure of a material at the surface can be significantly different from the bulk structure. The lack of uniformity is further aggravated by the presence of defects such as vacancies and impurities, sometimes intentionally added in the form of modifiers and promotors, especially in an industrial context. These variations in the surface structure give rise to much more complex adsorption sites than those imagined in Langmuir's model, with consequently more varied catalytic behaviour. Hence, more recent theories attempt to account for this complexity, at the cost of sacrificing the simplicity afforded by the Langmuir model. Langmuir's idea of chemisorption was extended from single atoms and molecules to consider more general adsorbate-substrate interactions, whereby several atoms present in the adsorbate interact in a specific way with several surface atoms of the substrate, known as the multiplet theory.[40] Whilst some catalytic reactions proceed with ease regardless of the method of preparation of the catalyst, typically reactions involving small molecules, other reactions involving more complex adsorbates demand a highly specific catalyst surface structure in order for the appropriate active sites to be present for adsorption.[41]

Further adding to the complexity of heterogeneous catalysis is the observa-

tion that the reaction being catalysed can also affect the surface structure, with catalysts adapting according to the conditions applied.[42] Indeed, upon adsorption of molecules from the gas phase, surface atoms actively reorganise to optimise bonding.[43] Moreover, the presence of adsorbates can induce the surface segregation already mentioned, affecting the catalyst composition at the interface.[44] Furthermore, in some cases it can be possible for a surface to undergo a non-catalytic reaction involving the reactants, thus changing the surface composition and the active phase of the catalyst. Hence, the catalyst surface can be seen as a dynamic system, which under appropriate conditions, can differ greatly from the stoichiometric surface at equilibrium, and in some cases, these dynamic changes in surface structure and compositions are key to the activity of the catalyst towards a given reaction.[45]

In addition to the changes to the catalyst surface that adsorption can induce, it is also important to consider the effects that coadsorbed species have on their respective geometries and stabilities. Under systems where there is a high coverage of adsorbates, lateral interactions between adsorbates results in a reorganisation of adsorbate geometry in order to reduce unfavourable steric interactions, and also improve attractive interactions, such as dipole-dipole interactions and hydrogen bonding, should these types of interaction exist in the system. Generally speaking, higher coverages result in less exothermic adsorption energies, as repulsive interactions between coadsorbed species weakens bonding to the substrate. In some cases, higher coverage can also encourage adsorbates to adopt coordination environments that differe from those observed at low coverages.[43]

As can be seen from the overview provided in the preceding paragraphs, rationally explaining the behaviour of heterogeneously catalysed reactions is greatly complicated by the highly variable, dynamic nature of surface structure and composition, and the important changes in adsorbate structure induced by coverage effects. At a first glance, such complexity may present a bleak outlook for scientific progress, but ingenious experimental techniques and theoretical tools ensure that these complexities are not completely insurmountable. Many so-called surface sensitive techniques offer a more detailed insight into the surface composition of catalysts and the bonding of adsorbates. For instance, IR spectroscopy can be performed on surface exposed to suitable probe molecules, such as CO or NO, revealing information about the nature of active sites from the vibration of the adsorbate-substrate bond, or from any changes in the vibrational frequencies associated with the adsorbate.[46] Other techniques can reveal important information about the electronic structure at the surface; these techniques, such as X-ray Photoelectron Spectroscopy (XPS), allow one to probe the

electronic band structure at the surface,[47] shedding light on the possible effects of additives and dopants by comparing with undoped samples. Temperature Programmed Desorption (TPD) studies can also provide detailed information about how strongly adsorbates are bound to the surface, and also reveal insights into reaction kinetics, as desorbed species are identified as the temperature is varied.[48,49] These techniques are just a few examples of the surface sensitive techniques available. Theoretical studies, such as those afforded by Density Functional Theory (DFT), can help to bridge the gap in understanding between the catalyst surface at the atomic scale and the interpretation of experimental results. Whilst investigations in heterogeneous catalysis remain challenging, combined theoretical and experimental studies allow for the most complete picture available of the interplay between catalyst structure, adsorbate geometry, and observable catalyst properties, such as activity and selectivity.

1.3 Halogens

The halogens are a class of elements appearing as group VII in the periodic table. The name *halogen* is derived from Greek, meaning "salt-forming", being coined in 1842 by Berzelius, who noticed the tendency of this class of elements to form salts by reacting with metals. The group consists of fluorine, chlorine, bromine, iodine, astatine, a radioactive element occurring naturally only in very small amounts in the Earth's crust, and speculatively tennessine, a superheavy element that has only been produced synthetically in limited quantities.[50] Of the four elements which occur in any significant abundance, Cl_2 and Br_2 are the most industrially important. Annual production of these two elements totals 75 Mton and 0.8 Mton, respectively, whilst annual I_2 production is 0.027 Mton and F_2 production stands at 0.02 Mton per annum.[51] Consequently, in this work, the focus will be exclusively on Cl_2 and Br_2 and their compounds.

1.3.1 Properties and Uses of Cl_2 and Br_2

Chlorine was discovered in 1808 by Sir Humphrey Davy, who named the element as such from the Greek, referring to its greenish colour. Although Carl Wilhelm Scheele (1742-1786) is recognised as having produced the gas in 1774, he did not identify it as an element. Scheele produced chlorine by reacting hydrochloric acid with manganese dioxide; at the time, HCl was essentially regarded as an element, known as *muriatic acid* (from the Latin *muria*, meaning salt), and in line with contemporary theories, identified the gas evolved as *dephlogisticated muriatic acid*.[52] Later, in 1785, Claude Louis Berthollet (1748-1822) observed that when bubbled through water

and exposed to light, the new gas evolved oxygen and left a solution of HCl, or *muriatic acid*. Hence, Berthollet identified the gas as *oxymuriatic acid*, believing it to contain oxygen which he had observed being released.[53] It was only after a rigourous compositional analysis of the gas that Davy concluded that it contained no oxygen and should be considered an element, and hence Davy is usually credited as the discoverer of chlorine. At standard temperature and pressure, Cl_2 presents as a pungent, poisonous green gas. Chlorine is a reactive gas and hence is not often found in its elemental form, but is highly abundant in the form of metal salts, most notably as NaCl, as well as many other minerals

Bromine was discovered by Antoine Jérome Balard (1802-1876) in 1824; the new element was extracted from brine residues obtained from sea water, after evaporation had taken place, and Balard recognised very quickly its relationship to chlorine and iodine, which had already been discovered. Balard obtained elemental bromine by treating magnesium bromide containing liquors, known as *bittern*, with chlorine. Bromine was evolved as Cl displaces Br from the salt, forming $MgCl_2$ as a byproduct.[53] Balard named the new element bromine, from the Greek meaning stench, in line with the naming convention adopted for other halogens, and the distinctive unpleasant odour that accompanies the element.[54] As with the discovery of chlorine, it is believed that earlier researchers had indeed isolated bromine, but had not identified the new substance as an element in the context of the theories of the time.[55] At standard temperature and pressure, bromine presents as a brown or dark orange, volatile liquid; like its relative chlorine, it has a distinctive odour, described as sharp and penetrating. Like chlorine, it is virtually never found in its elemental state in nature, however, whilst chlorine forms many salts and minerals, bromine containing compound in nature are more limited. Typically, bromine containing minerals are limited to silver compounds, as well as salts such as NaBr and KBr.

Table 1.1: Some physical and electronic properties of atomic and molecular chlorine and bromine. Values taken from Webelements.[56]

Units	Property	Chlorine	Bromine
	Atomic number	17	35
	Atomic mass	35.45	79.90
	Ground state electron configuration	$[Ne]3s^23p^5$	$[Ar]3d^{10}4s^24p^5$
	Term symbol	$^2P_{\frac{3}{2}}$	$^2P_{\frac{3}{2}}$
	Pauling electronegativity	3.16	2.96
$kJmol^{-1}$	First ionisation energy	1251.2	1139.9
K	Melting point	171.6	265.8
K	Boiling point	239.1	332.0
cm^3	Molar volume	17.39	19.78

As reflected in the production values, chlorine is used more widely in industrial applications than bromine. It is often used as a raw material for a multitude of industrial processes. Elemental chlorine is used in water treatment. By far the largest consumer of Cl_2 is the polyvinyl chloride (PVC) industry, accounting for nearly 40% of total Cl_2 production.[51] Furthermore, a 2014 estimate suggests that global demand for PVC is set to increase by 3.2% annually, hence it is likely that this will remain a major use of Cl_2 for the forseeable future.[57] Chlorine is also essential to the production of polyurethanes (PU); together with PVC, the polymer industry accounts for about 43 Mton of Cl_2 consumed annually. Polycarbonate (PC) production also accounts for a smaller amount of Cl_2 consumption, and together with PU it represents the importance of Cl in intermediate stages of production, rather than as a component of the final product, as both polymers require phosgene as a reactant, but production yields HCl as a byproduct.[58,59] Other important products requiring Cl_2 in their production are legion, ranging from bleaches, disinfectants and insecticides, to pigments, solvents and aerosols.[52]

Whilst Br_2 production is lower than that of Cl_2, bromine has several important uses, and is generally more specialised in its applications compared to chlorine, which is ubiquitous in industrial chemistry. The production of brominated flame retardants is the leading industry requiring bromine, accounting for the consumption of over half of all Br_2 produced. Additionally, bromine is used in a wide variety of more specialised compounds, such as pharmaceuticals, hydraulic fluids and perfumes.[60] Brominated biocides for water treatment are also increasing in popularity, being favoured over the traditional chlorine due to their more powerful action, as well as the fact that such compounds are much less heavily regulated than chlorine.[55] An increasingly important use of bromine in industry is the functionalisation of otherwise unreactive alkanes, increasing the options available for synthesis. As in the case of many processes using chlorine, such alkane functionalisation results in the generation of HBr as a byproduct.[61]

1.3.2 Production of Cl_2 and Br_2

Two main methods exist for the production of elemental chlorine: oxidation of hydrogen chloride, or alternatively, electrolysis of salt. Both methods have their advantages and disadvantages. Which method is favoured is often the result of a large number of factors, including the economic cost of the process, the supply of and demand for the reactants and products, respectively, environmental considerations, and technical or engineering limitations. For bromine, the smaller amounts produced entails some slightly different methods; for the most part, bromine is obtained from sea water by

ion exchange. However, electrolytic methods also exist for bromine production, and with the increasing use of bromine in industry and the resulting increase in the amount of HBr available, there is considerable interest in developing methods to recover Br_2 from the acid.

Chlorine production

Hydrogen Chloride Oxidation - the Deacon Process

Oxidation of hydrogen halides, producing the corresponding elemental halide and water, has long been a subject of heterogenous catalysis, particularly hydrogen chloride oxidation. The Deacon process was developed by Henry Deacon (1822-1876) in 1868, providing a catalytic process to convert HCl and O_2 into Cl_2 and H_2O over a $CuCl_2$-based catalyst.[62, 63] The overall reaction proceeds according the the following equation:

$$4HCl(g) + O_2(g) \rightarrow 2H_2O(g) + 2Cl_2(g); \ \Delta H^0 = -118 \text{ kJmol}^{-1}$$
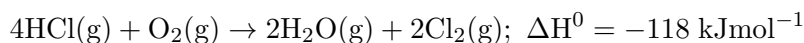
In an early example of environmental catalysis, the Deacon process was developed primarily to alleviate the negative impact of the Leblanc process. The Leblanc process was developed by Nicolas Leblanc (1742-1806) in 1790 as a means to produce sodium carbonate, which was in demand for the manufacture of soap, glass, and in particular textiles, since Na_2CO_3 was used to clean imported cotton before its eventual processing.[64] In the process, sodium chloride was treated with sulphuric acid, resulting in the formation of sodium sulphate, and waste HCl gas. The sulphate was then coal fired with calcium carbonate, yielding the desired Na_2CO_3, as well as waste HCl gas and calcium sulphide. Initially, the HCl gas was simply vented to the atmosphere, and the calcium sulphide waste, known as *galligu*, was simply dumped near plants utilising the Leblanc process, yielding toxic hydrogen sulphide gas upon weathering. Both of these waste products contributed to severe environmental pollution, especially in the North West of England, where much of the burgeoning British chemical industry was established. The negative impact of environmental pollution attributable to waste byproducts of the Leblanc process was the source of much grief to the local populace, and as such attracted legal attention, leading to the passage of the first of the Alkali Acts in 1863, which required that at least 95% of waste gases be recovered, leaving only a maximum of 5% that could be vented to the atmosphere.[65, 66] The Deacon process was developed in response to the legislation; since industrialists producing sodium carbonate were legally mandated to recover virtually all of the HCl byproduct by condensation, it was of economic interest to develop a process to convert undesirable HCl waste into a valuable product that could be sold. The Deacon process was integrated into chemical plants using the Leblanc process,

thereby making it more profitable for industrialists to observe the new laws, which required regular auditing of plants by government inspectors, and additionally imposed heavy fines for failure to comply with the regulations.

Figure 1.3: Left: An industrial scene in Widnes, Cheshire, UK, where extensive pollution due to the Leblanc process ultimately resulted in legislation to curtail HCl emissions. Right: Henry Deacon, the industrial chemist who devised the process taking his name to convert HCl to Cl_2, and thus alleviate some of the pollution caused by the Leblanc process. Owing to the extensive environmental damage inflicted in the locale of Widnes, the first plant utilising the combined Leblanc-Deacon process was established there.

The success of the Deacon process in ameliorating environmental pollution caused by the Leblanc process was, however, short-lived. More economical and less polluting methods to obtain sodium carbonate were developed at around the same time. Ernest Solvay (1838-1922) created an alternative method to produce Na_2CO_3 in 1865; the process is somewhat intricate and utilises ammonia to facilitate the reaction between NaCl and $CaCO_3$. Firstly, heating $CaCO_3$ induces its decomposition to CaO and CO_2 gas, which is then subsequently passed through a concentrated aqueous solution of salt and ammonia, yielding sodium bicarbonate and ammonium chloride. The desired sodium carbonate product is obtained from the bicarbonate by calcination, yielding water and CO_2 as byproducts, whilst CaO and NH_4Cl react to produce the only real waste product, $CaCl_2$, and regenerate NH_3. In this reaction, ammonia essentially functions as a homogeneous catalyst. The Solvay process was rapidly adopted across Europe, owing to its economic and environmental benefits over the Leblanc process, eventually rendering the Leblanc process obsolete.[64]

Whilst the Deacon process could be used to produce valuable chlorine from HCl independently of the Leblanc process, the copper chloride based catalysts utilised showed poor stability. Under typical reaction conditions, the catalyst is degraded by the formation of volatile copper chloride species. Hence, in spite of the relatively good activity and conversion rates achieved, the Deacon process was largely abandoned for Cl_2 production by the end of the 19th century, with electrolytic methods taking its place.[67] Throughout the 20th century, efforts were made to develop alternative Deacon catalysts, as whilst the electrochemical methods are feasible, they are very energy-intensive, and furthermore, Cl_2 production by salt electrolysis does not address the issue of surplus HCl produced as a byproduct of many industrial processes (PVC production, for example), as well as also producing caustic soda, which is not profitable due to its low value. Direct oxidation of HCl would provide a suitable method to recover Cl_2 from waste HCl and would be more cost-effective than electrolysis as it would consume less power. However, the success of these alternatives was rather limited. An example is the Shell-Chlor process, developed in the mid 20th century, which made significant improvements on the original Deacon catalyst by using potassium chloride additives in a $CuCl_2$ catalyst on a silica support, promoting catalyst stability. The additive improves the catalyst activity and thus lowers the typical operating temperature to achieve suitable HCl conversion, thus limiting the extent of the undesirable evaporation of the catalyst to volatile species.[68,69] Another attempt to produce a feasible Deacon catalyst was made in the 1980s with the MT-Chlor process, developed by Mitsui. This catalyst was also based on $CuCl_2$, but instead employed chromium oxide as an additive, and likewise saw similar improvements in stability and catalytic performance, improving significantly on the Shell-Chlor process in terms of stability.[70,71] However, despite the considerable improvements, the MT-Chlor process was not widely applied in industry, perhaps due to a reluctance to use chromium-based material owing to environmental concerns, and hence electrolysis remained the most popular method to produce Cl_2.[72,73]

It would not be until the 1990s that significant further progress would be made in the development of new Deacon catalysts. Whilst major developments throughout the mid 20th century in the composition of electrodes greatly improved the efficiency of electrolytic chlorine production, the industry remained to be one of the major consumers of electricity worldwide, and hence there remained an intense interest in developing a catalytic alternative. Sumitomo produced highly active and stable RuO_2-based heterogeneous catalysts for HCl oxidation, providing a much needed alternative to the earlier Deacon catalysts based on $CuCl_2$.[72,74] Experimental work in an

academic content has attempted to establish the origin of the high activity and good stability of the new RuO_2-based catalysts. Preliminary studies revealed through X-ray Photoelectron Spectroscopy (XPS) that a small amount of Cl is indeed present in the catalyst when exposed to HCl, however the X-ray diffraction pattern obtained was not substantially different from that of the stoichiometric catalyst, implying that the bulk catalyst remained largely unchanged. It can then be inferred that chlorine uptake must be limited exclusively to the catalyst surface. Additionally, High Resolution Core Level Shift (HRCLS) spectra show that for $RuO_2(110)$ exposed to a HCl atmosphere, increasing the temperature results in a shift in the Cl 2p levels to a higher binding energy, which can be attributed to a change from Cl being adsorbed at Ru coordinately unsaturated (Ru_{cus}) sites at lower temperatures, to the replacement of O_b with Cl at higher temperatures. This is mirrored in the HRCLS spectra for the O 1s levels. Low-Energy Electron Diffraction (LEED) studies also show that the catalyst exposed to a HCl environment is morphologically identical to the stoichiometric catalyst, and that $50 \pm 20\%$ of the bridging sites are occupied with Cl. CO oxidation studies corroborate the hypothesis; in the stoichiometric catalyst, the reaction proceeds with CO combining with O_b to evolve CO_2. CO_2 evolution is observed to decrease when a HCl atmosphere is present as temperature increases, as O_b atoms are gradually replaced by Cl.[75] The extent of bridging chlorination was determined from Auger electron spectroscopy to reach a maximum of 0.76 ± 0.08 ML, where 1 ML corresponds to complete replacement of O_b. It was proposed that this moderate Cl uptake in fact contributes to the remarkable stability of RuO_2 as a Deacon catalyst, with the partial chlorination affording sufficient stabilization to render further reduction of the catalyst unfeasible.[76]

The TiO_2-supported RuO_2 catalyst developed by Sumitomo is starting to be used in industry as a means to recycle HCl to obtain Cl_2, but electrolysis remains a major source of Cl_2 production, not least due to its well-established status and the not inconsiderable cost of ruthenium, the prices of which being highly volatile.

Salt Electrolysis - the Chlor-Alkali Process

Whilst observations of the electrochemical production of Cl_2 were made as early as 1800 by William Cruickshank (1745-1810), it would not be until the late 19th century that suitable electricity generators were available, hence delaying its economical application to industry.[52] The most common method of producing Cl_2 for most of the late 19th and early 20th centuries was the mercury cell process, first developed in 1892. In this method, electrolysis of brine yields Cl_2 at the anode, whilst sodium forms an amalgam

with mercury, which acts as the cathode. The amalgam is then directed to a separate reactor where it reacts with water, producing H_2 gas and caustic soda, whilst the mercury is recovered and recycled.[77] Whilst many plants operating this process still exist to the present day, there are plans to phase out the process in Europe, owing to mercury's high toxity. As of 2015, less than 20% of chlorine production in Europe was attributable to the mercury cell process,[77] with most of the production (64%) being accounted for by the membrane cell process, which relies on an ion exchange membrane to allow the separation of Cl_2 from the byproducts (H_2 and NaOH), since Na^+ ions originating from the formation of Cl_2 at the anode must diffuse across the membrane in order for NaOH to be formed at the cathode.[77]
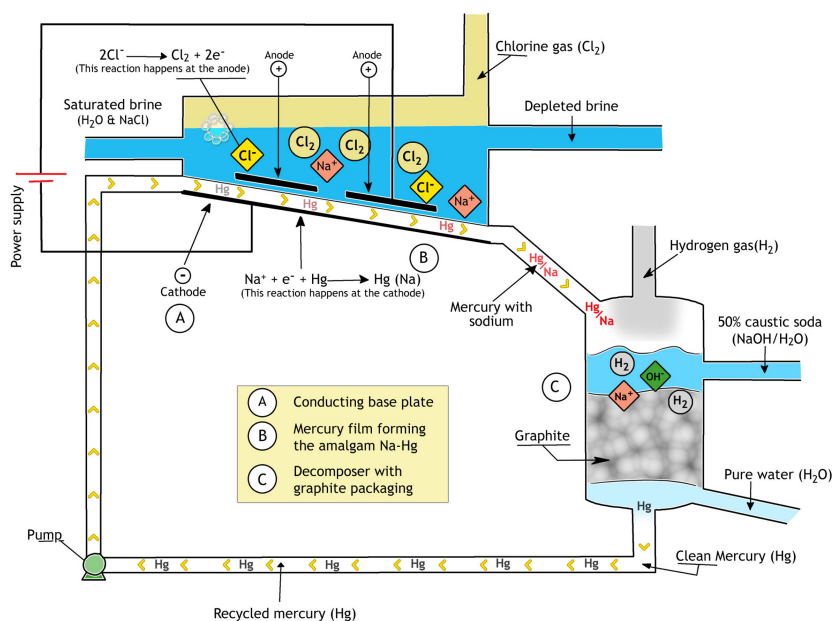
Figure 1.4: Schematic diagram depicting the mercury cell process for salt electrolysis. Reproduced from Eurochlor with permission.[77]

During the middle of the 20th century, whilst other researchers were aiming to develop improved Deacon catalysts with somewhat limited success, further advances were made in developing superior electrodes, namely Dimensionally Stable Anodes (DSAs).[78] Before the 1960s, plants operating the electrolytic chlor-alkali process used anodes based on materials such as lead, graphite and magnetite, which had a tendency to degrade over

1.3. HALOGENS

time.[79,80] It was fortuitously discovered, however, that 70/30 Pt/Ir coated Ti electrodes showed remarkable stability; naturally, this discovery was met with some resistance from industry leaders on the grounds of cost, but it soon became clear that despite the high initial investment, the new anodes would be sufficiently resistant to cover this initial cost. Indeed, it was reported that 10 years after the construction of first two plants utilising the new Pt/Ir coated Ti anodes in 1968, that the plant was still using the exact same electrodes with their original coating, and by the early 1970s, over half of all chlor-alkali plants were using these electrocatalysts worldwide.[81] Still, the Pt/Ir coated Ti electrodes were deemed to be in need of some improvement, not only because of the not inconsiderable cost of the metals required, but also because the electrodes were found to be unsuitable for plants using the mercury cell cycle, which was still popular across Europe in the 1970s. Specifically, problems arose with the sodium amalgam formed during the process inducing a short circuit, preventing the anode from functioning, and also the risk of the valuable metal comprising the electrode being dissolved into the amalgam.[81] This led to the development of the electrodes based on metal oxides, which showed much greater resistance to the adverse effects of mercury, as well as being generally more durable, and having a lower overpotential, making these electrodes more energy efficient.[82] After a periodic of research aiming to optimise the innovative new electrodes, the modern DSA was developed, being constructed of a co-precipitated mixed oxide of TiO_2 and RuO_2.[83] These electrodes showed excellent stability, being especially resistant to dissolution in amalgam, as well as showing good electrocatalytic performance. The high durability of the DSA was attributed to the fact that the RuO_2/TiO_2 mixture is a true mixed crystal, since RuO_2 and TiO_2 both adopt the rutile structure and have similar lattice parameters, hence the DSA shows greater mechanical durability compared to other electrodes which do not possess this property. Perhaps more importantly, from a commercial perspective, it was recognised that these mixed oxide electrodes would function highly efficiently even with a RuO_2 content of less than 50%, thus drastically reducing the cost, since RuO_2 is considerably more expensive than TiO_2. The lower RuO_2 content improves efficiency since RuO_2 is much more powerful as a chlorine electrocatalyst than for oxygen, hence reducing the amount of RuO_2 has the desirable effect of optimising the electrode overpotential, improving electrocatalytic performance.[81] Whilst DSAs might have originally been conceived to be applied to the mercury cell process, their introduction actually made the more environmentally friendly membrane cell method more appealing; before the introduction of the DSA, graphite anodes were often used, and hence the membrane cell process was not widely applied since graphite particules in the electrolye (as a consequence of routine electrode degradation)

would readily clog the membrane.[80] From the 1970s onwards, DSAs were widely adopted by the chlor-alkali industry, cementing the role of electrolysis as the primary means for producing Cl_2.
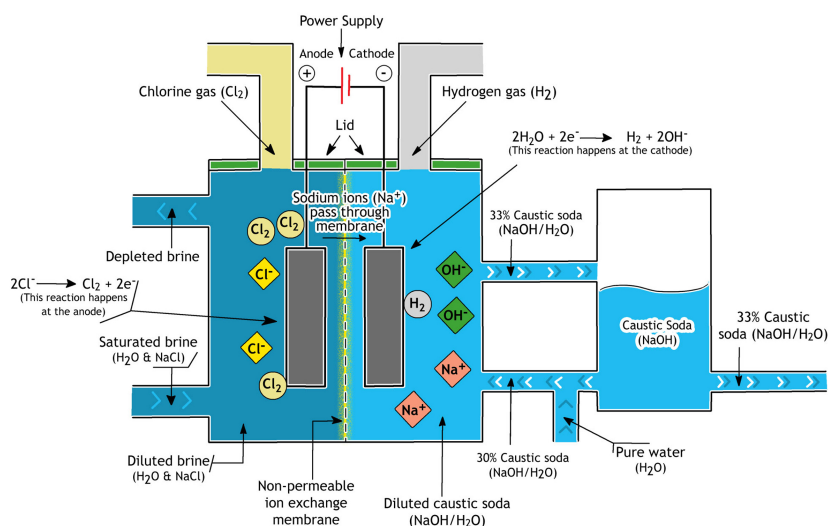
Figure 1.5: Schematic diagram depicting the membrane cell process for salt electrolysis. Reproduced from Eurochlor with permission.[77]

Bromine Production

Extraction by Displacement

Whilst bromine in general is a fairly rare element in nature, it forms a major component of sea water, which can contain as much as 65 mg/L.[55] Hence, both historically and up to the present, extraction from sea water, or concentrated salt lake brines, is and was the main source of bromine.[84] The bromine industry began in 1865 when Adolph Frank (1834-1916) developed a method to extract bromine from concentrated bromide present in the residues from carnallite ($KMgCl_3 \cdot 6(H_2O)$) production, a mineral obtained by evaporating brine in open ponds and used to obtain potash. The increase in demand for bromine can be attributed to the development of early photographic techniques by Louis Daguerre (1787-1851). Originally,

1.3. HALOGENS 27

Daguerre used light-sensitive silver iodide to produce photographic images, however, the process required a fairly long exposure of several minutes. Silver bromide shows a similar behaviour, but requires an exposure of only a few seconds, revolutionising the field of photography. The importance of this was highlighted by Jean Baptiste André Dumas (1800-1884), who specifically mentioned this application of bromine compounds in the eulogy of Balard that he delivered in 1879.[85] In the original process, MnO_2 and sulphuric acid were used to oxidise the bromide to elemental bromine, evolving water and leaving manganese sulphate in solution. This method was short-lived due to practical difficulties arising from the use of both solid and liquid reactants. The process was later modified so that chloride replaced MnO_2 as the oxidising agent, allowing for continuous production.[34] The method relies on the fact that bromide is more easily oxidised than chloride; the potential for the oxidation of Br^- to $\frac{1}{2}Br_2$ is -1.36V, compared to -1.09V for the oxidation of Cl^- to $\frac{1}{2}Cl_2$. Hence, chlorine essentially displaces bromide from the solution.[55] The Br_2 was then removed from the aqueous solution by "steaming out" the bromine, separating it from other minerals present in the brine. The vapour mixture was then passed through iron filings, extracting the bromine in the form of iron bromide, removing it from any contaminants. An improved version of this steaming-out process was developed in 1906, whereby steam blowing and chlorination occur simultaneously, increasing the efficiency of the process.[86] The dissolved chlorine and bromine are carried off with the steam, the mixture is condensed, and gravity separation allows the bromine to be collected as the lower fraction. Any chlorine dissolved in the steam mixture returns to the gas phase and is recycled for further oxidation of bromide.

An alternative process for extracting bromine from sea water, as opposed to concentrated brine, was developed by Herbert Henry Dow (1866-1930) in 1891.[87] The main innovation of this process was the use of air, rather than steam, to remove the bromine from the mixture, since it would be uneconomical to use steam given the relatively low Br concentration of sea water, compared to concentrated brine. The low concentration of bromine in sea water means that large quantities of the bromine stripping medium would be needed.[55] The process involves pumping sea water to the top of the air-blowing towers which extract the bromine. When the sea water has reached the top of the tower, sulphuric acid is added, in order to neutralise the slightly alkaline sea water (attributable to the presence of hydrogen carbonates) and thus prevent the undesirable further reaction of bromine hydrolysis.[88] Chlorine is also added to oxidise the bromide, as in the other processes discussed. As the sea water decends through the air-blowing tower, air pumped in the opposite direction extracts the bromine

and chlorine; the air-halogen mixture is then drawn through a sodium carbonate scrubber to extract the halogens, forming sodium bromide and chloride, sodium bromate, as well as CO_2. The salt solution is then directed to a reactor where bromine is then liberated by reaction with sulphuric acid.[55] The Dow Chemical Company made further modifications to this process in 1939; instead of using a sodium carbonate scrubber and treating the resulting salt mixture with sulphuric acid, the halogens blown out of the sea water are mixed with SO_2, which results in the formation of an acidic solution containing HBr, HCl, and H_2SO_4. This solution is then treated with chlorine and the bromine removed using steam in the ordinary way, with the H_2SO_4 and HCl solution remaining being recycled to acidify the sea water for the next cycle.[89,90] These new processes were developed largely in order to streamline the extraction process in light of increased demand for bromine in the early 20th century. The increased demand was due to the use of tetraethyllead in automobile engines as an anti-knocking agent; whilst tetraethyllead performed well to mitigate knocking caused by high sulphur content in fuels, the main drawback (apart from the environmental consideration, which were for the most part overlooked at the time) was that lead oxides could form in engine cylinders, hampering performance. Since it was discovered that ethylene bromide could be used to convert the lead oxide in lead bromides, which could be expediently removed from the engine via the exhaust (in spite of the environmental harm associated with such a practice), this became the main source of demand from bromine.[88] This would remain the case until the late 20th century, when lead fuel additives were phased out and flame retardant materials based on bromine became more popular.

To the present day, extraction of bromine from brine or sea water remains the most popular production method. This is because of the essentially limitless amount of bromine present in all the world's oceans; even if the concentration of bromide in sea water is rather low, the vast amount of sea water available renders this point somewhat moot. Today, the largest producers of bromine include primarily the United States, Jordan and Israel, as these countries possess salt lakes (namely the Dead Sea for Jordan and Israel, and the Smackover Formation in Arkansas for the US) which contain remarkably high levels of bromine.[34,91]

Electrolysis of Sea Water

In the early days of the bromine industry, investigations were made into the possibility of using electrolysis, rather than chlorine, as a means to oxidise bromide ions present in brine or sea water. The Wünsche electrochemical process was developed in Germany and used graphite electrodes separated

by a porous clay diaphragm; however, the process was short-lived, as Mg^{2+} at the cathode formed $Mg(OH)_2$ and H_2, with the magnesium hydroxide clogging up the pores of the diaphragm. The process was modified to result in the Kosseth electrochemical process. Here, a bipolar carbon plate replaced the graphite electrodes, with one side serving as the cathode, and the other as the anode. This set up prevented the excessive build up of $Mg(OH)_2$, since one can simply reverse the current to swap the anode and cathode to opposite sides of the carbon plate.[34, 55] The electrolytic method never became widely popular, largely due to the high power consumption compared to existing extraction processes.

Br_2 Production from HBr

Given the rise in the use of bromine in organic synthesis, and the increasing amounts of waste HBr produced as a result, methods to valorise the acid to recover bromine has attracted some recent attention from research.[61, 92, 93] Current methods rely on chemical oxidation (i.e. with chlorine) to convert HBr back to Br_2, similar to methods used to extract bromine from bromide containing solutions, and naturally such methods entail greater complexity and additional waste products. Hence, it is desirable to obtain a simpler and more environmentally viable method of recycling HBr. Several methods have been reported, but none are believed to be feasible on an industrial scale as of the present.[94]

Electrolytic methods have been investigated, not only as a means to recycle Br in HBr, but also in response to a growing demand for H_2 for fuel.[95] Attempts have been made both in the gas phase and in solution, but there have been significant issues with extracting the Br_2 produced. This is a major problem for electrolytic reactions in solution, since the aqueous mixture of HBr and Br_2 is extremely corrosive and often damages electrodes. In solution, solids capable of high bromide ion conduction have been considered, facilitating the separation of Br_2; the most successful to date have been based on LaOBr doped with alkaline earth metals. Whilst undoped LaOBr has a modest number of Br^- vacancies, which provide the mechanism for Br^- conduction, substitutional doping of La for alkaline earth metals increases the number of Br^- vacancies, thus increasing bromide anion conduction, allowing for a means of separating the bromine.[96] In the gas phase, investigations examined the use of a molten salt membrane, based on yttria stabilised zirconia saturated with a eutectic mixture of molten bromide salts.[97] However, both of these methods are not currently applied in industry, either because of issues with cost or efficiency. Further efforts built on the gas-phase molten salt membrane method, replacing the original graphite electrodes with platinum, testing different salt mixture compositions, and

varying the operating temperature.[98] The results showed a considerable increase in efficiency, but obviously platinum is not ideal for many industrial processes owing to its high cost, hence the authors indicated the need for further research into less expensive materials. More recent studies intended to address this by considering transition metal sulphides as electrodes for HBr oxidation; industrially, rhodium sulphide is used as an electrode material for HCl electrolysis, hence it seems reasonable to suggest that similar compounds may afford a good activity for HBr electrolysis.[99] These studies found that RuS_2 substitutionally doped with Ni or Co is a highly active as a HBr electrode material. The doped sample was found to be more active than pure RuS_2, but less so than the RhS_2 electrocatalyst considered initially. However, RuS_2 is considerably less expensive than RhS_2, and in addition, the new electrocatalyst was found to be much more resistant to corrosion than Pt, which had been used in earlier studies. Whilst these initial results are encouraging, such electrocatalysts are still a long way from being applied in an industrial setting.

Catalytic oxidation is a potential alternative to electrolysis for the conversion of HBr to Br_2, however, as with electrolysis, so far investigations of this avenue have been confined to a research setting, rather than to full industrial application.[100] Many of even the best efforts made since the middle of the 20$^{\text{th}}$ century have experienced setbacks such as poor catalyst stability under reaction conditions, or insufficient activity.[101] Whilst the highly exothermic nature of the catalytic process makes it attractive from an economic point of view compared to electrolytic methods, which require significant energy resources, the vast amounts of heat generated by the reaction has been identified as one of the main factors contributing to the volatisation of promoters, leading to catalyst degradation and reduced activity. Additionally, common contaminants, such as HCl and volatile organic compounds contribute to catalyst deactivation. Issues with excessive temperature were alleviated to some degree by using a concentrated aqueous solution of HBr, rather than anhydrous HBr. However, whilst some improvements were made, as of the present no further progress appears to have been made.[100] In more recent times, attention has turned to titania as a potentially successful HBr oxidation catalyst.

Very promising recent developments investigated the use of TiO_2 as a catalyst for HBr oxidation in the gas phase, similar to the use of RuO_2 as a Deacon catalyst for HCl oxidation. In catalytic tests, HBr conversion was recorded as being over 90% at 673 K.[45] Probing the Ti oxidation state, X-ray Photoelectron Spectroscopy (XPS) experiments showed the presence of Ti^{3+} states, as well as indicating the presence of small quantities of Br incorporated into the catalyst after exposure to a HBr atmosphere and var-

ious HBr/O_2 gas mixtures. Indeed, the catalyst was visibly changed after exposure to HBr, with the extrudates adopting a yellow hue after HBr exposure, rather than the more familar white colour associated with stoichiometric TiO_2. Complementary theoretical studies, discussed in more detail in Chapter 3, revealed that whilst stoichiometric TiO_2 would be inactive as an oxidation catalyst, under HBr oxidation conditions limited replacement of surface O atoms for Br induces the formation of defect states which render the catalyst active.[45] The self-limiting Br replacement was also found to promote catalyst stability, ameliorating some of the issues encountered with previous efforts to develop new HBr oxidation catalysts. These highly promising results offer a potentially viable method to prduce Br_2 from HBr on an industrial scale, and it can be expected that with some further academic study, catalyst performance will be optimised and the process will be applied industrially.

Some approaches have attempted to combine the alkane functionalisation and bromine recovery processes. Here, after the reaction between an alkane and Br_2, yielding a bromoalkane and HBr, the byproduct HBr is directed to a second reactor, where a reaction takes place with a metal oxide, yielding a metal bromide. Then, O_2 is introduced to the reactor, regenerating the metal oxide, and liberating Br_2, which can then be recycled for further alkane bromination.[102] In this context, the metal oxide is commonly termed a cataloreactant, as whilst the metal oxide is ultimately regenerated and is not consumed in the overall cycle, the reaction and regeneration steps happen sequentially, i.e. regeneration only occurs when O_2 is introduced. Whilst this method did result in a good degree of Br_2 recovery, selectivity towards the desired organic products proved to be an issue. Later work established a more concrete relationship between the reaction temperature and the product distribution.[103] Early tests of a scaled-up reactor have been performed, with good results, however more work will be needed before the process can be extended to a full industrial scale.

As can be seen from this overview, there are several potentially successful methods in development for the efficient conversion of HBr into Br_2. Evidently, the field presents some highly challenging problems, and there remains a great deal more to be investigated to ensure maximum efficiency, stability, and activity, before processes can be applied routinely in industry.

1.4 Vinyl Chloride

Chloroethylene, also know as vinyl chloride monomer (VCM) in industry, is a small organic compound, having the molecular formula C_2H_3Cl. It was

first synthesised in 1838 by Justus von Liebig (1803-1873) and Henri Regnault (1810-1878), who prepared the compound by dehydrochlorinating 1,2-dichloroethane (also known in industry as ethylene dichloride, or EDC).[104] In 1872, Eugen Baumann (1846-1896) repeated the synthesis, detailing the preparation method employed.[105] Notably, Baumann also noticed the formation of an insoluble, amorphous mass, when the substance was exposed to light.[106] However, these studies, did not directly lead to any further applications, and it would not be until the early 20th century that VCM would be rediscovered by Fritz Klatte (1880-1934), who prepared VCM in 1912 through the hydrochlorination of acetylene.[107] During the 1920s, Waldo Semon (1899-1999), whilst working at B. F. Goodrich and searching for suitable synthetic alternatives to natural rubber, expanded on Baumann's observation, and having prepared the polymer, began experimenting on manipulating its properties.[106] The new polymer, polyvinyl chloride (PVC), proved to be highly durable, waterproof and a cost-effective alternative to natural rubber. As the 20th century progressed, so did the development of PVC, as the burgeoning petrochemicals industry provided ample starting materials for PVC, and the versatile plastic became much in demand for a wide range of both specialised and consumer goods.

1.4.1   Properties and Uses of VCM and PVC

VCM is a highly soluble, colourless, flammable gas, possessing a slightly sweet odour. The compound is stable in the absence of oxygen and at low temperatures, but is liable to decompose into acetylene and HCl at elevated temperatures, and in an oxygen-rich environment, combustion readily takes place. VCM is toxic at high exposure, and is a known carcinogen.[104] The most important reactions of VCM, from an industrial perspective, are polymerisation reactions. Around 99% of all VCM produced goes on to be polymerised to PVC, with China being the largest producer of VCM.

Table 1.2: Some physical properties of VCM. Values taken from Dreher et al.[104]

Units	Property	Value
	Molecular weight	62.5
K	Melting point	119.4
K	Boiling point	259.8
kJmol^{-1}	ΔH_f^0	+35.2

PVC is a polymer obtained from VCM, with a typical polymer length of 700-1500 monomer units. PVC chains of a length of more than about 10

monomer units are insoluble in VCM, hence during polymerisation, PVC readily precipitates from its monomer.[108] The presence of Cl in the polymer results in its polarity, allowing for strong interactions between polymer chains, contributing to the mechanical strength of PVC. The length of polymer chains can be controlled, and this has a significant effect on the physical properties of the plastic. In practice, PVC is virtually always mixed with a variety of additives, such as stabilisers, lubricants, plasticisers and filler material. Stabilisers are needed since under heating, dehydrochlorination can occur. Stabilisers based on lead, or in more recent times, mixtures of metal compounds (carboxylates, napthalates and phenolates) including barium, cadmium, calcium and zince, amongst others, are used to neutralise the HCl evolved, and promote nucleophilic substitution reactions which limit further polymer degradation.[109] Internal and external lubricants are added to counter the naturally high viscosity of PVC, preventing the polymer from sticking to the interior of vessels, and allowing for ideal properties of the molten plastic. UV stabilisers prevent photodegradation, whilst filler materials such as TiO_2 are often added to improve the overall durability of the material. Hence, it can be seen that the physical properties of the plastic are highly dependent on the type and quantity of additives, allowing for highly versatile applications.[110]

Due to its versatility, low cost, and stability, PVC is one of the world's largest selling polymers, just behind polyethylene and polypropylene.[111] Early uses for PVC included insulation for wiring and waterproof fabrics, such as raincoats and shower curtains,[106] but today its use extends much further. PVC is ubiquitous in many areas, including construction (window frames, pipes, guttering, insulation and waterproofing), domestic products (electrical appliances and flooring), packaging (bottles, boxes and cling film), clothing (waterproofs, footwear and life jackets), medical items (sterile bags and tubing), and many more products. The items listed in this paragraph represent only a tiny fraction of the possible uses for PVC.[109]

1.4.2 Production of VCM and PVC

VCM Production

Two main methods for the industrial production of VCM exist: the hydrochlorination of acetylene, which was the original method applied by Klatte, and the thermal cracking of EDC, which in turn is produced by the chlorination of ethylene. The latter method is the most popular wordwide, whilst the former dominates in China, since cheap acetylene is readily available from extensive coal reserves.[112] Interest has also been growing in the direct oxychlorination of ethylene, cutting out the need to perform

thermal cracking on EDC and thus improving process efficiency.

VCM Production from Acetylene

Historically, production of VCM from acetylene was the main method employed, as acetylene was readily available from coal. Whilst the hydrochlorination of acetylene can take place in either the gas or liquid phase, industrially the gas phase reaction is favoured. Mercury chloride on activated carbon is the most popular catalyst for this process, owing to its high activity.[113, 114] In this method, it is essential that the input feed excludes not only common catalyst poisons, such as sulphur and phosphorus, but also unsaturated carbon compounds, as these can clog up the catalyst surface, elemental chlorine, as this can increase the risk of explosion, and water, since the the presence of water can cause corrosion inside the reactor.[110] Hence, reactants must be very pure to ensure to process proceeds correctly. The reaction is highly exothermic, and hence issues can arise relating to the volatisation of the $HgCl_2$ catalyst. This is alleviated by including additives, such as cerium, thorium or copper chlorides, or by making operational modifications which limit volatisation.[110]

By the mid-20th century, modifications were made to the process to allow VCM production from acetylene to take place without the need for costly purification of the acetylene. These modifications meant that ethylene and acetylene mixtures obtained from the cracking of napthalene could be directly fed into the reactor, producing a mixture of VCM and EDC, making the process more efficient by eliminating the need for separate hydrochlorination and chlorination steps. The EDC produced would then be cracked to produce VCM and HCl, ç which could be recycled and returned to the input gas feed. A process developed by Solvay achieved this by specifying very particular conditions, detailing a precise range of successful feed compositions, temperatures, and catalyst composition.[115] A slightly later method employed a technique whereby free radical acetylene precursors were formed, by either thermal or catalytic cracking, from a wide range of hydrocarbons at high temperatures, eliminating the need to separate appropriate fractions of pure hydrocarbons. Additionally, it was noted that it is much easier to separate the vinyl chloride product from the unreacted hydrocarbon mixture, than to separate the hydrocarbons before hydrochlorination. The free radicals would then be quickly quenched with either Cl_2 or HCl, yielding VCM.[116]

Due to the use of mercury in the aforementioned process, there has been considerable attention placed on finding less toxic alternatives, and recent international agreements have committed to the phasing out of mercury-

1.4. VINYL CHLORIDE 35

based substances in industry.[117] Academic studies have found that some carbon or silica supported metal chlorides are highly active as catalysts for acetylene hydrochlorination, and in particular it was discovered that gold chlorides are especially active.[118,119] Recent work shows that the remarkable activity is related to the stability of the intermediate formed between the metal and acetylene, and moreover that the reaction is highly selective towards the desired VCM product.[120,121] Hence, these catalysts offer a potentially viable alternative to the mercury based catalysts currently in use, being both active and environmentally acceptable.

VCM Production from EDC

As mentioned in the previous paragraph, VCM can be obtained from EDC by dehydrochlorination. In the liquid phase, this can be performed by treatment with an alkali, but this is undesirable as chlorine is incorporated into a salt, rather than a more useful substance which allows for facile recovery of the valuable chlorine. In the gas phase, however, the process is more industrially relevant, and can be performed either thermally or catalytically, with the former being more widely employed. The non-catalytic reaction occurs via a free radical mechanism according to the following equations:

$$CH_2ClCH_2Cl \rightarrow CH_2ClCH_2 \cdot + Cl\cdot$$

$$CH_2ClCH_2Cl + Cl\cdot \rightarrow CH_2ClCHCl \cdot + HCl$$

$$CH_2ClCHCl\cdot \rightarrow CH_2CHCl + Cl\cdot$$
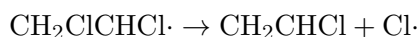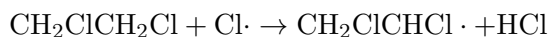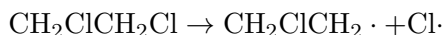
Hence, in this process, Cl· takes the role of the propagator, and consequently Cl_2 is often added to the input gas feed as a promotor. As is often the case with free radical type processes, impurities resulting from the various different combinations of radical species are present.[122] The catalytic method, on the other hand, shows better selectivity towards VCM, primarily due to the lower temperatures involved (200-400 ℃, compared to 400-650 ℃for the non-catalytic method). Typical catalysts include doped activated carbon materials, as well as catalysts based on silicates, alumina and zeolites.[104] Whilst the catalytic method shows better selectivity than the non-catalytic method, EDC conversion rates are similar, and the additional cost associated with the catalytic method provided an economic factor in favour of the non-catalytic method, which has been extensively optimised and is the favoured method in industry.

VCM Production from Ethylene

Whilst VCM can be obtained indirectly from ethylene, namely first by chlorination to EDC, followed by dehydrochlorination to VCM, given the inefficiencies inherent in this process, there is significant momentum towards the development of methods which allow for direct conversion of ethylene to VCM. Whilst the original copper chloride based Deacon catalyst was short-lived as a means of producing Cl_2, in the mid 20th century similar catalysts were applied to ethylene oxychlorination, obtaining EDC as the primary product, which can then be converted to VCM by the means already described. $CuCl_2$-based catalysts for ethylene oxychlorination are typically supported on alumina, and many various additives and promotors are included to optimise stability and performance.[123] Common additives include alkali metal chlorides, which are intended to promote catalyst stability, for example.[124] Stability of these catalysts has long been a major issue; whilst selectivity towards EDC is very good (around 99%), serious issues with catalyst volatilisation hamper performance, as the active phase is readily lost to the gas phase.[125]
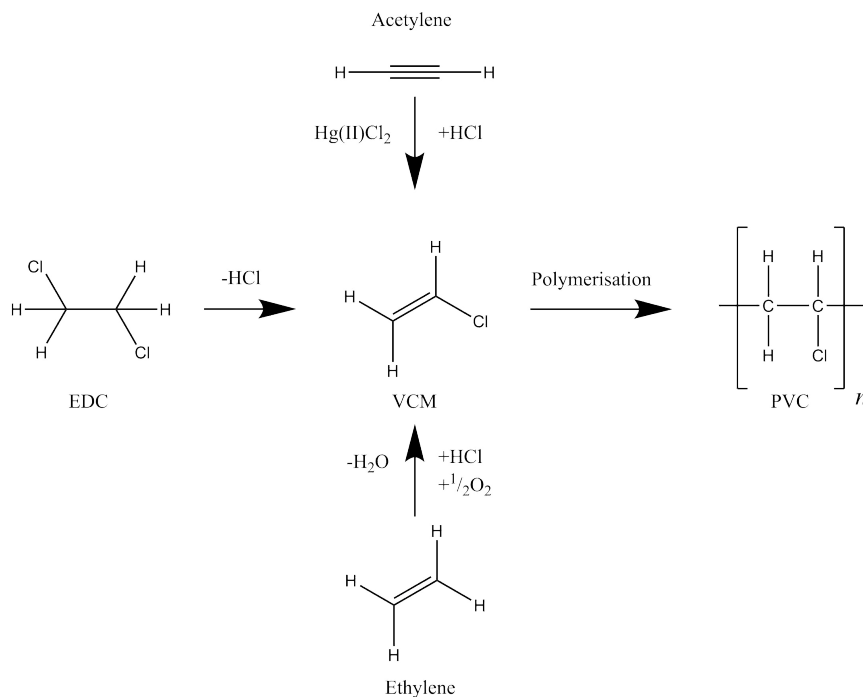
Figure 1.6: Production of VCM from ethylene, acetylene and EDC, and subsequent polymerisation of VCM to PVC.

1.4. VINYL CHLORIDE 37

Various experimental studies have attempted to understand the relationship between the composition and structure of $CuCl_2$-based catalysts, and their activity, selectivity and stability. In industry, the $CuCl_2$ active phase is typically supported on alumina. Whilst the alumina itself plays no role in catalytic activity,[126] it was observed that impregnation of the $CuCl_2$ into the alumina support, with solubility studies showing the presence of two distinct Cu-containing phases, the active $CuCl_2$ phase, as well as a surface copper aluminate,[127–129] with EPR studies suggesting the occupation of surface octahedral vacancies in the alumina by Cu.[130–132] UV-visible spectroscopy and Extended X-ray Absorption Fine Spectroscopy (EXAFS) studies showed that Cu atoms preferentially occupy these octahedral vacancies, and hence the active $CuCl_2$ phase was only evident with higher Cu loading.[133, 134] It was found by later studies that this phenoman explains the beneficial effect of the addition of La to the catalyst, a common practice in industry; La occupies the octahedral surface vacancies in the alumina more efficiently than Cu, thus increasing the fraction of Cu present in the active $CuCl_2$ phase, and improving catalyst performance.[124, 135] Later investigations including X-ray diffraction studies also found whilst that the active $CuCl_2$ phase has a tendancy to degrade to the crystallineparatacamite, $Cu_2(OH)_3Cl$, at room temperature (in contrast to the highly stable) surface aluminate, the active $CuCl_2$ phase is rapidly recovered from paratacamite under heating, hence it was confirmed that $CuCl_2$ and the surface aluminate are the only Cu-containing phases under typical Deacon conditions.[136, 137] Experimental investigations including further EPR and EXAFS studies into the mechanism of ethylene oxychlorination over traditional Deacon catalysts found that exposure of the catalyst to ethylene results in the formation of EDC, obtained from the $CuCl_2$ phase, and the appearance of a reduced $Cu(I)Cl$ phase, with comparative IR spectroscopy studies of both adsorbed CO and NO being used to identify the presence of the two Cu oxidation states and investigate the interplay between them.[138–140] The same spectroscopic techniques were used to investigate the precise mechanism of the regeratation of the active $CuCl_2$ after the reduced phase is exposed to the other reactants, O_2 and HCl; expose to oxygen results in the formation of an oxychloride of composition Cu_2OCl_2, recovering the Cu(II) oxidation state, whilst subsequent exposure to HCl results in the formation of the original $CuCl_2$, accompanied by the evolution of water.[141] Hence, the following reaction scheme was proposed:

$$2CuCl_2 + C_2H_4 \rightarrow C_2H_4Cl_2 + 2CuCl$$

$$2CuCl + \frac{1}{2}O_2 \rightarrow Cu_2OCl_2$$

$$Cu_2OCl_2 + 2HCl \rightarrow 2CuCl_2 + H_2O$$
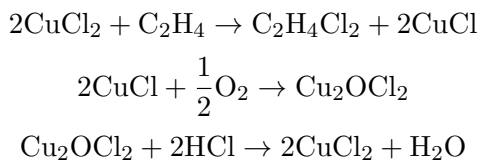
With this reaction scheme established, in situ catalytic tests with all of the reactants present were performed, tracking the oxidation state of the Cu through the reaction. These studies suggested that re-oxidation of Cu is the rate determining step, with competition between the adsorption of HCl and O_2 being responsible for slowing the rate of reoxidation.[135,142] Further investigations identified the role of K and Cs dopants frequently used in industrial catalysts as being responsible for improving the rate of reoxidation of Cu, due to the formation of mixed metal chlorides, thus improving catalytic activity.[143,144] Further experimental studies show for La and K co-doped $CuCl_2$ catalysts, in addition to both dopants acting in conjunction to improve activity, co-doping also enhances selectivity. It was found that La, which can act as a Lewis acidic site in its own right, increases the extent of dehydrochlorination, which results in HCl poisoning the surface and masking the Brønsted sites. The presence of K, on the other hand, has the opposite effect, masking the Lewis sites and increasing the number of Brønsted sites. Hence, in the co-doped sample, there is a synergistic effect between the two dopants, with an effective masking of both Lewis and Brønsted acidic sites, hence these catalysts showed better selectivity towards EDC, with reduced selectivity towards other chlorinated products.[145–148]

Given the success of the RuO_2 as Deacon catalyst, it is also reasonable to suggest that it may find utility as an ethylene oxychlorination catalyst, much in the same manner as traditional $CuCl_2$-based Deacon have been successfully repurposed for this reaction. Under ethylene oxychlorination conditions, there are three components of the input feed gas: C_2H_4, O_2 and HCl. Aside from the desired oxychlorination processes, it is also feasible that Deacon-style HCl oxidation can take place,[75,149] as well as oxidation of C_2H_4 by O_2, to the exclusion of HCl as a reactant. Clearly, this presents as potentially problematic, if oxidation of ethylene prevails over the oxychlorination reaction under reasonable conditions. Previous works have examined the utility of RuO_2 as a catalyst for partial oxidation of ethylene to valuable products,[150,151] such as aldehydes and epoxides, rather than full combustion, providing some insights into this aspect of the catalyst. These two processes compete, and even on successful selective ethylene oxidation catalysts, some degree of combustion is observed. TPD studies were conducted to determine the relationship between temperature and adsorption behaviour.[150] The stoichiometric $RuO_2(110)$ surface was exposed to C_2H_4 and C_2D_4 (i.e. without O_2) in order to investigate the adsorption behaviour of ethylene independently, and the isotopic labelling confirmed that in the absence of oxygen, no combustion can occur, with trace amounts of H_2O and CO_2 being attributed to background H_2 and CO, respectively. Further experiments then included oxygen, by first exposing the $RuO_2(110)$ surface

to 1.0 Langmuir O_2, achieving about 80% coverage. The new O-rich surface was then exposed to 0.6 Langmuir of C_2H_4 or C_2D_4. No desorption of C_2H_4, C_2D_4, or O_2 was observed, indicating complete consumption of these species through combustion, and the studies using C_2D_4 gave signals attributable to D_2O, confirming this notion. Additionally, no epoxide signals were observed, confirming complete combustion. In order to determine the origin of oxygen present in the combustion products, isotopic labelling experiments were performed, exposing the $RuO_2(110)$ surface to $^{18}O_2$. Since all of the oxygen present in the RuO_2 sample is ^{16}O, any ^{16}O detected in the combustion products must come from the lattice, whilst any ^{18}O observed must necessarily originate from O adsorbed on the coordinately unsaturated Ru positions. Hence, the experiments can reveal insights into the reaction mechanism. The tests showed that whilst lattice oxygen can be incorporated into combustion products, ethylene combustion is more extensive at igher $^{18}O_2$ coverages, suggesting that the presence of adsorbed oxygen is necessary to initiate combustion. High Resolution Electron Energy Loss Spectroscopy (HREELS) studies, supporting the TPD, revealed the role of temperature in facilitating C_2H_4 chemisorption; at 85 K, the C-C π bond persists, being relatively unperturbed compared to the gas phase, whilst at 260 K, a signal attributed to a C-C σ bond appears. The HREELS studies also show that ethylene requires the presence of coordinately unsaturated Ru sites at the surface, since pre-treatment of the surface with CO blocked the Ru active sites, preventing C_2H_4 adsorption. Further tests on a RuO_2 surface pre-treated with oxygen revealed the formation of C-O bonds, thus confirming the role of adsorbed O in facilitating the formation of reactive intermediates. Hence, the following mechanism for the initial stages of combustion was proposed; adsorption of ethylene at a vacant surface Ru site between two coadsorbed O atoms occurs, followed by the formation of a C-O bond and the conversion of the ethylene C-C π bond to σ bonding. The resulting oxametallacycle (OMME) intermediate features a Ru-O-C-C-Ru connectivity between two surface Ru sites. Because of the fairly large distance between Ru surface sites, it was proposed that rather than the C atom bonded to Ru in OMME directly interacting with a second O_{cus}, at higher temperatures and after subsequent H abstraction, facilitated by adsorbed O, rupture of the C-C bond takes place, yielding more mobile carbon containing species able to undergo further reaction with O_{cus} to form CO_2. These experimental results demonstrate the strongly oxidative character of RuO_2; not only does the catalyst readily facilitate complete combustion, but additionally no partial oxidation products, such as ethylene epoxide, are observed. It was also shown that coadsorbed O_{cus} is essential for combustion, as whilst O_b can participate in the reaction, being observed in the combustion products in the isotope labelling experiments, O_{cus} is necessary

to initiate the formation of the OMME intermediate, with O_b potentially being incorporated later in the reaction. Clearly, then, any successful RuO_2-based ethylene oxychlorination catalyst would need to consider the presence of adsorbed oxygen and its potentially detrimental role in facilitating complete oxidation.

Although ethylene oxychlorination has the advantage of providing a means of valorising waste HCl, the problem still remains that the main product, using the traditional $CuCl_2$ based catalysts, is EDC rather than VCM, and hence there is interest in developing more efficient methods. Higher temperatures allow for higher VCM selectivity, but also increase the risk of "deep" oxidation processes, whereby ethylene is combusted to carbon oxides and water, which is obviously highly undesirable.[104] Recent work has seen the development of new catalysts based on lanthanide elements, particularly CeO_2.[152] Like RuO_2, CeO_2 is a highly active and stable catalyst for HCl oxidation,[153–155] and hence ceria has attracted attention as a potential candidate catalyst for ethylene oxychlorination. Experimental tests showed highly promising results for CeO_2 as an oxychlorination catalyst; CeO_2 calcined at 1173 K showed remarkable selectivity towards the desirable chlorinated products, accounting for 98% of the total products. The high selectivity was attributed to the inhibition of CO_2 formation on chlorinated surfaces; whilst CeO_2 is active for CO oxidation to CO_2, competitive adsorption between Cl and carbon containing species prevents extensive combustion from taking place.[155] Cl can essentially poison the surface, as far as combustion processes are concerned. Comparing CeO_2 with traditional $CuCl_2$ catalysts, ceria produced a yield of chlorinated products about four times greater than that of $CuCl_2$, and additionally showed considerable stability, with no evidence of formation of volatile metal compounds and subsequent degradation of the catalyst. Another highly notable feature of CeO_2 as an oxychlorination catalyst is its ability to generate VCM at temperatures below that required for EDC cracking. Traditional catalysts tend to favour the formation of EDC, which is then subjected to thermal cracking to obtain EDC at around 773-823 K, whilst VCM was observed to be produced over CeO_2 at a mere 673 K, hence ceria presents as a potentially more efficient alternative to traditional catalysts, which typically favour EDC production. Catalytic tests showed that rather than VCM is formed sequentially from EDC, given the invariance of the EDC:VCM ratio with respect to C_2H_4 residence time. Furthermore, no VCM was produced when EDC alone was fed into the reactor at the lower temperature, indicating that the HCl and O_2 present in the input gas feed under oxychlorination conditions play a key role in modifying the catalyst surface to facilitate VCM formation. Given previous work which suggested that acidic sites on

the catalyst surface are important in the conversion of EDC to VCM,[147] additional experiments examining the temperature programmed desorption of NH_3 were conducted. The experiments showed that whilst NH_3 adsorption on clean CeO_2 is negligible, a large increase was observed when the catalyst had been previously exposed to oxychlorination conditions. Hence, it can be seen that the presence of acidic sites is correlated to VCM formation. It was proposed that CeO_2 employs a bifunctional mechanism to produce VCM, with redox sites on the surface being responsible for EDC production, whilst strongly acidic sites facilitate dehydrochlorination of EDC to VCM.

In light of the promising results for ceria, further studies examined the behaviour of other lanthanide compounds as oxychlorination catalysts, and the results showed that EuOCl is a potentially succesful candidate.[156] In addition to the very limited ethylene combustion activity exhibited by EuOCl, high VCM selectivity was also observed; at 12% C_2H_4 conversion, EuOCl produced VCM as 51% of its product distribution. Comparing with ceria, whilst CeO_2 showed a higher activity with 26% C_2H_4 conversion, only 31% of the product distribution was accounted for by VCM. Further N_2 sorption tests revealed that when accounting for differences in surface area between samples, EuOCl in fact shows a 1.5 times greater C_2H_4 conversion rate compared to CeO_2. Examing the effect of surface area and morphology of catalyst particles, EuOCl samples were produced by precipitation at a variety of calcination temperatures, as this is known to induce morphological variation. The samples showed complete suppression of combustion, with no CO or CO_2 being formed. The most active sample was obtained when EuOCl was calcined at 973 K, and when surface area was accounted for, it was found that this catalyst was a whole order of magnitude more active than CeO_2. Temperature Programmed Reaction (TPR) studies with H_2 were conducted to investigate the reducibility of the surface, and Temperature Programmed Desorption (TPD) studies with NH_3 were conducted to probe the surface for the strongly acidic sites necessary for VCM formation from EDC dehydrochlorination. Comparison of the NH_3 TPD spectra for EuOCl and CeO_2 showed that whilst both catalysts possess surface acidic sites, EuOCl has more strongly acidic sites which are necessary for EDC conversion to VCM, and hence shows the best VCM selectivity over EDC (although a significant proportion of C_2H_4 conversion is accounted for by combustion). Furthermore, the H_2 TPR studies showed that H_2 consumption, resulting from reduction of the catalyst, occurred at a much higher temperature for EuOCl compared to CeO_2, indicating that EuOCl is more resistant to reduction, affording EuOCl a less oxidative character than CeO_2, improving its selectivity towards chlorination by limiting combustion, which requires a more strongly oxidative catalyst. This was supported by tests conducted

under typical reaction conditions, which showed that whilst higher temperatures increased selectivity towards both VCM and the undesirable combustion, for EuOCl, combustion was observed to commence at a much higher temperature, with no combustion being observed up to temperatures as high as 773 K, and even then, no CO_2 and only CO was produced. Additionally, variation in the input feed composition, namely variations in the O_2 and HCl concentrations, had little effect on the catalytic performance of EuOCl, in contrast to CeO_2; this was attributed to the fact that the EuOCl surface is more stable and thus resistant to modification by input feed gases, whereas for CeO_2, higher HCl concentrations and lower O_2 concentrations result in the formation of surface chloride species, reducing the oxidative character of CeO_2 and favouring chlorination over combustion.

These innovative experimental studies support the notion that the composition and surface structure of catalysts under actual reaction conditions is central to determining their activity and selectivity, and the systems investigated provide some promising new avenues for developing more efficient and selective oxychlorination catalysts. However, as of the present, the classical $CuCl_2$-based Deacon catalysts still prevail, and a great deal more progress in investigating the new candidate catalysts will need to be made before industry is prepared to abandon the old catalysts, motivated by economic incentive.

In current industrial practices, VCM production is achieved using an integrated balanced approach. In this method, ethylene oxychlorination, ethylene chlorination and EDC dehydrochlorination reactors are combined, hence providing an operational means of obtaining VCM in large quantities and of high purity. In this method, ethylene is reacted with Cl_2 to produce EDC. The EDC is purified, then directed to a second reactor where dehydrochlorination takes place, producing VCM, which is then subsequently purified and removed as the product. The waste HCl from the EDC cracking is direct to yet another reactor, where ethylene oxychlorination takes place using traditional catalysts, producing EDC, which is treated in the same manner as EDC derived from ethylene chlorination. Obviously, this method consumes Cl_2, rather than relying exclusively on HCl as a chlorine source, hence there is still plenty of room for improvement to develop catalysts which can produce VCM directly by ethylene oxychlorination with HCl.[104]
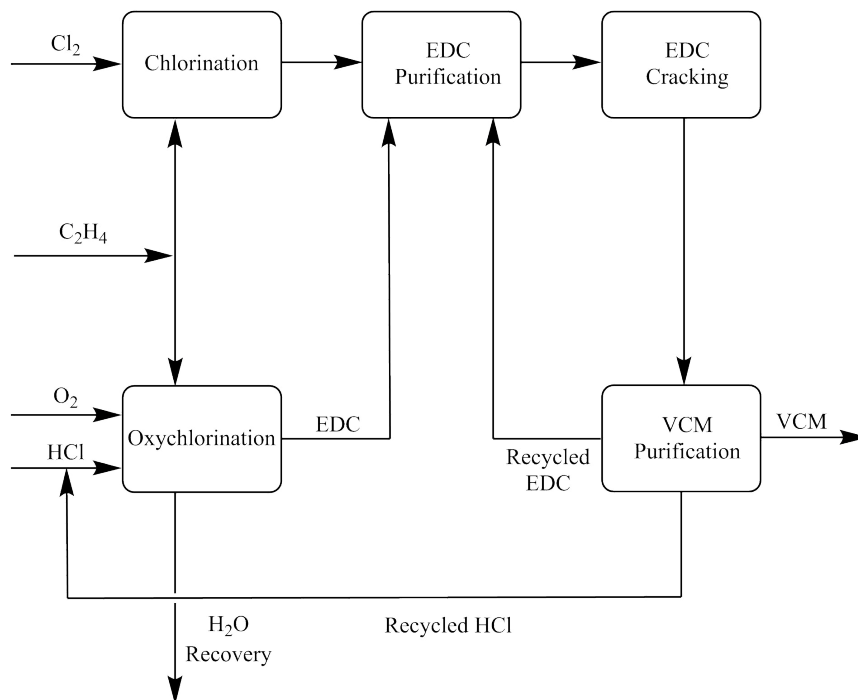
Figure 1.7: Simplified flow diagram depicting the operation of the integrated balanced process for VCM production.

PVC Production

PVC is produced from the polymerisation of VCM. Typically, plants incorporate VCM production from ethylene and VCM polymerisation to PVC, in order to avoid the costly enterprise of transporting VCM, since virtually all VCM produced goes into PVC production. Several different methods exist for the polymerisation of VCM; suspension polymerisation, which accounts for 80% of world PVC production, is the most popular. The two other main techniques are emulsion polymerisation and bulk polymerisation, which account for the remaining 12% and 8% of world PVC production, respectively.[110]

The basic principle of suspension polymerisation is that the reaction takes place within tiny droplets of VCM/demineralised water solution, suspended in a protective colloid granulating agent. These droplets essentially function as minature reactors. Polyvinyl alcohols are commonly used as protective colloids for the suspension medium.[157] A free radical initiator is included in the solution, so that when the reactor is heated, free radicals are formed and polymerisation commences. In practice, two initiators are often used,

usually a small amount of a more active, primary initiator, and a larger quantity of a less active secondary initiator which takes over from the primary initiator as the reaction progresses. Since the polymerisation reaction is highly exothermic, the reaction is controlled by managing the temperature via the reactor cooling jacket. As the reaction proceeds, a gel of PVC suspended in the VCM forms, until either a suffcient quantity of the monomer is consumed, or until a chain terminator is added, causing the reaction to cease. The PVC resin is extracted, and any unreacted VCM is recovered and reused.[110]

Bulk polymerisation is essentially the same as suspension polymerisation, but the process does away with the need for a suspension medium. Whilst grain sizes in suspension polymerisation are largely determined by the qualities of the suspension medium, in bulk polymerisation this is controlled by the operating conditions, i.e. the extent of mechanical agitation. The considerable heat evolved from the polymerisation reaction is removed by the evaporation of VCM and its subsequent condensation on the reactor walls. The main advantage of bulk polymerisation is that no drying stage is required, since residual VCM is absorbed by the porous PVC, and unlike suspension polymerisation, no additional ingredients other than the monomer and initiator are required. Additionally, the reactor design largely eliminates the need for a cooling jacket to control the reaction. However, difficulty in limiting the amount of residual VCM to comply with environmental regulations is a major drawback of bulk polymerisation, and the additional degree of control over polymer properties afforded by suspension polymerisation means that worldwide, bulk polymerisation is much less popular.[158]

Emulsion polymerisation is used to produce colloidal solutions of small PVC particles (0.1-3.0 μm). The particles are mixed with plasticisers to form a stable suspension, ready for use. The process, generally speaking, involves performing the polymerisation in the usual way, using an initiator to start the polymerisation of VCM, but with the addition of a surfactant substance. The surfactant used in emulsion polymerisation prevents the polymer particles from absorbing the plasticiser at room temperature, allowing for specialised applications of the polymer, such as coatings and moulded objects. The plastisol can be spread onto an object, or injected into a mould, and solidified by the application of heat treatment. PVC produced by emulsion polymerisation is import in the coating of fabrics, the manufacture of goods such as floor covering and wallpaper, as well as the production of common household articles.[110]

1.5   Objectives and Overview of the Thesis

As can be seen from the discussion provided in the preceding pages, improvements in industrial processes can be made by developing superior catalysts. In particular, it can be seen that with the growing use of bromine in industrial chemistry as a general means of functionalising unreactive alkanes derived from oil refining, there is demand for an efficient, economical and active catalyst to oxidise waste HBr generated by the functionalisation process, and thus recover the valuable bromine without the need for extensive lists of reactants and the consequent production of waste byproducts. Secondly, whilst catalytic processes exist to valorise waste HCl arising from a plethora of industrial processes, inefficiencies exist in the processes used to produce VCM, which is the main use of the recovered chlorine in the production of PVC. Hence, there is also an industrial demand for catalysts which are capable of selective oxychlorination of ethylene to VCM, utilising the abundant waste HCl, without the excessive production of less desirable chlorinated products, or the total combustion of ethylene.

In this thesis, theoretical investigations are conducted to explain the behaviour of transition metal oxide based materials as catalysts in halogen chemistry, and to investigate potential candidates for new catalysts. Density Functional Theory is applied to gain useful insights into the surface composition of catalysts, with *ab initio* thermodynamics studies providing a qualitative representation of the catalyst composition under typical reaction conditions. Energy changes for various elementary processes taking place on the surfaces are calculated along with corresponding activation energies, allowing for a rationalisation of experimentally observed selectivity. Calculated Density Of States (DOS) plots have also been obtained to provide a link between the observed catalytic behaviour and the electronic structure of the catalyst. The theoretical results, taken in consideration with corresponding experimental studies, reveal the relationships between the activity and selectivity of a catalyst, and its structure and composition.

The structure of the thesis is as follows: the next chapter, Chapter 2, describes the theoretical methods used to obtain the results, and provides an insight into the underlying theoretical considerations. In Chapter 3, ruthenium dioxide and titanium dioxide are considered as catalysts for hydrogen halide oxidation, and theoretical results are used to explain the interplay between their surface composition and their catalytic performance, particularly the extent of surface halogen uptake. This notion is extended in Chapter 4, where purely theoretical studies delve into the impact that dopants have on titanium dioxide as a catalyst for hydrogen halide oxidation, and how these doping phenomena can potentially allow for the rational design of

catalysts, optimised in terms of activity, selectivty and stability for particular reactions and conditions. In Chapter 5, ruthenium dioxide is considered as a catalyst for ethylene oxychlorination. Calculations are performed to gain deeper insights into the interplay between oxychlorination and combustion processes, and the role that surface composition has in affecting the energetics of key elementary processes. Finally, the main conclusions are summarised, and the most salient findings of the investigations detailed.

Chapter 2

Theoretical Approach and Experimental Techniques

The computational tools and methodology applied in this thesis are described herein. Firstly, a description of Density Functional Theory is provided, demonstrating how complex, multi-electron systems can be studied in a computationally expedient manner by the application of a few approximations for equations derived from the Schrödinger equation. Secondly, the practical implementation of computational methods is discussed. Finally, some specific techniques used in the thesis, namely transition state searches and *ab initio* thermodynamics, are detailed.

Since the research presented in the thesis was largely the result of combined theoretical and experimental studies, a brief introduction to the experimental methods is also provided, allowing for a theoretical appreciation of the techniques, and their interpretation in the context of the theoretical results.

2.1 Theoretical Methodology

2.1.1 Introduction

The Schrödinger equation is the cornerstone of all modern quantum chemical methods. Proposed by Erwin Schrödinger in 1926, it may be solved exactly and analytically for only the simplest of systems, i.e. a single-electron system:

$$\hat{H}\psi = E\psi \tag{2.1}$$

for the computational chemist, however, larger multi-electron systems are of primary concern. Hence, it is necessary to build on the Schrödinger equation, using appropriate approximations, in order to be able to study

more complex systems. Density Functional Theory (DFT) is the most popular approach used to investigate such systems, and all of the calculations detailed in this thesis were performed using DFT.

2.1.2   Density Functional Theory

For a system of N electrons, there are $3N$ spacial coordinates and N spin coordinates required in order to fully describe the system. For all but the simplest systems, any attempt to explicitly account for each electron in the wavefunction will be computationally infeasible. In 1964, Pierre Hohenberg and Walter Kohn offered a potentially less labourious method for dealing with larger systems containing a greater number of electrons (i.e. more than 10-20 atoms).[159] The Kohn-Hohenberg theory states that the ground state energy from the Schrödinger equation is a unique functional of the electron density, in the spirit of earlier theories such as those of Thomas,[160] Fermi,[161] and Dirac.[162] Consequently, observables are uniquely determined by the ground state electron density. Hence, the the dimensionality of the system is vastly reduced to one consisting of only three dimensions, representing a considerable simplification. Hence, DFT offers a computationally accessible way to determine the ground state properties of a system.

2.1.3   Formalism

The Schrödinger equation can be expressed as a Hamiltonian consisting of terms for the kinetic and potential energies of the system. Since the nuclei are much more massive than the electrons and, relative to the electrons, move very slowly, it is convenient to consider the nuclei to be fixed, with the electrons moving in the field defined by the nuclei. This approximation, known as the Born-Oppenheimer approximation, allows one to write the Hamiltonian in terms of the electronic kinetic energy, $\hat{T}$, the attractive potential defined by electron-nucleus interactions, $\hat{V}$, and the repulsive electron-electron interactions, $\hat{U}$:

$$\hat{H}\psi = \hat{T}\psi + \hat{V}\psi + \hat{U}\psi = E\psi \tag{2.2}$$

For a multi-electron system, the wavefunction, ψ, can be expressed as a function of the coordinates for each electron, i.e. $\psi(\mathbf{r}_1...\mathbf{r}_N)$, permitting one to now write the Hamiltonian as a sum over all of the electronic coordinates:

$$\hat{H}\psi = [-\frac{\hbar^2}{2m}\sum_{i=0}^{N}\nabla_i^2 + \sum_{i=0}^{N}V(\mathbf{r}_i) + \sum_{i=0}^{N}\sum_{i<j}U(\mathbf{r}_i, \mathbf{r}_j)]\psi = E\psi \tag{2.3}$$

In the above form, the equation is insoluble, since the wavefunction, $\psi(\mathbf{r}_1...\mathbf{r}_N)$, is unknown. Applying the Kohn-Hohenberg theory, however,

2.1. THEORETICAL METHODOLOGY 49

allows one to determine the single-particle wavefunctions from the electron density:

$$n(\mathbf{r}) = N \int d^3\mathbf{r}_2 \int d^3\mathbf{r}_3 \; ... \int d^3\mathbf{r}_N \psi^*(\mathbf{r}, \mathbf{r}_2, ..., \mathbf{r}_N)\psi(\mathbf{r}, \mathbf{r}_2, ..., \mathbf{r}_N) \quad (2.4)$$

That is to say, if the ground state electron density is known, the ground state wavefunctions may be constructed according to the reverse of the above equation. More formally, the first Kohn-Hohenberg theorem states that the ground state wavefunction is a unique functional of the ground state electron density:

$$\psi_0 = \psi_0[n_0(\mathbf{r})] \quad (2.5)$$

As such, all other ground state observables are also unique functionals of the ground state electron density:

$$\langle \hat{O} \rangle [n_0(\mathbf{r})] = \langle \psi[n_0(\mathbf{r})] | \hat{O} | \psi[n_0(\mathbf{r})] \rangle \quad (2.6)$$

Hence, the ground state energy is given by:

$$E_0 = E[n_0(\mathbf{r})] = \langle \psi[n_0(\mathbf{r})] | \hat{T} + \hat{V} + \hat{U} | \psi[n_0(\mathbf{r})] \rangle \quad (2.7)$$

For a given external potential, $v(\mathbf{r})$, (i.e. the attractive potential defined by the nuclear coordinates), one can write the more explicit expression:

$$E[n(\mathbf{r})] = T[n(\mathbf{r})] + U[n(\mathbf{r})] + \int v(\mathbf{r})n(\mathbf{r})d\mathbf{r} \quad (2.8)$$

The electron-electron interaction term, $U[n(\mathbf{r})]$, can be written as a sum of the electrostatic Coulomb term (known as Hartree repulsion) and the non-classical exchange-correlation term, $E_{xc}[n(\mathbf{r})]$:

$$E[n(\mathbf{r})] = T[n(\mathbf{r})] + \frac{1}{2} \iint \frac{n(\mathbf{r})v(\mathbf{r})}{|\mathbf{r} - \mathbf{r}'|} + \int v(\mathbf{r})n(\mathbf{r})d\mathbf{r} + E_{xc}[n(\mathbf{r})] \quad (2.9)$$

According to the Kohn-Sham theory,[163] the kinetic energy term, $T_s[n]$, can be expressed simply as the sum of the kinetic energies for each electron, reintroducing single-electron wavefunctions:

$$T_s[n] = -\frac{\hbar^2}{2m} \sum_{i=1}^{N} \int \phi_i^*(\mathbf{r})\nabla^2\phi_i(\mathbf{r})d\mathbf{r} \quad (2.10)$$

By re-writing the electrostatic Coulomb term and exchange-correlation term as potentials (i.e. as derivatives with respect to the electron density), they

may be collected together with the external potential, $v(\mathbf{r})$, as an "effective potential" that each individual electron experiences, with inter-particle interactions included in the effective potential as a mean field:

$$v_{eff}(\mathbf{r}) = v(\mathbf{r}) + \int \frac{n(\mathbf{r}')}{|\mathbf{r} - \mathbf{r}'|}d\mathbf{r}' + \frac{\partial E_{xc}[n(\mathbf{r})]}{\partial n(\mathbf{r})} \tag{2.11}$$

According to the Variational principle, the correct ground state wavefunction yields the minimal energy. Since the ground state wavefunction is a unique functional of the ground state electron density, it follows then that the correct density $n(\mathbf{r})$ will minimise the energy, in accordance with the second Kohn-Hohenberg theorem.

$$E_0 \leq E[n] \tag{2.12}$$

The expression for the energy can be minimised by means of Lagrangian multipliers to ensure the condition of othonormality of the single electron wavefunctions and a constant number of electrons, resulting in the Kohn-Sham equation:

$$[-\frac{\hbar^2}{2m}\nabla^2 + v_{eff}(\mathbf{r})]\phi_i(\mathbf{r}) = \epsilon_i\phi_i(\mathbf{r}) \tag{2.13}$$

By its very nature, an iterative approach is required to solve the Kohn-Sham equations. The terms for the electrostatic and exchange-correlation potentials require the electron density, $n(\mathbf{r})$, which can be determined from the Kohn-Sham orbitals $\phi_i(\mathbf{r})$, but of course this requires the electron density in the first place in order to evaluate $v_{eff}(\mathbf{r})$. Hence, in practice, a trial electron density is determined (typically based on an estimate of the atomic orbitals), which is used to evaluate the effective potential and obtain the Kohn-Sham orbitals. A new density may then be constructed from these orbitals, and the process is repeated as necessary until the ground state energy is sufficiently well-converged. When self-consistency to within an acceptable tolerance is achieved, one can be sure that wavefunctions obtained are accurate, from the variational principle. Therefore, the electron density obtained can be used to determine ground state observables in line with the first Hohenberg-Kohn theorem.

2.1.4 Approximations

The Kohn-Sham approach relies on separating terms which can be defined exactly from those that cannot. All of the exact terms are clearly defined, and all of the undefined non-classical terms, as well as various corrections, are collected in the exchange-correlation potential,$v_{xc} = \frac{\partial E_{xc}[n(\mathbf{r})]}{\partial n(\mathbf{r})}$, which in practice must be approximated in order to perform DFT calculations.

2.1. THEORETICAL METHODOLOGY 51

Exchange-Correlation Functionals

A wide variety of exchange-correlation functionals exist, with some being derived as limiting approximations in accordance with physical laws, and others relying on empirical fitting to experimental studies. In the simplified case of the uniform electron gas (i.e. $n(\mathbf{r}) = constant$), the exchange-correctional functional can be determined exactly. This can be extrapolated for a non-uniform electron gas by simply assuming that a non-uniform electron gas has the same exchange-correlation energy at a point r as a uniform electron gas which has the same density at point r. This is known as the Local Density Approximation:

$$E_{xc}^{LDA}[n(\mathbf{r})] = \int n(\mathbf{r})\varepsilon_{xc}^{hom}[n(\mathbf{r})]d\mathbf{r} \tag{2.14}$$

The exchange-correlation energy can be decomposed into separate terms for exchange and correlation energies:

$$E_{xc} = E_x + E_c \tag{2.15}$$

For LDA, the exchange energy term can be written exactly as determined from the Thomas-Fermi model:

$$E_{xc}^{LDA}[n(\mathbf{r})] = -\frac{3q^2}{4}(\frac{3}{\pi})^{\frac{1}{3}} \int n(\mathbf{r})^{\frac{4}{3}}d^3\mathbf{r} \tag{2.16}$$

The correlation energy term, however, must be approximated, typically derived by applying perturbation theory or resorting to Quantum Monte Carlo simulations. A popular implementation of the LDA is that of Perdew and Zunger (PZ81).[164]

DFT calculations employing the LDA can often be remarkably accurate in determining the atomic structure, elastic and vibrational poperties of many materials. This, however, can often be attributed to error cancellation. Furthermore, whilst the electron-correlation hole is very poorly estimated with the LDA, its spherical average and general properties which influence v_{xc} are broadly reproduced. The approximation has some serious limitations; often reaction energies for chemical processes and activation barriers are poorly reproduced, leading to a tendancy to overbind molecules on solids. Such limitations are hardly surprising, given its severe nature. Clearly, the inhomogeneous nature of an actual electron gas means that the LDA works from a highly simplified physical perspective. Whilst LDA can be acceptable for systems where the electron density is high and slowly varying, for most systems this is not applicable. An improved approach is the Generalised

Gradient Approximation (GGA), which whilst still semi-local, accounts for both the density at a given point r, and the density gradient at that point:

$$E_{xc}^{GGA}[n(\mathbf{r})] = \int n(\mathbf{r})\varepsilon_{xc}^{GGA}[n(\mathbf{r})\nabla n(\mathbf{r})]d\mathbf{r} \qquad (2.17)$$

Unlike LDA, there is no general form of the functional and hence there are many different schemes which allow the gradient to be included. As such, there are a wide variety of GGA functionals available. GGA functionals can cope better with systems that show greater variations in the electron density, as this information is accounted for in the gradient. Two popular GGA functionals are the Perdew-Wang (PW91)[165, 166] and the Perdew-Burke-Ernzerhof (PBE)[167] functionals. The PBE functional is used throughout this thesis, as it affords a good reproduction of electronic and geometric properties, is easily transferable between chemically different systems and is not overly demanding of computational resources.

More complex functionals also exist. Meta-GGA functionals, for example, include the kinetic energy in addition to the electron density and the electron density gradient. An example is the TPSS[168] functional. Other functionals, such as hybrid functionals, move away from a wholly *ab initio* approach and resort to empirical compromises to obtain the desired behavior. The popular B3LYP functional is an example. Whilst meta-GGA functionals can only offer a slight improvement on GGA functionals, they can be more computationally demanding. Hybrid functionals can also be very accurate, but owing to their semi-empirical nature, their behavior can be unpredictable at times, and they show limited transferability. *Ab initio* functionals such as LDA and GGA may be less accurate under some circumstances, however they are computationally efficient, their behavior is predictable for a wide range of systems, and errors are usually systematic in nature. Furthermore, more advanced functionals, such as the hybrids, are usually only necessary for systems with complex, long-range exchange and correlation effects, and hence are not usually needed for simple metallic and modified semiconducting system which are the primary focus of this thesis. Hence, under these circumstances, GGA functionals can be considered as a fair compromise between accuracy and reliability.

DFT+U Methods

For many systems, an appropriate choice of functional can be used to obtain accurate results.[169] For some systems, however, some important physical aspects are difficult to reproduce. An example of this is the band gap of semiconducting materials, which are routinely underestimated by LDA and GGA functionals. This originates from the self-interaction error, a spurious

interaction arising from the fact that each electron experiences the effect of the mean field to which it has itself contributed. This has the effect of elevating the energy of occupied bands, due to this unphysical repulsion of an electron against itself, hence band gaps for semiconductors are typically diminished compared to what experimental studies suggest. In regular LDA and GGA, there is no term included to account for this self-interaction energy. A popular solution involves adding a correction to cancel the self-interaction error:[170,171]

$$E_{DFT+U} = E_{DFT} + E_U - E_{dc} \tag{2.18}$$

Where E_U is the correction term and E_{dc} is a term to correct for double counting, since some contributions will have already been accounted for in the E_{DFT} term. The correction consists of a Hubbard-like U term for the on-site Coulomb interaction and a correction for the exchange, J. The method of Dudarev[172] uses spherically averaged terms for U and J as a simplification:

$$E_{DFT+U} = E_{DFT} + \frac{(U-J)}{2} \sum_{\sigma} [(\sum_{m_1} n_{m_1,m_2}^{\sigma}) - (\sum_{m_1,m_2} \hat{n}_{m_1,m_2}^{\sigma} \hat{n}_{m_2,m_1}^{\sigma})] \tag{2.19}$$

Where σ refers to the orbital spin, and m refers to the orbital index. Since J is often orders of magnitude smaller than U, the two values are often combined as $U_{eff} = U - J$, defining an "effective" Hubbard parameter account for both, for simplicity. Hence, this method allows for a simple parameter which can be included to account for the problems posed by the self-interaction error, and thus obtain more physically insightful results. A PBE+U approach is used in chapters 3 and 4 for the doped $TiO_2(110)$-based systems, in order to better account for correlation effects associated with filling of the normally vacant Ti 3d conduction band induced by dopant atoms.

DFT+D Methods

Many LDA and GGA exchange-correlation functionals also fail to describe van der Waals (vdW) forces and dispersions, since they fail to accurately describe long-range electron correlations, owing to their somewhat localised approach. Since vdW forces can have a major impact on structure and stability, for some systems with highly polarisable atoms, it is necessary to account for them with a correction term. In much the same way as DFT+U is applied, DFT+D methods include a dispersion correction, $E_{disp.}$ which is added to the DFT energy obtained using an uncorrected LDA or GGA functional:

$$E_{DFT+D} = E_{DFT} + E_{disp.} \tag{2.20}$$

The scheme of Grimme[173] uses the following expression as an empirical correction to the DFT energy:

$$E_{disp.} = -s_6 \sum_{i=1}^{M-1} \sum_{j=i+1}^{M} \frac{C_6^{ij}}{R_{ij}^6} f_{dmp.} R_{ij} \tag{2.21}$$

Where s_6 is a scaling factor based on the functional used, M is the number of atoms, C_6^{ij} is the dispersion coefficients between atoms i and j, and R_{ij} is the corresponding interatomic distance. The damping function $f_{dmp.}$ is used to alleviate unphysical interactions at short interatomic distance, having the following form:

$$f_{dmp.} = \frac{1}{1 + e^{-d(\frac{R_{ij}}{R_r})-1}} \tag{2.22}$$

Where R_r is the sum of the vdW radii of the atoms i and j, and d is a scaling factor. The empirical nature of this correction is a clear limitation; dispersion coefficients are independent of chemical environment, and are therefore not formally applicable to some situations. For systems where dispersion forces can play a significant role, however, inaccuracies in the correction are a compromise for being able to account for the dispersions in some approximate manner. A PBE+D approach is used in chapter 3 for the calculations concerning the halogen uptake of $RuO_2(110)$, in order to better account for dispersion effects associated with the higher polarisability of the introduced halogen atoms.

2.1.5   Implementation

Basis Sets

When performing DFT calculations in practice, it is necessary to approximate the Kohn-Sham orbitals with a set of basis functions. An unknown orbital can be described numerically as a set of known basis functions. Higher basis precision results in higher accuracy, at the cost of greater computational expense. Generally, there are two type of basis set used, localised basis sets, and plane-wave basis sets. In this thesis, all calculations have been performed using a code which employs only only plane-wave basis sets.

Plane-wave basis sets are used when dealing with extended, periodic systems, such as bulk solids and surfaces. Plane-wave basis functions are periodic, and thus they are able to reflect the translational symmetry typical of such systems. Hence, it is possible to model infinite systems using plane-wave basis sets. According to Bloch's theorem,[174] the wavefunction for an electron can be expressed as a plane-wave multiplied by a function reflecting

the periodicity of the lattice of interest:

$$\psi_{\mathbf{k}}(\mathbf{r}) = e^{i\mathbf{k}\cdot\mathbf{r}}u_{\mathbf{k}}(\mathbf{r}) \tag{2.23}$$

where $\mathbf{k}$ is the wave-vector, whose values are defined by the unit cell, and $\mathbf{r}$ is a position vector. Expanding the periodic function $u_{\mathbf{k}}(\mathbf{r})$ in terms of plane-waves of the reciprocal lattice, where $\mathbf{G}$ is the sum of the reciprocal lattice vectors:

$$u_{\mathbf{k}}(\mathbf{r}) = \sum_{G} c_{\mathbf{G}}e^{i(\mathbf{G}\cdot\mathbf{r})} \tag{2.24}$$

allows the whole wavefunction to be expressed as a sum of plane-waves:

$$\psi_i(\mathbf{r}) = \sum_{G} c_{i,\mathbf{k}+\mathbf{G}}e^{i(\mathbf{k}+\mathbf{G})\mathbf{r}} \tag{2.25}$$

To completely and accurately describe the wavefunction would require an infinite number of plane waves, which would render the calculation computationally intractable. Hence, in practice, a plane-wave cut-off energy is defined, where the sum includes only plane waves with a kinetic energy below the cut-off value (i.e. the summation only goes up to a maximum, pre-defined value of $\mathbf{G}$). In this context, then, a high plane-wave cut-off energy corresponds to high basis precision.

Pseudopotentials

The inclusion of high energy plane-waves the basis set allows one to describe short-length oscillations in the wavefunction, but also contributes significantly to the computational cost. Such oscillations are characteristic of tightly bound core electrons, close to the nucleus. Since these electrons often have a limited influence on chemical bonding and the physical properties of a material, it is computationally expedient to approximate the wavefunction within a certain distance from the nucleus with simple, analytical functions (e.g. polynomials, spherical Bessel functions), rather than with plane-waves.

Pseudopotentials replace the core region of the wavefunction with a smooth function which very roughly approximates the high frequency oscillations of the wavefunction. The core region is defined by a core radius; at this radius, the first and second derivatives of the pseudo-wavefunction must be the same as those of the all-electron wavefunction to ensure continuity. Outside of the core radius, the pseudo-wavefunction and the all-electron wavefunction are identical; this conditions is referred to as norm-conservation. Thus, the potential experienced by the valence electrons is approximated by the pseudopotential, which essentially combines the potential defined by the atomic
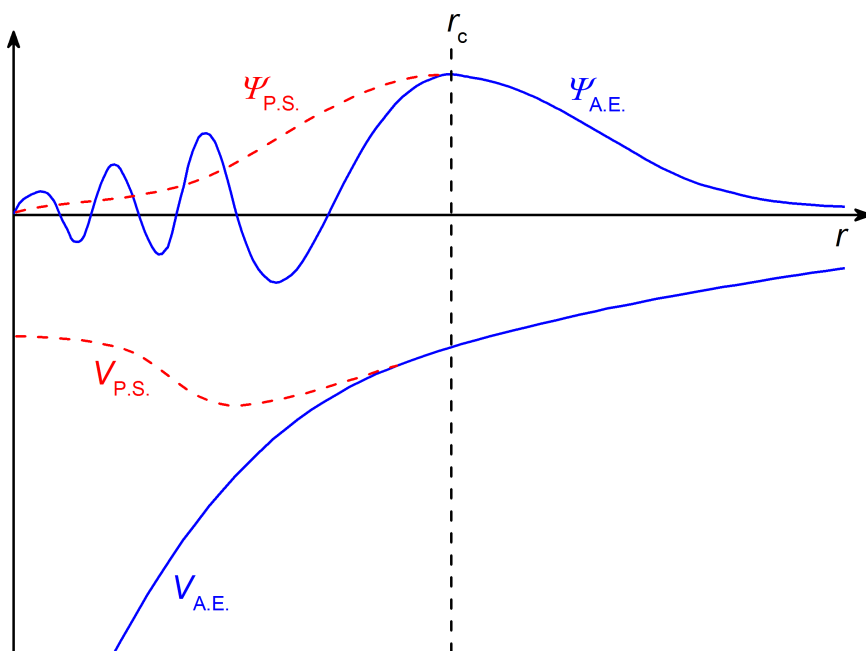
Figure 2.1: Schematic comparison of the all-electron radial wavefunction ($\psi_{A.E.}$) and its pseudo-wavefunction ($\psi_{P.S.}$) with their corresponding potentials. r_c defines the core radius; for $r > r_c$, the A.E. and P.S. wavefunction are identical.

nuclei with the effect of the core electrons.

There are two main types of pseudopotential used in computational chemistry: ultrasoft (US-PP)[175] and Projector Augmented Wave (PAW)[176] pseudopotentials. The popularity of these pseudopotentials can be attributed to the fact that they address the problems presented by atoms with strongly localised orbitals, particularly first-row transition metals. These elements either require a high plane-wave cut-off, in order to account for the rapid oscillations in the wavefunction closer to the nucleus, hampering computational efficiency, or alternatively they require an extension of the core radius, which limits transferability of the pseudopotental. Ultrasoft pseudopotentials alleviate this problem by relaxing the condition of norm-conservation; whilst this approach has been highly successful, it has the disadvantage of requiring several additional parameters to be specified, including several cut-off radii and the introduction of augmentation charges to compensate for the relaxation of norm-conservation, thus the use of ultrasoft pseudopotentials still requires extensive testing to ensure transferability. PAW pseudopotentials, on the other hand, avoid relaxing the condition of norm-conservation, and instead the pseudopotential is constructed in a consistent manner from the

2.1.   THEORETICAL METHODOLOGY   57

all-electron wavefunction, allowing for superior transferability.[177] Hence, in this thesis, PAW pseudopotentials are used throughout.

The principle of the PAW method is that within the augmention region (i.e. the parts of the valence wavefunctions within the core radius, the region of the wavefunction to be pseudised), a linear transformation maps the all-electron wavefunction, onto a smooth function, the pseudo-wavefunction. The core orbitals are considered to be frozen. Mathematically, a linear transformation T is defined which maps the pseudo-wavefunction, $\tilde{\psi}$, onto the actual wavefunction, ψ, for the valence states:

$$|\psi\rangle = T|\tilde{\psi}\rangle \tag{2.26}$$

The actual and pseudo-wavefunction are considered to be a sum of partial waves:

$$|\psi\rangle = \sum_i |\phi_i\rangle c_i \tag{2.27}$$

$$|\tilde{\psi}\rangle = \sum_i |\tilde{\phi}_i\rangle c_i \tag{2.28}$$

Within the augmentation region, Ω_R, where the transformation takes place, the operator T_R maps the actual and pseudo partial waves:

$$|\phi_{iR}\rangle = T_R|\tilde{\phi}_{iR}\rangle \tag{2.29}$$

outside the augmentation region, however, the all-electron and pseudo wavefunctions are identical:

$$|\phi_i\rangle = |\tilde{\phi}_i\rangle \tag{2.30}$$

hence the following expression for the transformation:

$$T = 1 + \sum_R T_R \tag{2.31}$$

Since the operator T must be linear, it follows that the coefficients of the partial waves, c_i, must themselves be linear functions of $\tilde{\psi}$:

$$c_i = \langle \tilde{p}_i|\tilde{\psi}\rangle \tag{2.32}$$

where $\tilde{p}_i$ is a projector function. One can then write the following expression for $|\psi\rangle$ by combining equations (2.27), (2.28) and (2.31):

$$|\psi\rangle = |\tilde{\psi}\rangle + \sum_i |\phi_i\rangle\langle \tilde{p}_i|\tilde{\psi}\rangle - \sum_i |\tilde{\phi}_i\rangle\langle \tilde{p}_i|\tilde{\psi}\rangle \tag{2.33}$$

Hence one can write the transformation T as:

$$T = 1 + \sum_i (|\phi_i\rangle - |\tilde{\phi}_i\rangle)\langle \tilde{p}_i| \tag{2.34}$$

The transformation can be applied completely analogously to generate operators which yield expectation values for observations commensurate with the all-electron solution when applied to the pseudo wavefunction:

$$\tilde{O} = \hat{O} + \sum_{i,j} |\tilde{p}_i\rangle(\langle\phi_i|\hat{O}|\phi_j\rangle - \langle\tilde{\phi}_i|\hat{O}|\tilde{\phi}_j\rangle)\langle\tilde{p}_j| \qquad (2.35)$$

Hence, the PAW method provides a simple means of constructing pseudo-wavefunctions which can greatly increase computational efficiency and be used just as one would use the all-electron wavefunction to calculate observables.

Sampling of the Brillouin Zone

As a consequence of using Bloch's theorem to expand the wavefunction as a set of plane-waves, it is possible to replace integrals performed over an infinite system in real space with integrals performed over a finite system in reciprocal space. This finite reciprocal space of particular interest is often referred to as the Brillouin zone. Numerical integration of a function is performed by evaluating the function at a set of discrete points and summing the values, with appropriate weighting. Given the imperative for computational efficiency when performing DFT calculations, methods have been developed to ensure that one can optimise the number, weighting and distribution of these integration points in the Brillouin zone (known as k-points).

The Monkhorst-Pack scheme[178] is one of the most popular methods for achieving efficient k-point sampling of the Brillouin zone, and is the scheme used throughout this thesis. The general principle of the Monkhorst-Pack scheme is that k-points should be equally spaced throughout the Brillouin zone. A higher density of k-points only improves accuracy up to a limit, since integrals evaluated at k-points close in the Brillouin zone are almost the same, hence only a finite number of k-points are needed to achieve good accuracy.

2.1.6   Transition State Searches

Identifying transition states and calculating activation barriers for processes is often an important task for the computational chemist. Transition State Theory relates the activation barrier to the rate of a process, hence providing some kinetic insights into the process. A minimum energy path (MEP) exists between two local minima on a potential energy surface (PES); the potential energy maximum along the MEP corresponds to a saddle point on the PES, i.e. a transition state. Several methods exist to determine the

MEP between two local minima, and thus identify the transition state for the process.

Nudged Elastic Band (NEB) Method

The Nudged Elastic Band method[179–181] is suitable where the initial and final states associated with the process are known. By interpolating between these two points, a series of images is generated, representing a sequence of intermediate structures that link their geometries. Each image is optimised simultaneously in an attempt to trace out the MEP. Spring forces between each of the images ensure that the images remain equally spaced along the MEP (like an elastic band, hence the name of the method), rather than allowing them to "slide down" the PES towards the local minima of the initial or final states. Hence, the image which represents a maximum along the MEP should be closest to the transition state, if the NEB calculation was successful.

For each image, the path direction is defined by the vector along the line defined by the two adjacent images. Mathematically, for image i, the path direction vector, $\boldsymbol{\tau}_i$, is given by:

$$\boldsymbol{\tau}_i = \mathbf{r}_{i+1} - \mathbf{r}_{i-1} \tag{2.36}$$

The true force on the image can then be determined as the component perpendicular to the path direction:

$$\nabla E(\mathbf{r}_i)^{\perp} = \nabla E(\mathbf{r}_i) - (\nabla E(\mathbf{r}_i) \cdot \boldsymbol{\tau}_i) \tag{2.37}$$

Of course, the spring forces which keep the images evenly distributed along the MEP also contribute a component perpendicular to the path direction. Hence, in the NEB method, the perpendicular component of the spring force is projected out. We can define the spring component parallel to the path direction:

$$\mathbf{F}_{i(spring)}^{\parallel} = (\mathbf{F}_{i(spring)} \cdot \boldsymbol{\tau}_i) = k(|\mathbf{r}_{i+1} - \mathbf{r}_i| - |\mathbf{r}_i - \mathbf{r}_{i-1}|)\boldsymbol{\tau}_i \tag{2.38}$$

where k refers to the spring constant. Hence, combining these expressions for the true force perpendicular to the path and the spring force parallel to the path gives the expression which must be minimised in order to "nudge" the elastic band closer to the MEP:

$$\mathbf{F}_i = \mathbf{F}_{i(spring)}^{\parallel} - \nabla E(\mathbf{r}_i)^{\perp} \tag{2.39}$$

Climbing Image Nudged Elastic Band (CI-NEB)

A disadvantage of the NEB method is that images are rarely found exactly at the maximum; taking the difference between the energy of the initial state and the highest energy image results in an underestimation of the activation energy. Hence, in practice an interpolation is used to estimate the maximum of the MEP, often with large uncertainty. The Climbing Image Nudged Elastic Band (CI-NEB)[182] method offers a solution at no additional computational expense. After a few iterations with the traditional NEB method, the highest energy image is identified. For subsequent iterations, a different expression for the force is used:

$$\mathbf{F}_{i \ max.} = -\nabla E(\mathbf{r}_{i \ max.}) + 2\nabla E(\mathbf{r}_{i \ max.})^{\parallel} \qquad (2.40)$$
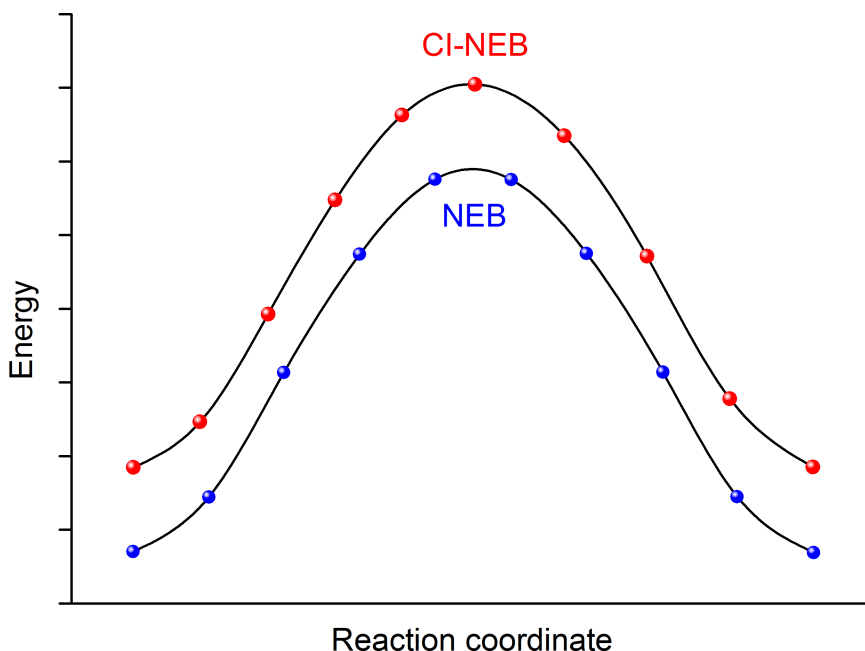
Figure 2.2: Schematic comparison of NEB and CI-NEB methods for locating the saddle-point. Notice how the NEB method must interpolate between the two highest energy images to locate the saddle-point. Not to scale.

This means that the true force along the MEP is inverted; consequently, the so-called "climbing image" is pushed up the PES along the path direction, but still moves down the PES perpendicular to the MEP, ensuring that the climbing image remains on the MEP and successfully converges to the

saddle point. This eliminates the need to interpolate to the saddle point, as is usually the case with the regular NEB method, and can be used to obtain accurate activation energies. The CI-NEB method is used predominantly in this thesis.

2.1.7 *Ab Initio* Thermodynamics

Whilst DFT calculations can provide valuable insights into chemical behavior, formally such calculations apply to rather unrealistic conditions ($T = 0K, p = 0Pa$). Hence, it is often necessary to extrapolate DFT results to apply to more experimentally relevant conditions, which include factors such as temperature and pressure. *Ab initio* thermodynamics combines DFT results with results obtained from statistical thermodynamics studies or from experimental data.[183, 184]

The Gibbs free energy can be expressed as the sum of the Helmholtz free energy and a term for the expansion work:

$$G = F + pV \tag{2.41}$$

For a solid, the Helmholtz free energy can be further decomposed into terms for the total electronic energy of the solid, the vibrational free energy and the configurational free energy:

$$g_{sol.} = E_{sol.} + F_{vib.} + F_{conf.} + pV \tag{2.42}$$

It can be readily seen that for solids under the actual reaction conditions, most of these terms can be safely neglected. Clearly, for a solid, expansion work is negligible and the pV term can be ignored. Since the temperatures under experimental conditions ($< 800K$) are far below the Fermi temperature, the electronic configurational free energy will be virtually frozen out, and for solids the vibrational term is also negligible due to atomic confinement. Hence, to a good approximation, for our purposes the molar Gibbs free energy, or chemical potential, μ, can be approximated to the total electronic energy, which can be obtained from DFT:

$$\mu_{sol.} \cong E_{sol.} \tag{2.43}$$

Considering now the terms for the gas phase species, the chemical potential for an ideal gas at a given temperature and pressure can be expressed in terms of a reference pressure, p_0:

$$\mu_{gas}(T, p) = \mu_{gas}(T, p^0) + k_{\mathrm{B}}T\ln(\frac{p}{p^0}) \tag{2.44}$$

The chemical potential can be expressed in terms of enthalphy, h, and entropy, s:

$$\mu_{gas}(T,p) = h_{gas}(T,p^0) - Ts_{gas}(T,p^0) + k_\text{B}T\ln(\frac{p}{p^0}) \qquad (2.45)$$

This expression can be written equivalently to allow for some simplifications:

$$\mu_{gas}(T,p) = [h_{gas}(T,p^0) - h_{gas}(T=0K,p^0)]$$
$$+ [h_{gas}(T=0K,p^0) - E_{gas}]$$
$$+ E_{gas} - Ts_{gas}(T,p^0) + k_\text{B}T\ln(\frac{p}{p^0}) \qquad (2.46)$$

Clearly, $[h_{gas}(T,p^0) - h_{gas}(T=0K,p^0)] = \Delta h_{gas}$, and $[h_{gas}(T=0K,p^0) - E_{gas}] = E_{ZPE}$, since one can infer that any contributions to $h_{gas}(T=0K,p^0)$ not accounted for by E_{gas} can be attributed to the zero-point energy vibrations, E_{ZPE}. Hence, one arrives at the following expression for the chemical potential:

$$\mu_{gas}(T,p) = \Delta h_{gas} + E_{ZPE} + E_{gas} - Ts_{gas}(T,p^0) + k_\text{B}T\ln(\frac{p}{p^0}) \quad (2.47)$$

E_{gas} is the calculated DFT energy for the molecule, E_{ZPE} can be determined from calculated vibrational modes ($\frac{h\nu}{2}$ eV per mode contribution), and Δh_{gas} and $s_{gas}(T,p^0)$ can be determined from experimental gas phase thermochemical data, which can be found easily in online databases (e.g. the NIST webbook).

Hence, by combining expressions for the Gibbs free energy of a solid, with the obtained expression for gas phases species, the Gibbs free energy change for processes where a solid or surface reacts with a gas phase species can be determined for a specific temperature and pressure.

2.2   Experimental Techniques

The DFT calculations presented in the results section were supported by experimental studies conducted by collaborators from both the Pérez-Ramírez group at ETH Zürich and by Dr. Detre Teschner at the electronic structure group at FHI Berlin. A variety of techniques were applied to test the predictions made from the theoretical results, and thus provide complementary evidence supporting the claims made according the theoretical results. The experimental methods applied include: High Resolution Transmission Electron Microscopy (HRTEM), Temporal Analysis of Products (TAP), and Prompt Gamma Activation Analysis (PGAA).

2.2. EXPERIMENTAL TECHNIQUES   63

2.2.1   High Resolution Transmission Electron Microscopy

High Resolution Transmission Electron Microscopy (HRTEM) allows one
to obtain highly detailed images of nanoparticle surfaces. The basic princi-
ple of HRTEM is very similar to that of optical microscopy, except instead
of light, a high energy electron beam is used to obtain structural informa-
tion about the sample. The electrons are focused into the incident primary
beam by magnetic condenser lenses; when the primary beam strikes the
sample, some of the electrons are transmitted through the sample, whilst
some are diffracted as a Fourier transform of the periodic potential, thus
retaining structural information about the sample. The diffracted electrons
are re-focused and brought together with the transmitted electrons using
an objective lense. The interference between the transmitted and diffracted
electrons is used to generate a high-resolution image of the sample.
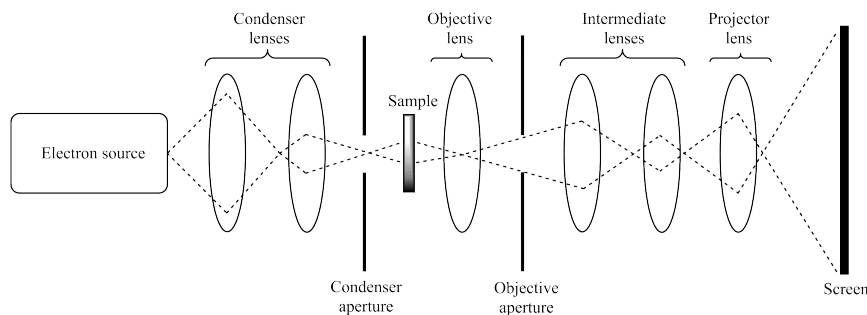
Figure 2.3: Simplified schematic diagram depicting a typical HRTEM setup.

HRTEM can be used in conjunction with computational results to probe the
surface structure under given conditions, hence any calculated distortions
and rearrangements in the surface structure induced by the relvant condi-
tions can be seen via HRTEM in the form of surface amorphisation. HRTEM
experiments can shed light on this phenomena by providing visual confirma-
tion of the nature and extent of any changes in the surface structure of the
catalysts. Furthermore, elemental mapping using Energy-Dispersive X-ray
Spectroscopy (EDXS) allows for a determination of surface the composition
of the sample, and thus in cases where surface structural rearrangement is
accompanied with a change in surface composition,the technique allows one
to identify atoms of different elements, and hence determine their role in
the structural distortion. The technique relies on the face that the incident
electron beam can cause surface atoms of the sample to eject a core electron
as a result of the bombardment. Subsequently, an electron from a higher
energy level fills the newly formed core vacancy, emitting X-ray radiation

the process. In EDXS, the X-ray spectrum emitted as a result is analysed to identify the atoms responsible for the spectrum, the principle being that different elements have their own unique X-ray signature. Hence, the technique allows one to obtain an intuitive perspective on the relationship between the surface composition, and theoretical insights into the surface structure at the atomic scale.

In this thesis, HRTEM is used to investigate the extent of halogen uptake by RuO_2 and TiO_2 under hydrogen halide oxidation conditions, and provides an experimental means of testing the conclusions drawn from the computational results.

2.2.2   Temporal Analysis of Products

Temporal Analysis of Products (TAP)[185] is a technique used to obtain kinetic and mechanistic insights into gas-solid interactions in heterogeneous catalysis. As the name suggests, the technique allows for a sub-millisecond resolution of catalytic performance. Kinetic data obtained from more traditional steady-state techniques typically only provide information on the slowest, rate-defining steps of a complex series of elementary processes. Furthermore, the observed kinetics obtained from steady-state techniques is a complex function of the gas phase composition and the structure and composition of the catalyst, making it difficult to extract precise structure-activity relations. Clearly, this is an issue for systems where the catalyst structure and composition depends strongly on the reaction conditions. Transient techniques, such as TAP, allow one to decouple elementary processes and probe systems which are less easily observed under steady-state conditions. TAP is a highly versatile technique, and is especially useful in investigating heterogeneous catalysts which are highly sensitive to the input gas feed composition, and thus experimental techniques must account for this.

In TAP experiments, a narrow gas pulse is injected into one side of the reactor, whilst the other side of the reactor is kept under continuous high vacuum. Hence, the pressure gradient along the reactor length drives the diffusion of the gas through the reactor. The sample chamber is filled with catalyst particles, and gas transport takes place through the reactor and the porous catalyst sample. At high pressures, gas diffusion is dominated by collisions between gas particles. However, during TAP experiments, the low pressures inside the reactor mean that interactions between the gas particles and the solid catalyst dominate (rather than collisions between only gas particles). This is known as the Knudsen diffusion limit, hence TAP experiments provide information on gas-solid interactions, affording insights into the elementary processes taking place on the catalyst surface.[186]
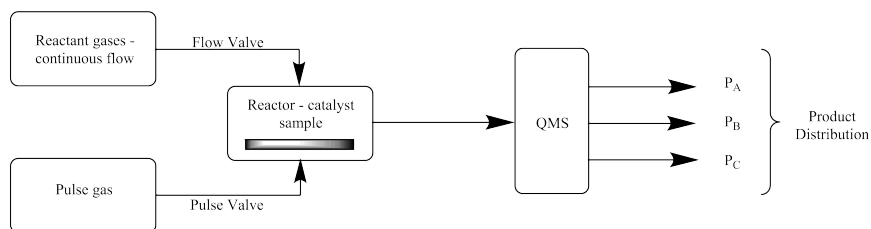
Figure 2.4: Simplified schematic diagram depicting a typical TAP setup. Reactants gases can be introduced into the reactor either via the continuous flow valve, or the pulse valve; the reactants pass through the reactor due to the UHV conditions inside the apparatus, since there is a pressure gradient from the input gas to the exit vent. Reactant may either adsorb on the catalyst surface, and subsequently desorb, or a reaction may take place. The product distribution is obtained by identifying the gases present through Quadrupolar Mass Spectrometry (QMS), and the intensity of the QMS signal corresponds to the contribution of that gas to the total product distribution.

In the context of the thesis, TAP studies are used to probe the relationship between activity and selectivty of rutile-based catalysts for halogen chemistry, and the changes in the surface structure induced by different temperatures and partial pressures of the input gases.

2.2.3   Prompt Gamma Activation Analysis

Prompt Gamma Activation Analysis (PGAA) is a modern *operando* spectroscopic technique, meaning that it can be applied to catalysts under actual reaction conditions and is thus appropriate to establish relationships between structure and activity. Clearly, this makes it an ideal technique to understand the behaviour of catalysts which are highly sensitive to applied reaction conditions. Indeed, the technique has already been used successfully to investigate the rutile type catalysts which are the primary focus of this thesis, providing detailed insights into the nature of HCl oxidation over RuO_2.[187,188]

The principle of the PGAA technique is based on the neutron capture of the atomic nuclei present in a sample. The sample placed in the path of a neutron beam, and upon irradiation, the neutrons captured by the atomic nuclei induce the emission of gamma radiation, referred to as prompt gamma radiation. The frequency of this prompt gamma raditation is element specific, allowing for the identification of elements present in the sample, whilst the intensity of radiation of a given frequency can be used to determine the concentration of the element responsible for the signal. After the emission

of prompt gamma radiation, the now unstable nucleus emits yet another gamma photon, referred to as delayed gamma radiation, along with a decay particle, returning the nucleus to its original state. Hence, PGAA is a non-destructive technique and can be used to investigate catalytic behaviour without significantly perturbing the system. In this thesis, PGAA
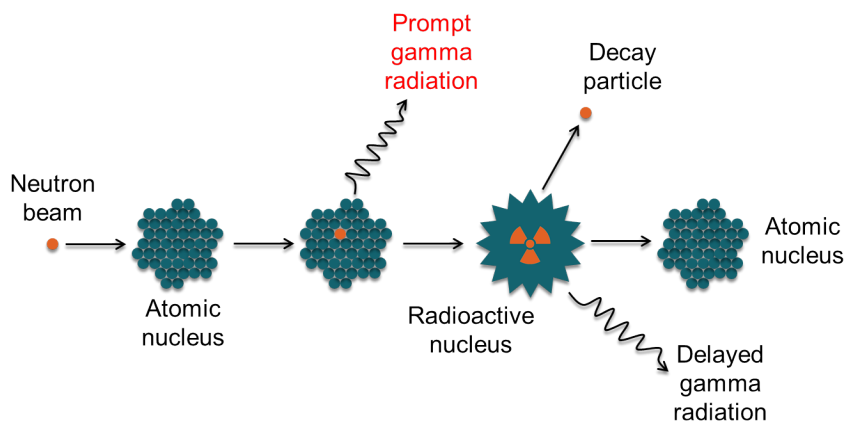
Figure 2.5: Schematic depicting the principles of PGAA.

is used to bridge the gap between the calculated halogen uptake of TiO_2 and RuO_2 under hydrogen halide oxidation conditions. As earlier studies have showed, the varying halogen uptake of different rutiles under hydrogen halide oxidation conditions means that in many cases, the active catalyst phase is structurally (and hence electronically) quite different from the stoichiometric catalysts that one might start with when performing experiments. PGAA studies allow for the simultaneous measurement of the catalyst activity as a function of its composition, which can be varied by altering the input gas feed. Hence, PGAA studies can provide information on catalyst activity which corresponds to the theoretical insights into the catalyst structure and composition obtained from *ab initio* thermodynamics studies.

Part II

Results

UNIVERSITAT ROVIRA I VIRGILI
THEORETICAL STUDIES OF HETEROGENEOUS CATALYSIS FOR HALOGEN CHEMISTRY
Michael David Higham

Chapter 3

Interplay between surface chemistry and performance of rutile-type catalysts for halogen production

The oxidation of HBr proceeds according to the following chemical equation:

$$4\mathrm{HBr(g)} + \mathrm{O_2(g)} \rightarrow 2\mathrm{H_2O(g)} + 2\mathrm{Br_2(g)}; \ \Delta\mathrm{H}^0 = -276 \ \mathrm{kJmol^{-1}}$$
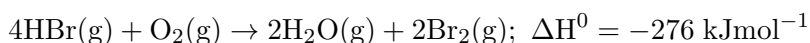
In this chapter, the catalytic activity of several rutile transition metal oxides (namely $\mathrm{IrO_2}$, $\mathrm{TiO_2}$ and $\mathrm{RuO_2}$) for HBr oxidation is investigated. Comparison is made to the superficially similar catalytic HCl oxidation, known as the Deacon process, which has already been studied extensively. Particular attention is devoted the stability of the catalysts, and their surface structure and composition under reactive conditions. DFT calculations investigate the key mechanistic steps in the overall reaction and provide kinetic and thermodynamic insights. Further calculations investigate the extent of halogen uptake and provide the basis for *ab initio* thermodynamics studies which illuminate the likely surface composition of the catalysts under real conditions. Experimental results obtained from studies conducted by collaborators from both the Pérez-Ramírez group at ETH Zürich and by Dr. Detre Teschner at the electronic structure group at FHI Berlin are presented and compared with the theoretical results, affording a detailed perspective on the structure, composition and activity of these catalysts.

3.1   Previous Work

3.1.1   RuO$_2$ Catalysed HCl Oxidation

It has already been established that halogen uptake by rutile catalysts under hydrogen halide oxidation conditions is a notable feature and plays an important role in the structure and activity of said catalysts, as discussed in the overview of the experimental studies in Chapter 1. Complementary computational studies showed that replacement of the bridging oxygen atoms (O$_b$) of the 110 surface by Cl is exothermic by -0.15 eV, suggesting that this is where Cl is incorporated into the surface.[149] The mechanism of O$_b$ replacement depends on the formation of H$_2$O$_b$, arising from the recombination of O$_b$H, which in turn results from HCl dissociative adsorption. Evidently, this replacement is selective, and is thus self-limiting, being confined exclusively to the O$_b$ site, since none of the other oxygen sites are able to abstract H from HCl, and therefore are unable to leave in the form of H$_2$O.
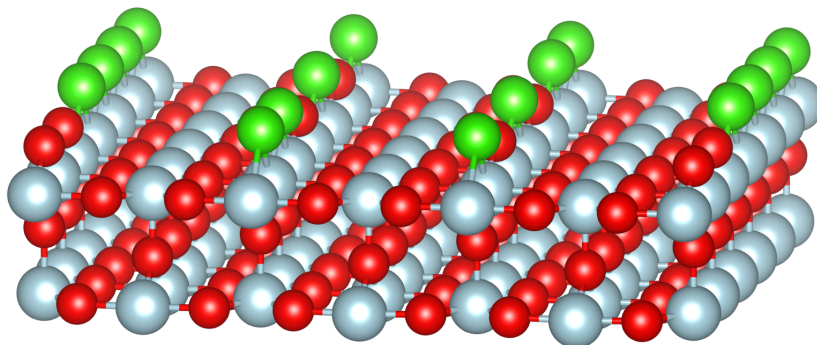
Figure 3.1: Schematic model of the RuO$_2$ surface with extensive replacement of O$_b$ for Cl$_b$. Legend: Ru, blue; O, red; Cl, green

Further studies show that the impact of Cl uptake does not appear to be detrimental to the Deacon activity of the catalyst. The precise mechanism of the Deacon reaction depends on the extent of Cl uptake, since the replacement of O$_b$ for Cl$_b$ fundamentally alters the dimensionality of the catalyst. In the fully chlorinated case, the RuO$_2$(110) surface is completely one-dimensional, with stable rows of inactive Cl$_b$ defining rows of

Table 3.1: Elementary processes of the Deacon reaction

Description	Equation
Oxygen adsorption	$O_2 + 2^* \rightarrow O_2^{**}$
Oxygen dissociation	$O_2^{**} \rightarrow 2O^*$
HCl dissiative adsorption	$HCl + O_b + ^* \rightarrow Cl^* + O_bH$
Chlorine recombination	$2Cl^* \rightarrow Cl_2 + 2^*$
H transfer	$O^* + O_bH \rightarrow OH^* + O_b$
Water formation	$OH^* + O_bH \rightarrow H_2O^* + O_b$
Water desorption	$H_2O^* \rightarrow H_2O + ^*$

active Ru_{cus} sites for adsorption. In this case, only coadsorbed O_{cus} can promote HCl dissociative adsorption by H abstraction. For stoichiometric $RuO_2(110)$, on the other hand, both O_{cus} and O_b may participate in this role, giving the catalyst a more two-dimensional character. The reaction mechanism is proposed to take place firstly with HCl dissociative adsorption. Where available, O_b may facilitate H abstraction from HCl, however in the case where the majority of O_b has been replaced with Cl_b, O_{cus} must perform this role, originating from O_2 dissociative adsorption on Ru_{cus}. Two equivalents of HCl must be adsorbed in order for H_2O to be evolved as a leaving group. In the case where O_b is preserved, this leads to a Mars-van Krevelen type mechanism, as the H_2O yielded involves the active participation and removal of O_b, which must then be subsequently replenished from either the bulk or from the gas phase.[149] On the other hand, if virtually all of the O_b sites are replaced by Cl_b, then a Langmuir-Hinshelwood type mechanism is proposed, with the H_2O evolved necessarily originating from coadsorbed O_{cus}.[189] Finally, the catalytic cycle is closed by Cl recombination, which is determined to be the rate determining step. The elementary processes described are presented in Table 3.1.

Studies to determine volcano relations,[190] where the reaction rate is plotted as a function of a descriptor such as the O_2 dissociation energy, show that whilst stoichiometric RuO_2 lies near the maximum of the volcano, chlorinated RuO_2 shows only a comparatively small decrease in activity, attributed to a slight increase in the exothermicity of O_2 dissociation on the chlorinated surface.

3.1.2   TiO$_2$ As a Catalyst for HCl and HBr Oxidation

TiO_2 has attracted interest as a potential catalyst for hydrogen halide oxidation processes, and experimental studies, discussed in Chapter 1, have found it to show good activity and stability. Whilst TiO_2 is geometrically very

similar to RuO_2, the two compounds are vastly different in terms of their electronic structure, with TiO_2 being a semiconductor, rather than metallic like RuO_2. Theoretical studies suggest that stoichiometric TiO_2 is a poor Deacon catalyst,[190] this largely being attributed the highly endothermic dissociative adsorption of O_2.[92, 191] However, further studies have demonstrated that the presence of electronic structure defects dramatically alters the activity of the catalyst. For instance, it has been shown that adsorption of a Lewis acid on $TiO_2(110)$ is enhanced by the presence of a coadsorbed Lewis base (or indeed vice versa).[192] Oxygen vacancies in the TiO_2 lattice have a similar effect, since the removal of O leaves two unpaired electrons behind, essentially making the surface Lewis basic.[193] It was proposed that these electrons occupy the conduction band, facilitating adsorption of electronegative species (i.e. O_2) by donating from the conduction band into the adsorbate, resulting in stronger binding.[194]

Clearly, under conditions appropriate for hydrogen halide oxidation, the presence of oxygen vacancies in the lattice cannot facilitate O_2 dissociative adsorption. Such defect formation would not be favoured under the oxidising conditions, with any potential vacancies being rapidly occupied with oxygen readily available from the gas phase. In light of the highly endothermic O_2 dissociative adsorption energy for stoichiometric TiO_2, one might then expect TiO_2 to be a poor catalyst for HCl and HBr oxidation. Indeed, DFT calculations showed that whilst O_2 dissociative adsorption is thermodynamically unfeasible. However, the basic character of surface oxygen atoms still permits dissociative adsorption of HBr, forming O_bH and Br_{cus}. Two equivalents of HBr may be adsorbed in this manner, followed by O_bH recombination to form water, which is subsequently desorbed, leaving a vacancy at the bridge position. Br_{cus} then rapidly occupies this vacancy. The overall process is exothermic by 0.73 eV, making it thermodynamically feasible, hence providing a reasonable mechanism to explain the observed presence of Br in the sample.[45] This process appears to be analogous to the Cl uptake observed in $RuO_2(110)$ during HCl oxidation.[149] The impact of halogen uptake on electronic structure, however, differs greatly between RuO_2 and TiO_2. Both Cl and Br have an additional valence electron compared to O. For RuO_2, this has neglible consequences, since RuO_2 is metallic and the presence of an additional electron compared to the stoichiometric sample does not substantially change its overall electronic structure. TiO_2, on the other hand, is a semiconductor, hence the "extra" electron provided by Br is accommodated in a defect state located in the band gap, essentially forming Ti^{3+}, in line with the experimental studies discussed in Chapter 1. The presence of Ti^{3+} facilitates O_2 dissociative adsorption, thus permitting the reaction to continue on the modified surface analogously to the Deacon

3.1. PREVIOUS WORK   73

process. Similarly, Br recombination to form Br_2 is found to be the most
energy-demanding step. It is proposed that this also explains why the HCl
oxidation activity of TiO_2 is poor; even though Cl uptake, like Br uptake,
would allow for the appearance of active Ti^{3+} defect states, recombination
of Cl_2 is even more energy demanding than Br_2 recombination, owing to
the stronger Ti-Cl bond afforded by the greater electron affinity of Cl.

The effect of the electronic structure of the modified surface on the activity
can be understood by considering the relative energies of the defect state
compared to the adsorbed species. For stoichiometric TiO_2, the highest
occupied levels of the valence band are much lower in energy than the lev-
els associated with O_2 π^* antibonding orbitals, into which electrons from
the catalyst must be donated in order to facilitate dissociative adsorption.
Hence, the process is energetically unfeasible. The Ti^{3+} defect states, on
the other hand, lie at a much higher energy in the band gap, close to the
bottom of the conduction band. Since these are now the highest occupied
levels of the catalyst, electrons will be donated from here to the O_2 π^* an-
tibonding orbitals. As the defect levels are slightly higher than O_2 π^*, the
process is now exothermic.

The fact that stoichiometric TiO_2 is inactive as a HBr oxidation catalyst
stands in stark contrast to the high activity of the Br-containing modified
surface which is obtained under reactive conditions. This phenomenon can
be considered as a form of self-doping; the incorporation of Br into the
TiO_2 surface drastically alters the electronic structure of the system, and
moveover these defects are stable under reaction conditions. Clearly, in
order to correctly understand catalytic activity, one must not restrict one-
self to consider only the structure and composition of the catalyst under
ambient conditions. Evidently, it is necessary to attempt to systematically
describe the activity of rutile hydrogen halide oxidation catalysts with a
consideration of the effects that the reaction conditions may have on the
catalyst and its activity. Continuing in this chapter, computational studies,
supported by experimental results, illuminate the interplay between surface
chemisty and catalytic performance.
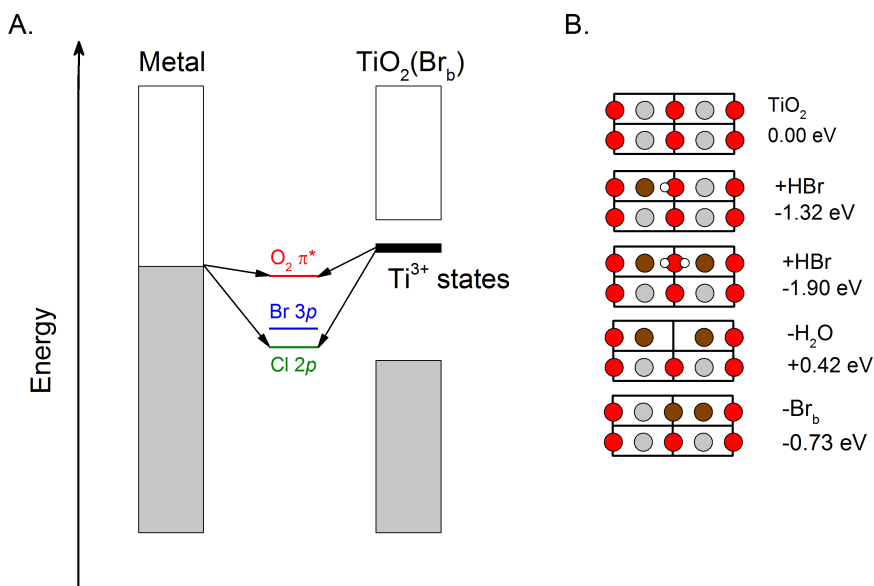
Figure 3.2: A: Schematic band structure comparison for a metallic system and Br self-doped TiO_2. B: Schematic depiction of the bromination path. Adapted from Moser et al.[45]

3.2 Computational Results

In light of previous work which suggests that halogen uptake of rutile catalysts plays a key role in determining their activities, it is important to rationalise this behaviour. To this end, computational techniques may be employed to obtain an atomic scale understanding of phenomena observed experimentally at a macroscopic scale. By simply modelling the catalyst surface as a sufficiently large periodically repeated cell, one can simulate halogen uptake by replacing oxygen atoms in this cell for halogen atoms. Calculations can then be performed to optimise the geometry of the system and determine the thermodynamic feasibility of this process, thus offering an insight into the extent of halogenation and the impact this has on the structure of the surface.

Whilst DFT calculations by themselves can reveal a great deal of information, formally they only refer to the system at 0 K and 0 Pa. pressure, which are somewhat artificial conditions if the aim is to understand the structure and activity of the system under the applied reaction conditions. Hence, in this work, *ab initio* thermodynamics studies are performed in order to extrapolate DFT results to relevant temperatures and pressures. Whilst this necessarily involves making some approximations, there is great value

in obtaining theoretical results which have a direct correspondence to experimental studies. The *ab initio* thermodynamics results offer a general overview of the extent of halogen uptake that can be expected under industrial conditions which can be readily understood in the context of real-life experiments.

To understand the reaction kinetics, and hence the overall reaction mechanism, it is necessary to have a clear perpective on the energetics of each of the elementary steps. The kinetics of a reaction are related to the activation barriers of the elementary processes. Hence, DFT calculations are applied to determine the reaction profile for the systems of interest. The calculated activation barriers can be viewed in conjunction with experimental kinetic data to rationalise the reaction mechanism.

### 3.2.1 Computational Details

Density functional theory (DFT), as implemented in the Vienna ab initio simulation package (VASP) version 5.3.3,[195, 196] was applied to slabs representing the rutile (110) facet, for both RuO_2 and TiO_2. For all rutile-type catalysts, the (110) surface represents the largest contribution to the surface in the Wulff construction of the nanoparticles.[197] For example, RuO_2 exhibits 43% of the (110) facet and a complementary 42% of the (101) facet.[187] For calculations involving $RuO_2(110)$, a p(2×1) supercell was employed, with a k-point sampling of $4 \times 4 \times 1$, using the scheme of Monkhorst and Pack.[178] For calculations involving $TiO_2(110)$, the chosen slab corresponds to a p(2×2) supercell, with a k-point sampling of $4 \times 2 \times 1$. In both cases, slabs consisting of five layers were interleaved by a 15 Å vacuum. The top two layers of the slabs were optimised, while the remaining bottom three were fixed. Forces were converged to within 0.015 eVÅ^{-1}. In order to eliminate the spurious electrostatic interactions associated with asymmetric relaxation of the slab, a dipole correction was applied to the vacuum. The exchange-correlation functional PBE,[167] as well as PBE+U[170–172] for TiO_2, was employed, with $U_{eff} = 4.5$ eV for Ti. Inner electrons were replaced with PAW,[176] and the valence states were expanded in plane-waves with a cut-off energy of 450 eV. Spin-polarised calculations were performed as necessary. Transition states were identified by CI-NEB.[182]

Ab initio thermodynamics studies were performed using DFT results for the lowest energy surface configurations to determine the surface composition under typical experimental conditions as a function of the partial pressures, p(HX), p(H_2O), and p(X_2); (X = Cl, Br). For RuO_2, DFT calculations were performed over 33 different configurations (besides the clean $RuO_2(110)$ surface) containing up to 6 X atoms per p(2×1) surface unit cell

of the $RuO_2(110)$ slab. Here, the functional of choice was PBE-D2,[173] thus including dispersion contributions. These may be relevant for the very polarisable Br atoms. Various configurations were tested for different relative positions of X atoms. For each configuration, the energy for the replacement of O atoms with X was calculated according to the following reference equation:

$$RuO_2 + 2nHBr \rightarrow RuO_2@X_n + nH_2O + \frac{n}{2}X_2$$
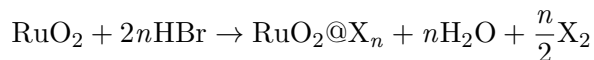
where n is the number of X atoms incorporated. The most energetically favourable configurations were obtained for each X atom incorporated. Similar calculations were also performed to investigate the Br uptake of $TiO_2(110)$. DFT calculations were performed for 4 distinct configurations investigating the incorporation of up to 2 Br atoms into a $p(2 \times 2)$ cell at 6-coordinate bridging sites. For both RuO_2 and TiO_2, the lowest energy configurations determined from DFT were used in combination with experimental gas-phase thermodynamic data for the relevant molecular species (viz. HCl, HBr, Cl_2, Br_2, and H_2O) from the NIST reference tables.[198] Hence, the number of halogen atoms incorporated into the unit cell under typical experimental conditions was determined as a function of the partial pressures $p(HBr)$, $p(H_2O)$, and $p(Br_2)$.

3.2.2 Halogen Uptake of RuO_2

The extent of halogen uptake of RuO_2 was investigated computationally by replacing surface and immediate subsurface oxygen atoms in the stoichiometric $p(2x1)$ cell for halogen atoms. More oxygen atoms were replaced sequentially, and different configurations were tested in order to determine the most stable configuration for a given number of halogen atoms present in the slab. The energy for the replacement was calculated with reference to the stoichiometric slab and the halogen halide, with lattice oxygen entering the gas phase as H_2O. Hence, the following equation was used to determine the energy of replacement, ΔE_r:

$$\Delta E_r = E_{RuO_2@X_n} + nE_{H_2O} + \frac{n}{2}E_{X_2} - E_{RuO_2} - 2nE_{HX} \qquad (3.1)$$

Here, n is the number of X atoms incorporated into the slab, $E_{RuO_2@X_n}$ refers to DFT energy of the halogenated slab, E_{RuO_2} is the energy for the stoichiometric slab, and E_{H_2O}, E_{X_2} and E_{HX} are the energies for the gas phase molecular components H_2O, X_2 and HX, respectively.

The energies for RuO_2 bromination are most exothermic for configurations corresponding to the substitution of two O atoms($\Delta E_r = -1.97$ eV, 2A, Table 3.2), and remain significantly exothermic for up to four Br atoms

3.2. COMPUTATIONAL RESULTS 77
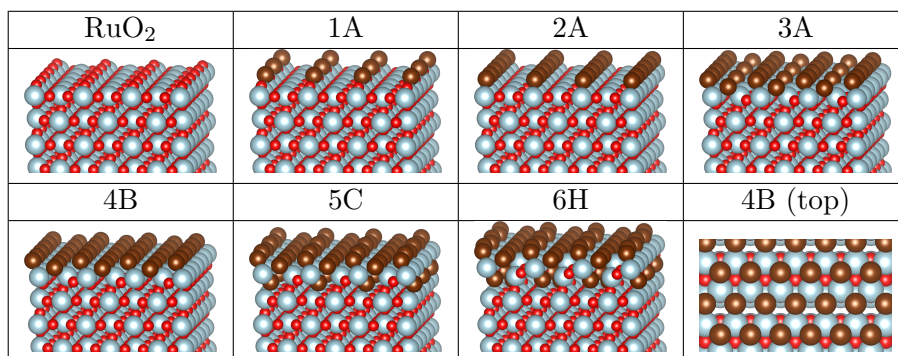
Figure 3.3: Depiction of surface structure and composition of RuO_2@Br with successive Br uptake. The labels refer to the most stable configurations for a given number of Br incorporated, as in Table 3.2. Notice the distinctive hexagonal arrangement of Br atoms at higher coverages (i.e. more than 4 Br per p(2×1) cell), evident when looking along the (001) direction. Legend: Ru: blue; O: red; Br: brown.

($\Delta E_r > -1$ eV, 3A and 4B, Table 3.2). Upon addition of the first sub-surface Br atom, the bromination becomes less exothermic ($\Delta E_r = -0.50$ eV, 5C, Table 3.2), and eventually it becomes slightly endothermic after the addition of a further Br atom ($\Delta E_r = 0.30$ eV, 6H, Table 3.2). Notably, the incorporation of four or more Br atoms into the lattice already leads to a considerable degree of structural rearrangement. The surface Br atoms relax such that they form a hexagonal arrangement. Furthermore, considering factors unaccounted for by the above methodology, such as configurational entropy or other surface orientations, extensive subsurface bromination is well within the bounds of possibility. The present calculations only aim at establishing the lowest energy configurations and do not provide any indication as to how the bromination occurs. For RuO_2 chlorination, the process is only exothermic for up to two Cl atoms incorporated into the surface ($\Delta E_r = -0.93$ eV, 2A, Table 3.2), with subsequent Cl addition being endothermic. While incorporation of up to four Cl atoms is moderately endothermic ($\Delta E_r = 0.71$ eV, 4B, Table 3.2), subsequent chlorination of the subsurface layers is considerably more so, reaching $\Delta E_r = 1.81$ eV and 3.21 eV for five and six Cl atoms, respectively (5C and 6H, Table 3.2).
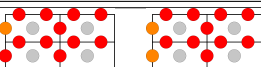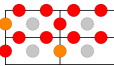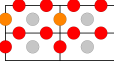
Table 3.2: Schemes of the incorporation of halogen atoms (X = Br, Cl) into a
(2×1) cell of the $RuO_2(110)$ surface. Configurations considered the various relative
positions of up to 6 halogen atoms. Configurations 4F, 5G, 6G, and 6H depict the
halogen substitution into the subsurface layer, whereby the surface configurations
are identical to 3A, 4B, and 5C. Legend: Ru: blue; O: red; X (Br or Cl): orange;
two X atoms eclipsing one another: purple. Free energy values of Br (blue values)
and Cl (red values) atom substitution are also presented below the corresponding
configuration. Blue boxes indicate the lowest free energy cases.

| | Free Energy of halogen substitution / eV | | | | | |
	1	2	3	4	5	6
A	-1.462	-1.972	-1.520	0.849	0.476	6.423
	-0.817	-0.926	0.137	3.428	3.122	9.322
B	0.334	-0.928	1.563	-1.373	5.422	1.296
	1.071	0.363	3.242	0.712	8.781	5.050
C		0.700	-0.589	0.576	-0.503	3.244
		1.834	1.122	2.622	1.831	8.661
D		2.614	0.344	0.911	2.076	1.296
		3.558	2.308	3.157	6.498	5.050
E		1.257	1.991	7.512	1.438	2.625
		2.784	3.629	9.501	3.461	7.827
F				1.744		6.504
				2.954		10.136
G				0.201 (+4B)		0.647 (+5C)
				2.316		3.515
H						0.303 (+5C)
						3.207

3.2.3 Halogen Uptake of TiO_2

The calculations for TiO_2 show that, unlike RuO_2, Br uptake is endothermic for incorporation of both one and two Br atoms, with $\Delta E_r = 0.43$ eV and 1.33 eV, respectively (1A and 2B, Table 3.3). The lowest energy configuration for two Br atoms had them both occupying bridging sites in diagonal fashion, as this would result in minimal repulsion between them. This is in line with the experimental results. Additionally, the free energy of substitution of a Br atom into TiO_2 is much lower than those of RuO_2 chlorination and bromination, reflecting the resistance of TiO_2 to halogenation.

Table 3.3: Scheme for the incorporation of bromine atoms into a (2×2) cell of the $TiO_2(110)$ surface. The number of substituted halide atoms (1-2) as well as their relative position in the lattice (A-C) was computed for 4 different configurations. The free energy values of Br substitution for all configurations are tabulated. Blue boxes indicate the lowest free energy cases.

	1	2	Free Energy of Br substitution / eV 1	2
A			0.431	1.589
B				1.328
C				1.344

3.2.4 *Ab initio* Thermodynamics

From the calculations detailed in the previous subsection, the most stable configurations for each halogen atom incorporated were identified and used for the *ab initio* thermodynamics studies. The chemical potentials for the gas phase species were obtained according to Equation 2.47 and the chemical potentials for the solid state components were approximated as being equal to the DFT energy, in line with Equation 2.43. Hence, using the chemical equation for halogen substitution, the change in the Gibbs free energy for halogen substition as a function of the partial pressures of the gas phase

components was obtained from the following expression:

$$
\begin{aligned}
\Delta g_{sub.} = {} & E_{\mathrm{RuO_2@X_n}} - E_{\mathrm{RuO_2}} \\
& - 2n\mu_{\mathrm{HX}}(T, p^0) + \frac{n}{2}\mu_{\mathrm{X_2}}(T, p^0) + n\mu_{\mathrm{H_2O}}(T, p^0) \\
& - 2nk_{\mathrm{B}}T\ln(\frac{p_{\mathrm{HX}}}{p^0}) + \frac{n}{2}k_{\mathrm{B}}T\ln(\frac{p_{\mathrm{X_2}}}{p^0}) + nk_{\mathrm{B}}T\ln(\frac{p_{\mathrm{H_2O}}}{p^0})
\end{aligned} \tag{3.2}
$$

The partial pressures were varied independently with $\ln(\frac{p}{p^0})$ ranging between -10 and 10, corresponding to a pressure range of between approximately 10^{-4} and 10^4 bar. The temperature was set such that the calculations are commensurate with typical industrial conditions. The studies showed that for RuO_2 the partial pressures of the products of the substitution process, X_2 and H_2O, have only a very limited impact on surface halogenation (Figure 3.4). The most stable composition varied much more with variable HX pressure, thus indicating that this is the dominant factor in surface and subsurface halogenation.

Comparing the plots for RuO_2 chlorine uptake with that for Br uptake as a function of the hydrogen halide partial pressure, it can be clearly seen that whilst in both cases higher HX partial pressures are associated with a greater uptake of the halogen, bromination is much stronger than chlorination. Indeed, for RuO_2 bromination, even at the lowest HBr partial pressures and highest Br_2 and H_2O partial pressures, one would still expect to observe at least 1 Br atom per $p(2 \times 1)$ cell. Comparing RuO_2 bromination with TiO_2 bromination, there is a marked difference between the two systems, with Br uptake of TiO_2 being very limited, only being observed for high HBr partial pressures. RuO_2, on the other hand, shows extensive uptake even at lower HBr partial pressures (Figure 3.5). Condensing all of these results, it can be seen that TiO_2 shows a remarkable resistance to halogenation. With low product partial pressures (i.e. initial conditions with limited Br_2 and H_2O present), HBr partial pressures of around 10 bar are required in order to observe even one Br atom incorporated into the $p(2 \times 2)$ surface cell. RuO_2, on the other hand, could feasibly be expected to exhibit a Br uptake of 4 Br atoms per $p(2 \times 1)$ cell. This is especially notable given that the TiO_2 cell used is twice as large; for comparably sized cells, at HBr partial pressures of around 10 bar, one would expect around 8 times as much Br in RuO_2 compared to TiO_2. Similarly, Cl uptake under HCl oxidation conditions at comparable partial pressures for all components showed moderate Cl uptake, with an expected uptake of 2 Cl atoms per $p(2 \times 1)$ cell for HCl partial pressures of around 10 bar (Figure 3.6). Clearly, the structure and composition, and by extension activity, of rutile-type catalysts are highly sensitive to to reaction conditions.

Surface	Energy / eV	Surface	energy
4B	0.712	4B	-1.373
2A	-0.926	2A	-0.928
1A	-0.817	1A	-1.462
Clean	0	Clean	0
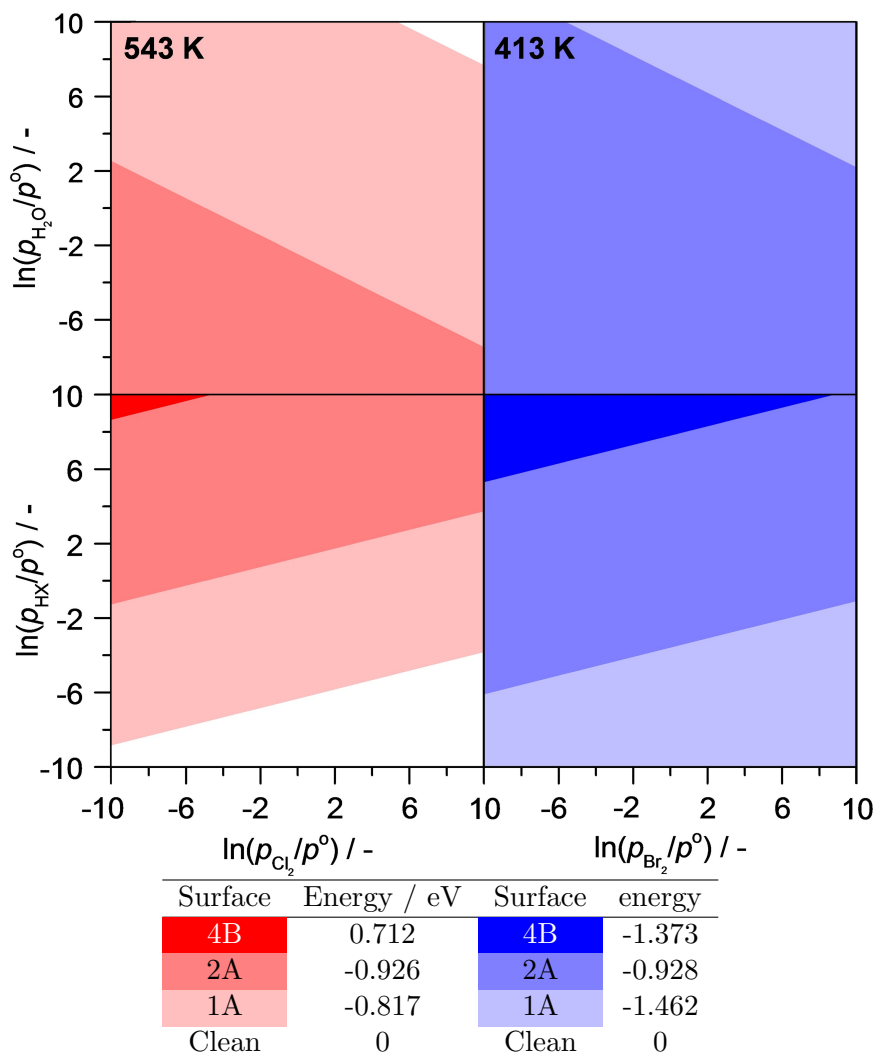
Figure 3.4: *Ab initio* thermodynamics for Cl (red) and Br (blue) substitution on
$RuO_2(110)$ surfaces. The colour shades correspond to the surface configurations
having the lowest energy under the simulated conditions, tabulated in Table 3.2.
The partial pressures of HX (top) and H_2O (bottom) were fixed at 1 bar.

RuO$_2$ Chlorination		RuO$_2$ Bromination		TiO$_2$ Bromination	
Surface	Energy / eV	Surface	Energy / eV	Surface	Energy / eV
6H	3.207	4B	-1.373	2B	1.328
4B	0.712	2A	-0.928	1A	0.431
2A	-0.926	1A	-1.462	Clean	0
1A	-0.817	Clean	0		
Clean	0				
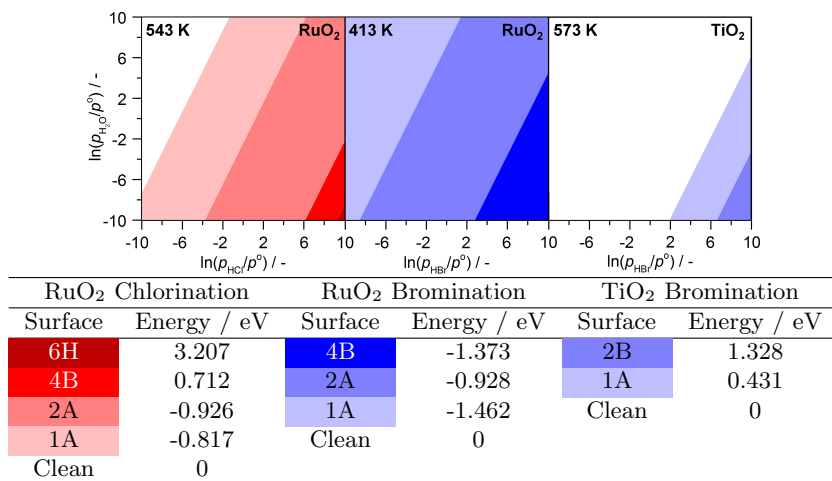
Figure 3.5: *Ab initio* thermodynamics of the Cl (red) and Br (blue) substitution on RuO$_2$(110)and TiO$_2$(110) surfaces. The color shades denote the surface configurations in Figs. 3.2 and 3.3 having the lowest energies under the simulated conditions. The partial pressures of Cl$_2$ and Br$_2$ were fixed at 1 bar.
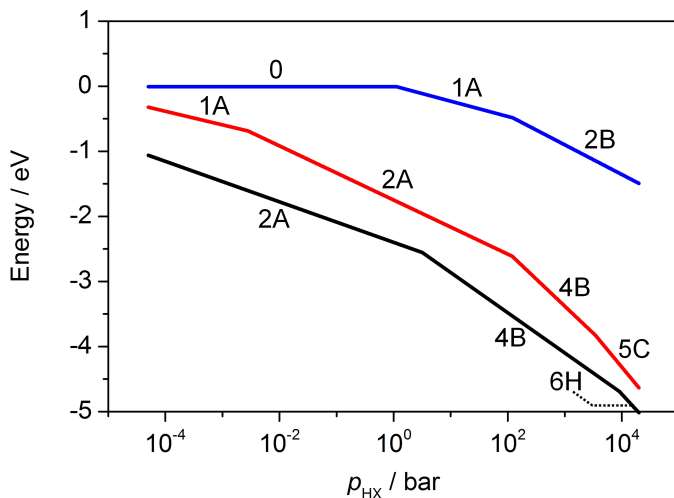
Figure 3.6: Free energy of substitution versus the partial pressure of the hydrogen halide for the bromination of TiO$_2$ (blue) and RuO$_2$ (black), as well as for the chlorination of RuO$_2$ (red). The partial pressures of X$_2$ and H$_2$O were fixed at 10^{-4} bar. The temperature was set to 573 K (TiO$_2$) and 393 K (RuO$_2$) for bromination and 523 K (RuO$_2$) for chlorination. The labels in the plot refer to the schematics presented in Figure 3.2 for RuO$_2$ and Figure 3.3 for TiO$_2$.

3.2.5 Modelling of the Reaction Mechanism

Further calculations were performed to investigate the mechanism for HBr oxidation over a variety of rutile-type catalysts when halogen uptake is accounted for. The overall process involves four key stages: HBr dissociative adsorption, O_2 dissociative adsorption, Br_2 evolution and H_2O evolution. For all of the systems investigated here (RuO_2@Cl, RuO_2@Br, TiO_2@Br and IrO_2@Br), dissociative adsorption of O_2 from the gas phase was found to be exothermic, and especially so for the RuO_2 and IrO_2 based systems. This is unsurprising in light of previous works; it has already been established that O_2 dissociative adsorption is highly exothermic for stoichiometric RuO_2 and IrO_2, and since these systems are metallic, the adsorption is limited only by the number of free sites available.[199] For TiO_2@Br, on the other hand, any O_2 dissociative adsorption depends on the presence of Ti^{3+} defect sites resulting from self-doping caused by Br uptake.[45] Basic surface sites, such as O_b and coadsorbed O_{cus}, facilitate HBr dissociative adsorption by abstracting H. Whilst the HBr dissociative adsorption energies were found to be comparable for RuO_2@Cl, RuO_2@Br and TiO_2@Br, for IrO_2@Br the value was considerably more exothermic. Conversely, for Br_2 recombination, the process was most endothermic for IrO_2@Br, at 3.05 eV, compared to 2.44 eV for TiO_2@Br and 1.90 eV for RuO_2@Br. In this case, Br is much too strongly adsorbed on IrO_2, hindering the eventual Br_2 evolution. Water evolution was also endothermic for each of the systems, albeit to a lesser extent than Br_2 evolution.
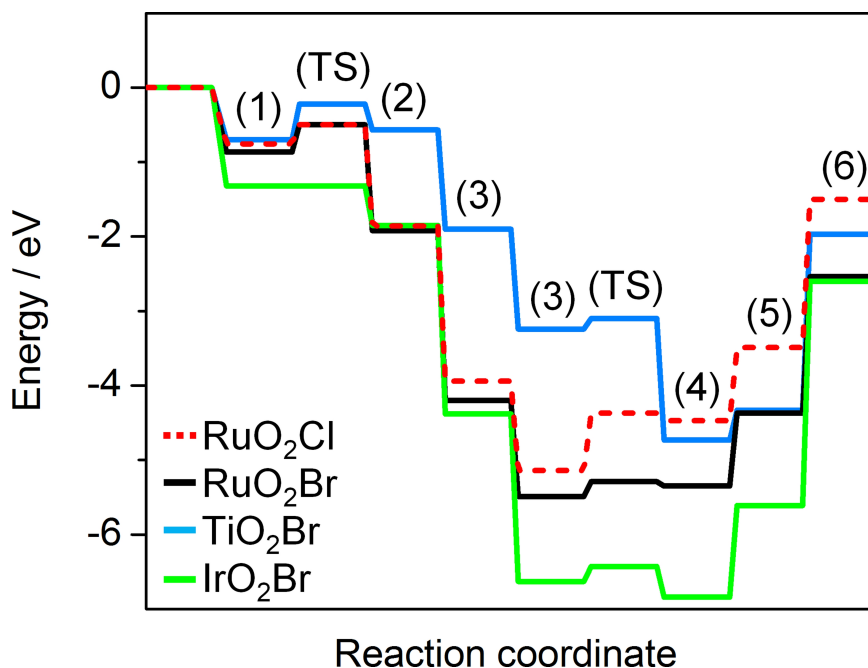
Figure 3.7: Reaction profiles of HBr (solid lines) and HCl (dashed line) oxidation on halogenated rutile-type catalysts. Herein, (1) is the molecular O_2 adsorption and (2) is the dissociated state after the transition state (TS). Subsequently, two HX molecules are adsorbed in steps (3), followed by the transition state (TS) for the OH recombination to water (4). Finally, both water (5) and molecular halogen (6) are desorbed from the surfaces. The profile corresponds to half a stoichiometric reaction: $O_2 + 2HX \rightarrow O * +H_2O + X_2$, thus step (3) occurs only twice and an oxygen atom is left on the surface in the final state. Adapted from Moser et al.[200]

3.3   Experimental Evidence

A variety of experimental techniques were applied by collaborators from both the Pérez-Ramírez group at ETH Zürich and by Dr. Detre Teschner at the electronic structure group at FHI Berlin. Advanced techniques were carefully selected to provide the most detailed insights into the activity, structure and composition of the catalyst under actual reaction conditions, and to offer the best comparison with the computational results. These experimental studies were performed in parallel with and are complementary to the computational results presented in this thesis.[200]

3.3.1   HRTEM

HRTEM experiments were performed for both RuO_2 and TiO_2 nanoparticles, with images obtained before and after exposure to HCl and HBr. The untreated samples showed sharp, clearly defined particle edges, demonstrating a high degree of crystallinity, which would be expected for the stoichiometric samples. For both RuO_2 and TiO_2, no significant change in size of the nanoparticles was observed after treatment with HCl or HBr, indicating that the bulk structure of the nanoparticles had been largely preserved. This corroborates the theoretical results which suggest that any structural changes are limited to the surface and immediate subsurface layers of the catalyst. Whilst the TiO_2 nanoparticles remained mostly unchanged by HCl and HBr treatment, RuO_2 showed a significant amorphisation of the catalyst surface. The amorphisation of the RuO_2 surface after HBr exposure was particularly extensive, implying a high degree of rearrangement of the geometry of the surface layers. This strongly supports the theoretical results which suggest that Br uptake by RuO_2 is extensive and causes a major rearrangment of the surface structure. EDXS analysis revealed that for TiO_2, neglible quantities of Cl were to be found in the sample, compared to small amounts of Br. The small amounts of Br detected are in line with the limited extent of bromination predicted by the *ab initio* thermodynamics studies. For RuO_2, on the other hand, the EDXS analysis showed a significant incorporation of Br into the surface layers, and only a moderate degree of Cl uptake. This again corresponds to the theoretical results, which predict a moderate Cl uptake and an extensive Br uptake by RuO_2. The EDXS analysis combined with the observation of amorphisation at the nanoparticle surface confirms the simulations which revealed that high Br concentrations in the surface and subsurface layers precipitate a major structural change to accommodate the larger Br atoms.
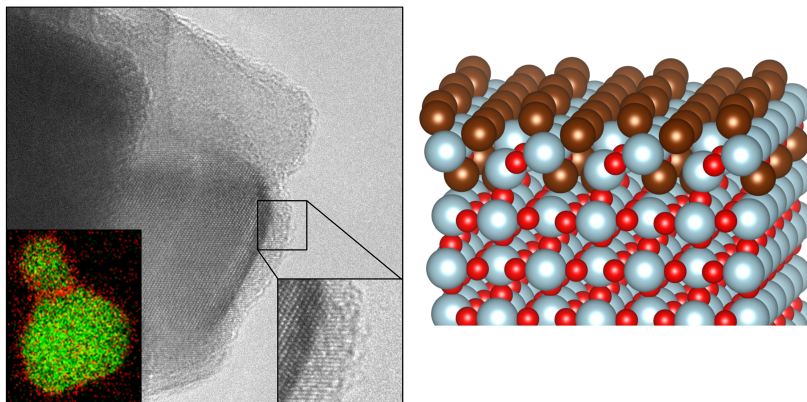
Figure 3.8: Left: HRTEM image of RuO_2 after treatment in HBr at 393 K. Right: Calculated surface geometry for RuO_2 with a high degree of surface O replacement for Br, presented for comparison. The bottom left inset in HRTEM micrograph depicts the averaged elemental mapping of the RuO_2 particle using EDXS, with Ru shown in green and Br shown in red. The bottom right inset shows a magnified image of the amorphised particle edge. HRTEM micrograph adapted from Moser et al.[200]

3.3.2   TAP

TAP studies were performed to investigate reactant consumption and product evolution as a function of time. Firstly, an individual pulse of either HBr or HCl (i.e. without O_2 present) was applied to IrO_2, RuO_2 and TiO_2. It was observed that the normalised peak responses for HBr were delayed compared to those for HCl for each of the catalysts (by 0.17s for IrO_2, 0.44s for RuO_2, and 0.82s for TiO_2, Figure 3.9). This implies that the dissociative adsorption of HBr is more exothermic than that of HCl, since the delay in the peak response can be attributed to HBr molecules adsorbing on the surface, rather than simply passing through the apparatus to the detector. When the catalysts are exposed to a mixture of HBr and O_2, it was observed that the delays in the peak maxima for IrO_2 and TiO_2 were reduced, along with the the integrated peak area, indicating consumption of HBr (i.e. oxidation to Br_2 and H_2O). For RuO_2, on the other hand, no significant reduction of the peak maximum was observed, implying the presence of O_2 does not affect HBr dissociative adsorption greatly. When the catalysts were exposed to a mixture of HCl and O_2, only RuO_2 showed any notable reduction in the integrated peak area compared to the HCl-only pulses, indicating that only RuO_2 is capable of any significant conversion of HCl.
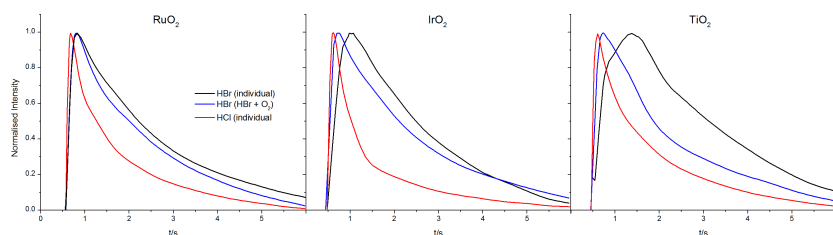
Figure 3.9: Normalised transient responses of HBr and HCl after individual (HBr, black; HCl, red), and simultaneous (HBr+O$_2$, blue) pulse experiments at 623 K. Adapted from Moser et al.[200]
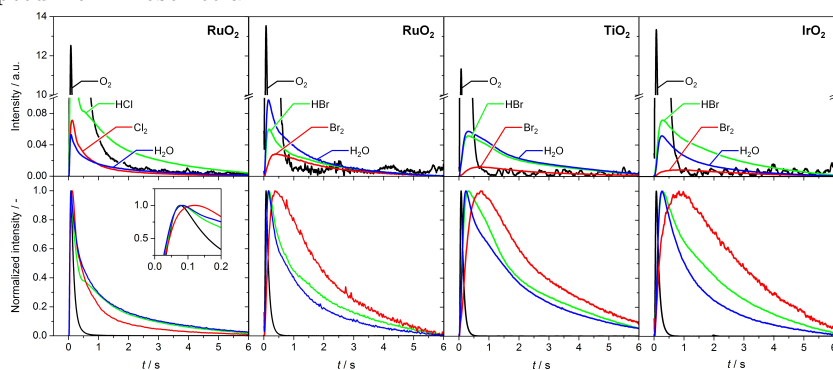
Figure 3.10: Transient (top) and normalised transient (bottom) responses of reactants (HCl, HBr, O$_2$) and products (Br$_2$, Cl$_2$, H$_2$O) at 623 K upon simultaneous pulsing of HX and O$_2$ over rutile-type catalysts. The colour code applies to both the top and bottom rows. The break in the y-axis in the top plots enables a better visualiszation of the product responses: Cl$_2$, Br$_2$, and H$_2$O. The inset in the bottom left plot magnifies the region at the maximum of the normalised transient responses. Adapted from Moser et al.[200]

Turning now to the product responses (Figure 3.10), it can be seen that HBr conversion is more efficient than HCl conversion over RuO$_2$, since the product response for H$_2$O (which forms in stoichiometric amounts with either Br$_2$ or Cl$_2$) is more intense for the HBr/O$_2$ mixture. Comparing the H$_2$O response for HBr oxidation for each of the catalysts, it was observed that RuO$_2$ showed the most intense signal, followed by TiO$_2$ and finally IrO$_2$, which implies that RuO$_2$ is the most active in HBr oxidation, with IrO$_2$ being the least active. It is also seen that in every case, the H$_2$O signal reaches its maximum before the X$_2$ signal (where X is either Cl or Br), suggesting that halogen recombination is the most energy-demanding step.

3.3.3   PGAA

PGAA experiments were perfomed to provide deeper insights into the halogen uptake of the catalysts. Whilst the PGAA experiments were not possible for IrO_2 (since the neutron excitation and radioactive decay of Ir leads to the emission of very intense gamma radiation, thus saturating the detector and overshadowing the halogen signal), results were obtained for RuO_2 and TiO_2. TiO_2 was found to exhibit halogen coverages of 0.57 and 0.48 for Br and Cl respectively, at $O_2 : HX = 0$. With increasing oxygen partial pressure, these values decrease to 0.40 (Br) and 0.36 (Cl). The Cl coverage on RuO_2 is close to 1 at $O_2 : HCl = 0$ and reaches 0.86 at $O_2 : HCl = 9$. Most notably, however, was the extensive Br uptake observed for RuO_2. The value obtained exceeded the theoretical surface coverage by a factor of 300%, with the Br coverage increasing from 0.65 to 1.48 as the $O_2:HBr$ ratio was decreased from 9 to 1, thus indicating that extensive subsurface bromination had taken place. It was also observed that coverage was affected by temperature, with the halogen coverage on TiO_2 decreasing from 0.41 (Br) and 0.54 (Cl) to 0.27 (Br) and 0.38 (Cl), respectively. In all cases, the halogen coverages on TiO_2 were found to be significantly lower compared to RuO_2. Examining the catalyst activity as a function of halogen coverage, it was observed that for TiO_2, small increases in Br coverage correspond to an increase in activity, with the Br coverage remaining low. For RuO_2, however, larger Br coverages were observed to result in a decrease in activity. Thus, an optimal halogen coverage between the observed values for TiO_2 and RuO_2, at which the bromine formation rate would be maximal, is likely to exist.

The impact of product inhibition was investigated by the addition of Br_2 to the input gas feed. It was observed that for Br_2 input of more than 2% volume, the uptake of Br by TiO_2 had already stabilised at a coverage of 0.43, indicating that only very limited Br uptake can be attributed to Br_2, with HBr being mostly responsible. With a higher proportion of Br_2 included in the input gas feed, a distinct decrease in activity was observed. For a Br_2 proportion of 4%, the Br_2 formation rate decreased by 55%. Considering the reaction rate versus the Br_2 partial pressure, an apparent reaction order of -0.44 was observed. Since the theoretical reaction order for Br_2 dissociative adsorption is -0.5, it seems plausible that the decrease in activity associated with a higher proportion of Br_2 in the input gas feed can be attributed to competitive adsorption between Br_2 and HBr on the surface. In comparison, previous studies examining the product inhibition caused by Cl_2 for the Deacon reaction over RuO_2 gave a greater inhibition effect of 1.00. This is attributed to the fact that the activity of TiO_2 to HBr oxidation relies on the formation of localised Ti^{3+} defect states, meaning that the catalyst,

under reactive conditions, is more able to discriminate between potential adsorbate species. On the other hand, for metallic systems such as RuO_2, site competition is promoted since the effect of defects is screened by the conduction band, making adsorption sites essentially chemically equivalent and thus unable to differentiate between electron- rich and electron-poor species.
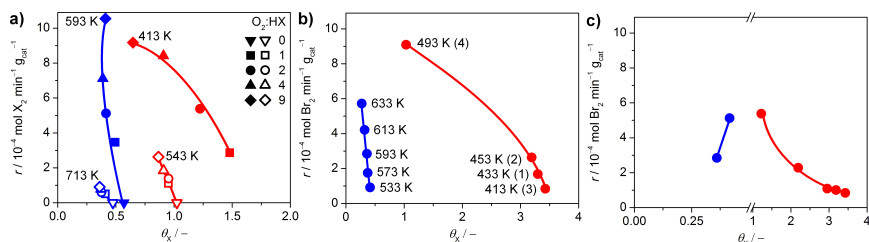
Figure 3.11: Rate of halogen formation from HBr (solid symbols) and HCl (open symbols) oxidation as a function of the halogen coverage over TiO_2 (blue) and RuO_2 (red) showing the dependence on the feed O_2:HX ratio at constant temperature (a). The O_2:HX ratio was increased from 0 to 9, except for the HBr oxidation over RuO_2 where the order was inverted from 9 to 1. Dependence of the rate on the catalyst bed temperature at O_2:HBr=2. The temperature for TiO_2 was increased from 533 K to 633 K (b). The order of measurements for RuO_2 is indicated with numbers in parenthesis. Rate of bromine formation versus the bromine coverage (c). Coverages exceeding unity indicate the occurrence of subsurface halogenation. Adapted from Moser et al.[200]
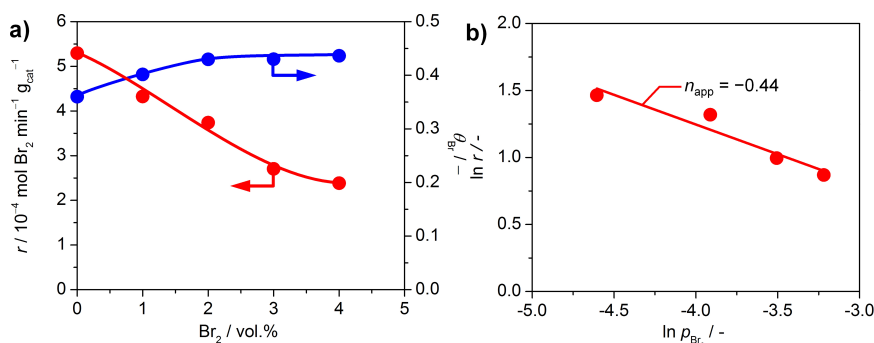
Figure 3.12: Rate of bromine formation (red) and bromine surface coverage (blue) versus the volumetric feed of bromine over TiO_2 at 593 K and O_2:HBr = 2 (a). Rate of bromine formation versus partial pressure of bromine (b). Adapted from Moser et al.[200]

3.4   Summary

Viewing the experimental and theoretical results collectively, a general picture of halogen chemistry over rutile-type transition metal oxides emerges. Whilst one might have expected that HCl and HBr oxidation processes would proceed in a substantially similar manner, it is clear that their interactions with different potential catalysts are markedly different. In every case, one observes HX dissociative adsorption, owing to the acidity of HX and the presence of basic sites on the catalyst surfaces. However, depending on the combination of hydrogen halide and metal oxide, a highly variable degree of surface halogenation can take place. For HBr oxidation over TiO_2, a modest degree of replacement of O_b by Br takes place. For RuO_2, HCl oxidation conditions result in a moderate Cl uptake with significant O_b replacement, whilst HBr oxidation conditions result in extensive bromination, which is not confined to the most labile surface sites, but in fact includes a significant degree of subsurface bromination and the appearance of a distinct and highly amorphous surface phase with a high Br concentration. The extent of halogenation depends partially on the metal oxide system in question, with semiconductors such as TiO_2 being limited in their halogen uptake owing to a limited capacity to form defect states. On the other hand, for metallic systems such as RuO_2 and IrO_2, the extent of halogenation depends on the relative strength of M-X bonds compared to M-O bonds at the surface.

Clearly, the surface structure and composition has a major impact on the activity of the catalyst and the mechanism by which HX oxidation occurs, demonstrating the multifarious nature of rutile oxides in HX oxidation.

3.5   Conclusions

By applying an integrated approach consisting of DFT calculations and experimental techniques, a detailed analysis of the surface chemistry of HBr and HCl oxidation on a variety of rutile catalysts, namely RuO_2, IrO_2, and TiO_2, has been obtained. It was found that the structural stability of HX oxidation catalysts depends on the interaction of the hydrogen halide molecule with the catalyst surface. The combined HRTEM, DFT, and TAP studies reveal that the amorphisation of the RuO_2 particle surface after treatment with HBr is due to structural distortion of the clean surface geometry after extensive bromination, and that strong bromination, and thus surface amorphisation, also occurred during the HBr oxidation reaction. The impact of HCl is much more limited, leading to less pronounced amorphisation as a result of the comparably unfavourable energetics of oxygen substitu-

3.5. CONCLUSIONS   91

tion, restricting the Cl replacement to the surface. The computed bromine substitution into the TiO_2 lattice is endothermic, suggesting only limited potential for bromination. The TAP experiments support these results, indicating a stronger interaction of rutile-type materials with HBr than HCl. Both the computational results and TAP experiments indicate that halogen evolution can be considered to be the most energy demanding step, with the activity of the catalysts for HBr oxidation increasing in the following order: $IrO_2 < TiO_2 < RuO_2$. Both the HBr and HCl oxidation reactions follow a Langmuir-Hinshelwood type mechanism on surfaces with a low to moderate degree of halogenation, whilst for the high coverages seen for RuO_2 under HBr oxidation conditions, the reaction mechanism may involve active participation of surface atoms through the replacement of surface oxygen atoms, reminiscent of a Mars-van-Krevelen type mechanism. Indeed, it is possible that both mechanisms contribute to the overall reaction, the extent to which depending on the halogen uptake. The halogen uptake is the key descriptor linking stability and activity of the catalytic systems. For RuO_2, *ab initio* thermodynamics studies show that under typical HCl reaction conditions, a moderate amount of O_b is replaced with Cl, whilst under typical HBr oxidation conditions, extensive surface and subsurface bromination occurs. This is in agreement with the PGAA studies, which showed that the steady-state surface halogen coverage reaches 86-100% for chlorine and 75-300% for bromine, proving that subsurface bromination does indeed take place. This is further supported by the HRTEM images, which show signicant changes in the RuO_2 surface after exposure to HBr. PGAA studies also showed a decrease in the halogen coverage on RuO_2 can be induced by increasing the operation temperature and elevating the O_2:HX feed ratios. The theoretical results also show that for TiO_2, only a limited Br uptake is observed, and only then at high HBr partial pressures. This is also supported by the PGAA studies, which show that the halogen coverage of TiO_2 is limited to 30-50% as a result of its self-doping mechanism with bromine. An increase in the temperature and the O_2:HX feed ratio induces higher activity, but does not significantly affect the halogen coverage on TiO_2. The addition of Br_2 to the gas feed over TiO_2 does not affect the bromine coverage, but inhibits the reaction at an apparent order of 0.44, indicating a competitive adsorption of Br_2 and HBr on the active sites. As a result of these studies, it was determined that it would be desirable to combine the exceptional low-temperature activity of RuO_2 with the stability of TiO_2 against strong surface halogenation by designing new Ru-Ti mixed oxide catalysts for HBr oxidation with an optimal balance between activity and stability. Such systems, along with other several other modified TiO_2-based systems, are examined in the next chapter.

Chapter 4

Doping Strategies for Rutile Transition Metal Oxides in Hydrogen Halide Oxidation

As seen in the previous chapter, the remarkable activity of $TiO_2(110)$ as a catalyst for HBr oxidation can be attributed to the formation of Ti^{3+} defects, originating from self-doping by Br incorporation into the surface under reactive conditions. $RuO_2(110)$ is also an active HBr oxidation catalyst, but suffers from extensive Br uptake, which ultimately poisons the surface, blocking the active sites. In light of these two extremes, it is of interest to develop new catalysts based on the principles established in the previous chapter. A catalyst combining the inherent reactivity of RuO_2 with the stability of TiO_2, for example, could prove to be a highly successful catalyst. In this chapter, several TiO_2-based systems are investigated. Systems featuring substitutional doping, such as TiO_2@Br (i.e. the active phase obtained when stoichiometric TiO_2 is exposed to HBr oxidation conditions) and TiO_2@Ru (i.e. substituting one surface Ti atom for Ru) are considered, along with a system containing both Ru and Br dopant atoms, in comparison to the stoichiometric catalyst. Interstitial doping of boron into TiO_2 is also examined. The theoretical studies show that a careful choice of dopant and host system affords a powerful degree of control in determining the electronic structure, and by extension, catalytic activity of a system. Valuable insights into the strategies available for rationally designing superior catalysts are obtained.

4.1   Computational Details

Density Functional Theory (DFT) as implemented in the Vienna Ab initio Simulation Package (VASP), version 5.3.3,[195, 196] was applied to slabs representing the rutile (110) facet for all of the TiO_2-based systems. A p(2×2) supercell was employed in all cases, with a k-point sampling of $4 \times 2 \times 1$, using the scheme of Monkhorst and Pack.[178] Slabs consisting of five layers were interleaved by 15 Å of vacuum, with the ionic coordinates of the top two layers of the slabs being optimised, while the remaining bottom three were fixed. Forces were converged to within 0.01 eV/Å^{-1}. In order to eliminate the spurious electrostatic interactions associated with asymmetric relaxation of the slab, a dipole correction was applied to the vacuum. The exchange-correlation functional PBE+U[167, 170–172] was employed, with $U_{eff} = 4.5$ eV applied to Ti to accurately account for correlation effects. Inner electrons were replaced with PAW,[176] and the valence states were expanded in plane-waves with a cut-off energy of 450 eV. Spin-polarization was included as required.

4.2   Previous Work

4.2.1   Substitutional Doping of Ru in TiO_2(110)

Mixed Ru and Ti oxides have attracted investigative attention for several decades, especially owing to the ubiquity of Dimensionally Stable Anodes (DSA) of such composition applied in the electrochemical oxidation of HCl to Cl_2.[78, 201, 202] Early experimental and theoretical studies examined the effect of Ru dopant atoms in a rutile TiO_2 matrix and the effects this has on the electronic structure, and by extension, the optical and electronic properties of the material.[203, 204]

Mössbauer spectroscopy studies using obtained spectra with very similar structures for stoichiometric RuO_2 and Ru-doped TiO_2. The results show that it can be confirmed rather unambiguously that for mixed Ru-Ti oxides, Ru is present as Ru^{4+}, particularly since the isomer shift obtained for Ru-doped TiO_2 (-0.25 mm/s) corresponds not only to that of stoichiometric RuO_2 (-0.26 mm/s), but also many other compounds known to contain Ru^{4+}. Additionally, the virtually identical quadrupolar splitting values for RuO_2 and Ru-doped TiO_2 (0.50 mm/s and 0.55 mm/s, respectively) imply a very similar electric field gradient for Ru atoms in both systems and suggests that Ru is present as a substitutional dopant in the TiO_2 lattice.[205] Further experimental studies probed the electronic structure using optical absorption spectroscopy, and found that for Ru-doped TiO_2, absorption bands were observed in the spectrum indicating the presence of impurity

states located in fundamental band gap of TiO_2, attributable to Ru^{4+}, with the Ru^{4+} states being located approximately 1.2 eV above the edge of the top O 2p valence band.[203, 206]

Early theoretical studies investigated the electronic structure of bulk mixed Ru-Ti oxides, examining a range of Ru concentrations. For $Ru_{\frac{1}{4}}Ti_{\frac{3}{4}}O_2$, Ru impurity states were observed in the calculated Density Of States (DOS), occupying the TiO_2 band gap, with the impurity band being of a width of ~ 1.2 eV, with the edges of this band separated from the top of the O 2p valence band and the bottom of the Ti 3d conduction band by ~ 0.5 eV in both cases. Reducing the Ru concentration (and thereby increasing the Ru–Ru dopant separation) to achieve a composition of $Ru_{\frac{1}{24}}Ti_{\frac{23}{34}}O_2$ resulted in a narrowing of the Ru impurity band to ~ 0.37 eV, whilst the barycentre of the Ru impurity band and the TiO_2 fundamental band gap remained largely unchanged, at ~ 1.0 eV above the O 2p manifold.[204] This in fair agreement with the experimentally determined values of ~ 1.2 eV. To determine the symmetry and localisation of the Ru impurity states, the charge density around the Ru atom was calculated. The defect states were identified as possessing a t_{2g}-like symmetry, localised on the Ru dopant atom.

More recent theoretical studies investigated the presence of Ru impurities in a TiO_2 lattice, along with several other combinations of host rutile lattice and dopant metal atom,[44] examining in particular the stability of dopant atoms in the host material. The solubility of Ru in bulk TiO_2 was determined by defining a solubility energy, $E_{sol.}$, according the following equation:

$$E_{sol.} = E_{M_gM_hO_2} + E_{M_hO_2}(1F.U.) - E_{M_hO_2} - E_{M_gO_2}(1F.U.) \qquad (4.1)$$

M_hO_2 and M_gO_2 refer to the host and guest metal oxide systems, respectively. Hence, $E_{M_gM_hO_2}$ refers to the bulk energy of the mixed system with one atom of the host metal replaced with an atom of the guest metal in a $(2 \times 2 \times 2)$ cell, and $E_{M_hO_2}$ refers to the energy of a $(2 \times 2 \times 2)$ cell of the pure guest metal oxide. The terms $E_{M_hO_2}(1F.U.)$ and $E_{M_gO_2}(1F.U.)$ denote the energies for one formula unit of the pure host oxide and the pure guest oxide, respectively. A moderately endothermic solubility energy of 0.63 eV was obtained, which at a first glance might suggest that the substitutional incorporation of Ru into a TiO_2 matrix would be thermodynamically unfavourable. However, it is important to note that the model used does not account for configurational entropies arising from the disorder in the distribution of Ru throughout the TiO_2 bulk matrix, which would present a significant exothermic contribution to the solubility.[207] Hence, one can consider this value to be an upper estimate for the endothermicity of the solubility, making such a process within the bounds of possibility under

real experimental conditions. Electronic structure calculations corroborate earlier work, with impurity states appearing in the TiO_2 band gap under substitutional doping of a transition metal whose rutile oxide is metallic (i.e. Ir and Ru). Segregation energies for the dopant species were also calculated to determine whether dopant atoms are more likely to be found at the surface or deeper in the bulk of the slab. Segregation energies were calculated according the the following expression:

$$E_{seg.} = E_{M_gM_hO_2}(M_g^s) - E_{M_gM_hO_2}(M_g^b) \tag{4.2}$$

where $E_{M_gM_hO_2}(M_g^s)$ refers to the energy of the slab with the impurity atom located in the surface layer, and $E_{M_gM_hO_2}(M_g^b)$ refers to the energy of the slab with the impurity atom located in the bulk of the slab (i.e. in the third of five layers, according to the model used). It was found that for the (110) index, the segregation energy for a Ru atom in a TiO_2 matrix was found to be 0.33 eV, implying that it is thermodynamically slightly more feasible for Ru to be located in the bulk, rather than at the surface. It was also noted, however, that the inclusion of configurational entropy in this case would tend to favour locating the impurity atom at the bulk, hence in practice one can assume that the themodynamic barrier for surface segregation will be greater than the calculated value. In order to investigate the effect of oxidative conditions on surface segregation, further calculations examined the potential for "induced" segregation arising from adsorption of atomic oxygen at surface sites. The oxygen-induced surface segregation was calculated according to the following expression:

$$E_{seg.}(O) = \min[E_{O-M_gM_hO_2}(M_g^s), E_{M_gM_hO_2}(M_g^s) + \frac{1}{2}O_2]$$

$$- \min[E_{O-M_gM_hO_2}(M_g^b), E_{M_gM_hO_2}(M_g^b) + \frac{1}{2}O_2] \tag{4.3}$$

where $E_{O-M_gM_hO_2}(M_g^s)$ and $E_{M_gM_hO_2}(M_g^s)$ refer to the energy of the slab with the dopant atom at the surface, with and without oxygen adsorbed on the surface, respectively. Likewise, $E_{O-M_gM_hO_2}(M_g^b)$ and $E_{M_gM_hO_2}(M_g^b)$ refer to the energy of the slab with the dopant atom located in the bulk, with and without oxygen adsorbed on the surface, respectively. It was calculated whether adsorption of $\frac{1}{2}O_2$ on the surface is exothermic relative to oxygen remaining in the gas phase, and the lowest energy option was taken to determine the segregation energy. The calculated oxygen induced segregation enery for Ru in a $TiO_2(110)$ slab was determined to be -0.38 eV, showing that the presence of oxygen adsorbed on the surface strongly favours segregation of Ru to the surface compared to the clean slab. The results imply then that under oxidative conditions, one can expect to

find at least some dopant Ru atoms located at the surface, making them potentially available as active sites for adsorption.

Further computational studies examined the adsorption behaviour of mixed Ru-Ti rutile oxides under electrochemical HCl oxidation conditions.[208] Based on earlier work, it was established that the oxygen adsorption energy can be considered as a descriptor for electrochemical HCl oxidation.[209, 210] Calculations were performed to determine the effect of the relative position of Ru dopant atoms in a mixed rutile Ru- Ti- oxide system, with several configurations covering all of the potential sites for Ru. It was found that whilst the adsorption behaviour at the Ru dopant atom was substantially similar to that of stoichiometric RuO_2, neighbouring Ti atoms were affected by the presence of Ru; when Ru was placed at the surface, at the $M_{cus.}$ site, the calculated adsorption energy for atomic oxygen (relative to water, according to the equation: $\Delta E(O^c) = E(O^c) - E(^c) - E(H_2O) + E(H_2)$, where $E(O^c)$ and $E(^c)$ are the energies of the slab with and without adsorbed O, respectively, and $E(H_2O)$ and $E(H_2)$ refer to the energies of the corresponding molecules) was found to be $\sim$1.6 eV, compared to $\sim$1.7 eV for stoichiometric RuO_2, but when Ru was placed at the bridging site (with the O atom adsorbed on Ti), the energy $\Delta E(O^c)$ was calculated to be $\sim$3.2 eV, compared to $\sim$5.1 eV for stoichiometric TiO_2. It was also found that this effect strongly depends on the proximity of Ti atoms to the Ru dopant. Previous studies identified an optimal $\Delta E(O^c)$ at around 3.2 eV (since this corresponds to the lowest overpotential for Cl_2 formation under electrochemical HCl oxidation conditions).[209] $\Delta E(O^c)$ values close to this optimal were found for systems with Ru located in a variety of different environments within the system, and for different O coverages, demonstrating that in a real sample, suitable absorption sites will be found under a wide range of conditions. Additional calculations also attempted to simulate the composition of the DSAs used in industry ($Ru_{0.3}Ti_{0.7}O_2$), and found that for this composition, $\Delta E(O^c)$ values remained close to the optimal 3.2 eV for a wide range of different configurations in terms of the Ru environment. It was ultimately proposed that the improvement of activity at Ti sites in Ru-doped TiO_2 was attributed to the donation of electron density from Ru to Ti, corresponding to the studies focusing of heterogeneous catalysis, rather than electrocatalysis.[208]

Clearly, the extensive work already conducted on Ru-doped TiO_2 systems reflects their potential utility and hence it is of interest to further rationalise the behaviour of these systems and to establish further relationships between electronic structure and catalytic activity in the context of heterogeneous catalysis, complementing the exisiting electrochemical studies. It is furthermore of interest to investigate the inclusion of dopants in addition

to Ru in TiO_2, and this concept will be introduced in the next section.

4.2.2 Multiple doping of TiO_2

Given previous results[45] that demonstrate the importance of Br substitu-
tional doping for surface O under HBr oxidation conditions, and the key
role this plays in the catalyst activity, it is illustrative to consider this fac-
tor in conjunction with any proposed modifications of stoichiometric TiO_2
(i.e. substitutionl Ru doping). As far as the author is aware, however,
no previous studies exist considering specifically the effect of Br uptake on
Ru-doped TiO_2. It can still be useful though to review other studies which
consider multiple doping of TiO_2 to gain an insight into the interplay be-
tween these factors.

Previous works show that defective Ti^{3+} states originate from the fact that
when replacing surface O for Br, there is a change in the anionic oxidation
state (from O^{2-} to Br^-) which needs to be compensated by a change in
the oxidation state in one of the cationic species.[45] As has been established,
substitutional doping of Ru for Ti does not induce any such changes since in
both stoichiometric RuO_2 and TiO_2, the transition metal adopts the same
4+ oxidation state, and hence no charge compensation is required.[203] How-
ever, further doping with different species that do not match the oxidation
state of the species that it displaces should induce defect formation. Triggs
et al. also considered doping of TiO_2 with both Ru and Ta. Earlier works
examined Ta doping of TiO_2 and found that such samples showed higher
conductivity than stoichiometric TiO_2.[211] This was attributed to the forma-
tion of Ti^{3+} defect states; since Ta formally adopts a 5+ oxidation state, it is
necessary for charge compensation to occur when Ti^{4+} is replaced by Ta^{5+}.
Mössbauer studies on TiO_2 containing both Ru and Ta showed features
which can be attributed to both Ru^{4+} (as in the Ru-only doped sample)
and Ru^{2+}, suggesting that Ru acts as an electron trap, with the formation of
reduced Ru sites being favoured over reduced Ti sites which are observed for
Ta-only doped TiO_2.[205] Additionally, optical absorption spectroscopy stud-

ies provide further evidence for this phenomenon, with bands associated
with the Ru^{2+} oxidation state appearing in the spectrum at higher Ta con-
centrations, in addition to Ru^{3+} related bands at lower Ta concentrations,
which is consistent with the overall charge compensation. Analogous studies
which examine doping of TiO_2 with both Ru and Nb yield virtually identical
optical absorption spectra, supporting the interpretation of the Ta doped
spectra since both Ta and Nb behave as electron donor species in TiO_2.[203]

Hence, it can be seen that when other dopants are present in a TiO_2 matrix
in addition to Ru, any charge mismatches induced by substitutional doping

of Ti for species with a different oxidation state are preferentially compensated for by defect formation on Ru rather than Ti. Since it has already been established that substitution of O for Br in otherwise stoichiometric TiO_2 results in the formation of Ti^{3+} defect states, it is plausible that the same phenomenon ocurring in Ru-doped TiO_2 would result in the formation of Ru^{3+}. Hence, it is of interest to investigate this possibility and determine its role in HBr oxidation processes.

4.2.3 B-doped TiO_2

It has been established that substitutional doping in TiO_2 can induce defect formation[203, 204] which can improve the activity of the material towards oxygen dissociation under hydrogen halide oxidation conditions.[45] In the case of HBr oxidation, replacement of surface O for Br results in the formation of one Ti^{3+} defect state per Br atom incorporated. Dissociative adsorption of oxygen, however, necessarily requires two adjacent active sites on the catalyst surface. Hence, it is of interest to consider potential dopants which can yield multiple defect states per dopant atom incorporated.

Many experimental studies on B-doped TiO_2 have been conducted, since the system has attracted attention for photonic applications which intend to modify the light absorption behaviour of TiO_2 so that absorption in the visible part of the spectrum is possible. Whilst X-ray Photoelectron Spectroscopy (XPS) provide clear information on the oxidation state of B in B-doped TiO_2 samples, suggesting that incorporated B exists in the B^{3+} oxidation state,[212, 213] different UV-visible reflectance absorption spectroscopy studies have yielded somewhat contradictory results regarding the optical behaviour of B-doped TiO_2. Whilst one study recorded a red-shift in adsorption compared to undoped TiO_2, with the band gap being reduced to 2.93 eV from 3.18 eV,[213] another found a blue-shift in adsorption, indicating that the band gap hand increased after B doping.[214] Further experimental studies suggest that these discrepancies orginate from the highly varaible morphology of the doped samples. TiO_2 exists as several polymorphs (anatase, brookite and rutile), and all of these polymorphs may coexist in samples. For instance, he observed blue-shift in adsorption observed for B-doped TiO_2 was attributed to a lower rutile to anatase ratio induced by B doping (since stoichiometric rutile has a slightly smaller band gap than anatase).[215] Clearly, the wide range of structural possibilities makes it challenging to identify the precise cause of experimentally observed phenomena,[216] and the exact morphology of samples used in experimental studies depends strongly on the preparation method used.

Comprehensive theoretical studies examined the geometric and electronic

structure of the doped materials and attributed the apparent experimental discrepancies to variations in the B dopant environment. Boron may be incorporated into the TiO_2 lattice either substitutionally or interstitially. Substitutional doping can potentially occur via the replacement of either Ti or O for B. Substitution of Ti for B was found to be energetically unfeasible, attributed to the large difference in size of the B and Ti atoms. The red-shift in adsorption was attributed to the appearance of gap states near the bottom of the conduction band, arising from substitutional doping of O for B, with excitation from the valence band to the empty gap states explaining the reduction in absorbed frequency.[217,218] It was also found that the B impurity state was somewhat delocalised, with the B impurity state overlapping with the O 2p valence states. The B dopant atoms donate electron density to neighbouring O atoms, which in turn affect the oxidation state of Ti, implying not only that B exists in a somewhat oxidised state, but its presence can also affect nearby Ti atoms. The observed blue-shift was accounted for by the population of the bottom of the conduction band arising from B interstitial doping; this results in an increase in the absorbed light frequency due to the so-called band-filling mechanism, whereby electrons occupied in the top of the conduction band are excited to the lowest unoccupied states, which are now slightly higher in energy due to the partial occupation of the bottom of the conduction band.[219]

Theoretical studies aimed at relating the various experimental results with specific structural environments were conducted.[220] Focusing on the rutile (110) facet, a comprehensive selection of configurations were investigated, covering a variety of substitutional and interstitial B doping environments. It was found that for anionic substitutional doping, the most stable configurations accommodated B doping atoms at positions located in the horizonatal plane, bonded in a three-coordinate trigonal planar manner parallel to the plane of the 110 surface, with the subsurface position being more stable. For cationic substitutional doping, the tested configurations were found to be largely unstable compared to anionic substitutional doping, with the subsurface positions again being the most stable. For interstitial doping, several configurations featuring the B dopant atom located in different cavities within the TiO_2 lattice found the most stable configuration accommodated the B atom in a 4-coordinate environment with O. It was also noted that the 4-coordinate interstitial position was the most stable of all, moreso than any of the tested substitutional configurations. Investigating the electronic structure of the interstitially doped system, the calculated Projected Density Of States (PDOS) showed that the B 2p impurity states appear at the bottom of the O 2p valence band; no impurity states were observed in the band gap. It was also noted that the increase in the Ti-O

bond distance induced by the B impurity causes a shift in the Ti 3d conduction band to a slightly higher energy, widening the band gap; this was suggested as another possible explanation for the experimentally observed blue shift in light absorption.

In this study, only interstitial doping of B in TiO_2 is considered, since it is established to be the most stable manner in which B may be incorporated into the TiO_2 lattice. Investigations focus on the electronic structure and the adsorption behaviour of key components in hydrogen halide oxidation processes, a novel application of this material. The study examines the interplay between electronic structure and catalytic activity, and comparisons are made between related systems.
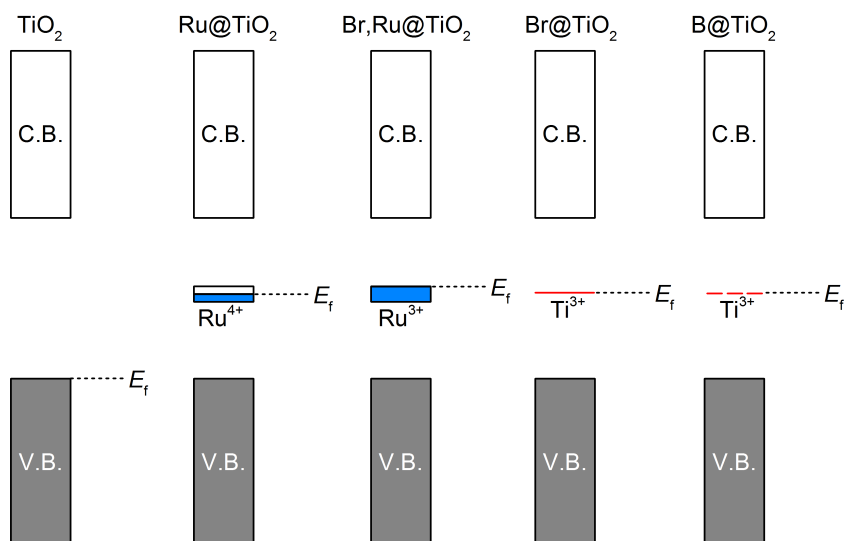
Figure 4.1: Schematic diagrams depicting the various changes in the electronic structure in the fundamental band gap of TiO_2 induced by dopant atoms.

4.3 Results

The electronic structure of the materials investigated can be visualised through Density of States plots (DOS). The DOS plots obtained allow for a convenient, qualitative measure by which the different systems may be compared. DOS plots were generated for Ru-doped TiO_2, Br-doped TiO_2, Ru- and Br-doped TiO_2, and B-doped TiO_2, along with the host system,

undoped TiO_2, to afford a clear comparison. Values for the workfunction, ϕ, were also obtained for some of the most important systems. Adsorption energies for species relevant to hydrogen halide oxidation were calculated for a selection of systems.

4.3.1   Density of States

Undoped TiO_2 is a semiconductor, and as such has a small band gap. The calculated band gap of ~ 1.5 eV is much smaller than the experimentally observed value (~ 3.2 eV),[221] most likely owing to the inherent difficulties in DFT in reproducing band gaps for semiconductors due to the self-interaction error. In this study, however, it is primarily of interest to compare related systems in a consistent manner, hence the presence of such systematic errors does not greatly affect the qualitative interpretation of the results. The DOS shows the usual features: the occupied valence band, primarily composed of O 2p states, and the unoccupied conduction band, consisting of vacant Ti 3d states.

As has already been established, substitutional doping of TiO_2 with species whose oxidation states are different from the element being displaced tends to cause defect states to appear in this band gap. As previously studied,[45] the self-doping that originates from Br uptake in clean TiO_2 gives rise to Ti^{3+} defect states, which are clearly visible in the calculated Br-doped DOS. The defect states appear as a small, localised, partially occupied density of states just below the Ti 3d conduction band.

Doping of Ru in TiO_2 also contributes states to this gap, with a band attributed to Ru 3d appearing in the mid gap. Otherwise, the overall structure of the DOS appears to be substantially the same as for stoichiometric TiO_2. implying that the Ru states are, generally speaking, simply contributing to the existing electronic structure, without inducing any major changes in it. Rather than a more localised impurity state appearing, as with Br doping of TiO_2, a much broader band appears for Ru-doped TiO_2, reflecting the metallic character of RuO_2.

Combining these two doping strategies, however, appears to have a more profound effect, with a large band appearing just below the Fermi level, in the middle of the band gap. This can be attributed to the formation of Ru^{3+} defect states arising from Br self-doping in a manner completely analogous to that of clean TiO_2.[45] While Br self-doping of clean TiO_2 yields a single, localised defect state, the same process in Ru-doped TiO_2 yields a defect band in the midgap. As with Ru-only doped TiO_2, the slight overlap of Ru d states leads to a broadening of the defect states. Clearly, such a broadening is not observed for Br-doped TiO_2. The DOS appears to be similar

4.3. RESULTS 103

to that obtained for Ru-only doped TiO_2, but the change in Ru oxidation state arising from Ru^{3+} defect formation causes an increase in the density of states of the impurity band below the Fermi level, as the DOS is shifted down in energy.

Introducing interstitial B atoms into TiO_2 results in the formation of multiple defect states, in comparison to only one with Br self-doping, as evidenced from the DOS plots, with two large peaks being visible for B-doped TiO_2 (appearing below the Fermi level above the valence band), along with a smaller partially filled contribution just below the Ti 3d conduction band. For Br-doped TiO_2, on the other hand, only one can be seen just below the Fermi level. As with the comparison between Ru-doped TiO_2 and Ru- and Br- co-doped TiO_2, there is no radical difference between Br-doped TiO_2 and B-doped TiO_2, with both types of doping resulting in localised Ti^{3+} defect states. It is notable, however that the introduction of B results in an increased number of these states, reflecting the oxidation of B to B^{3+} and the subsequent redistribution of its electrons among neighbouring Ti atoms. This was confirmed by further calculations to determine the spin density of the system. The visualisation clearly shows the appearance of two localised defect states at adjacent neighbouring surface Ti atoms, indicating their reduction to Ti^{3+} and the presence of a single unpaired electron occupying the defect states. This is also reflected in the DOS, since the defect states are only evident in one of the spin channels, indicating unpaired electrons. The third electron originating from B is somewhat more delocalised, with a small spin density appearing on the subsurface Ti atoms closest to the interstitial B. This is likely reflected in the DOS as the broader defect state appearing just below the conduction band. Furthermore, the calculated spin denisty shows that the two localised surface defect states have unpaired electrons of the same spin, whilst the subsurface defect has an unpaired electron of the opposite spin, which further supports the interpretation of the DOS. Since the broader defect band appears only in the spin channel opposite to the two narrower defect states, it can be assigned with some degree of confidence.
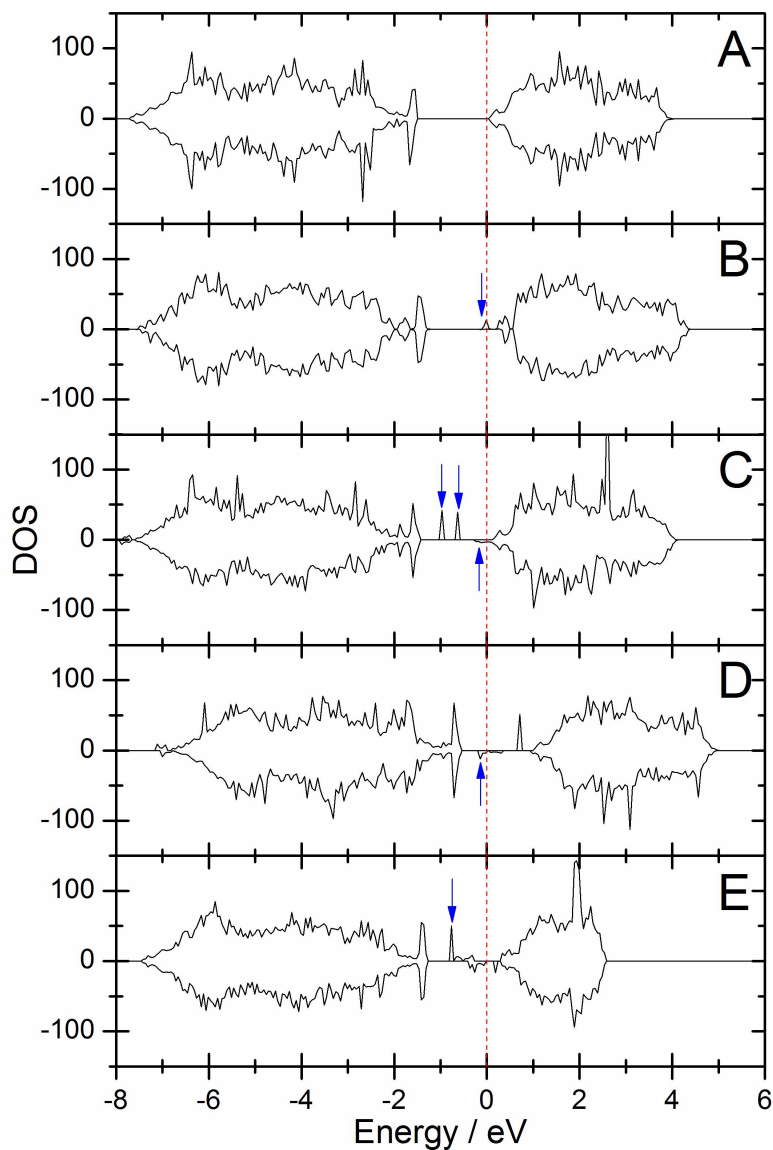
Figure 4.2: Computed DOS plots for a variety of TiO_2-based systems. A: Clean TiO_2. B: Br-doped TiO_2. C: B-doped TiO_2. D: Ru-doped TiO_2. E: Ru- and Br-doped TiO_2. The Fermi level is set to zero and is indicated by the red dashed line. Defect states are indicated with blue arrows where appropriate.
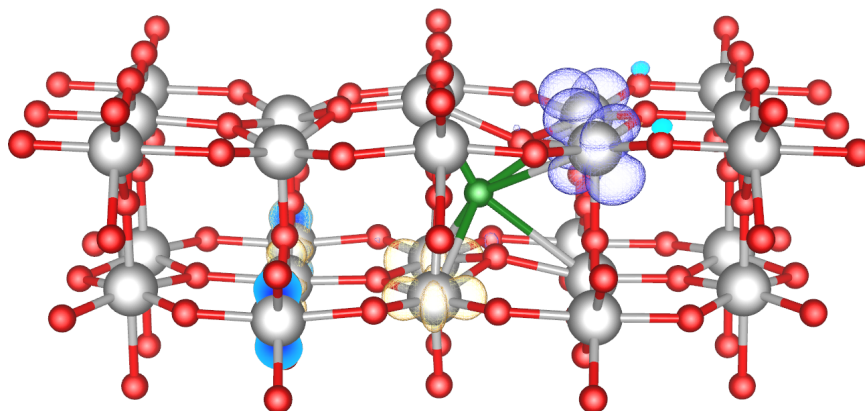
Figure 4.3: Spin density plot for B-doped TiO_2. Note the presence of excess spin density on adjacent surface Ti atoms, indicating that they are indeed defective, formally Ti^{3+} centres. Legend: Ti: grey; O: red; B: green. The blue spin density regions correspond to the spin up channel, whilst the yellow spin density regions correspond to the spin down channel, in accordance with plot C in Figure 4.2.

4.3.2 Work-functions

In addition to calculating the DOS for each of the systems, the work-function also determined for several of the most important to provide further insights into the relative Fermi levels of the materials. For stoichiometric TiO_2, a work-function of 6.86 eV was obtained. For both B-doped TiO_2 and Ru- and Br- doped TiO_2, a reduction of the work-function was observed, confirming the presence of occupied gap states responsible for an increase in the Fermi level. For Ru- and Br-doped TiO_2, a work-function of 5.44 eV was obtained, and for B-doped TiO_2 the work-function was calculated to be 6.44 eV.

Table 4.1: Selected work-functions for several of the systems investigated.

System	ϕ / eV
Stoichiometric TiO_2	6.86
B-doped TiO_2	6.44
Ru- and Br- doped TiO_2	5.44

4.3.3   Adsorption and Reactivity

Adsorption energies for species relevant to hydrogen halide oxidation processes were calculated, namely atomic O, Cl and Br (relative to $\frac{1}{2}X_2$, where X is O, Cl or Br), as well as dissociated and undissociated O_2. From the calculated adsorption energies, it is immediately evident that doping of TiO_2 with species that induce the formation of defects can greatly enhance the adsorption of relevant species, especially oxygen dissociative adsorption. Whilst the adsorption of every species tested is endothermic for stoichiometric TiO_2, for both of the doped systems investigated, Ru- and Br-doped TiO_2 and B-doped TiO_2, the inverse is true. Adsorption of atomic O is endothermic by 2.16 eV for stoichiometric TiO_2. It is notable that atomic O adsorption for the Ru- and Br-doped system is more exothermic when adsorption takes place on the Ru site (-1.58 eV), rather than a Ti site (-0.25 eV). The most exothermic atomic O adsorption energy was observed for B-doped TiO_2, at -2.24 eV. The energy for dissociated O_2 (i.e. 2O) is especially remarkable; for stoichiometric TiO_2, the value obtained is very endothermic at 4.55 eV, compared to that of B-doped TiO_2 which is strongly exothermic at -1.77 eV. It is also of interest that the adsorption energy for 2O is more exothermic for B-doped TiO_2 than for Ru- and Br-doped TiO_2 (-1.41 eV). Similarly, the energy for dissociative adsorption of O_2 over Ru- and Br-doped TiO_2 is less exothermic than the sum of the atomic O adsorption energies over Ru and Ti. In contrast, the adsorption energy for undissociated O_2 is rather similar for B-doped TiO_2 and Ru- and Br-doped TiO_2 (-1.49 and -1.41 eV, respectively).

Similar trends are observed for halogen adsorption. Both of the doped systems show exothermic adsorption energies for both Cl and Br, whilst stoichiometric TiO_2 yields endothermic values (0.52 and 0.69 eV for Cl and Br, respectively). B-doped TiO_2 gives the most exothermic values, with atomic Cl and Br adsorption energies at -1.96 and -1.65 eV, respectively. For Ru- and Br-doped TiO_2, the adsorption energies are most exothermic when adsorption takes place at Ru (-1.48 and -1.20 eV for Cl and Br, respectively), rather than at Ti (-0.80 and -0.43 eV for Cl and Br, respectively). As a general trend, Br adsorption appears to be more exothermic than Cl (the only exception being stoichiometric TiO_2). For the doped systems, Br adsorption is more exothermic by 0.32 eV on average.

Table 4.2: Calculated adsorption energies for species relevant for HX oxidation on a variety of systems.

System	$E_{ads.}(\text{O})$	$E_{ads.}(\text{O}_2)$	$E_{ads.}(\text{2O})$	$E_{ads.}(\text{Cl})$	$E_{ads.}(\text{Br})$
Stoichiometric TiO$_2$	2.16	1.35	4.55	0.52	0.69
B-doped TiO$_2$	-2.24	-1.49	-1.77	-1.96	-1.65
Ru & Br doped TiO$_2$ (@Ru)	-1.58	-1.41	-0.73	-1.48	-1.20
Ru & Br doped TiO$_2$ (@Ti)	-0.25	-1.41	-0.73	-0.80	-0.43

4.4 Discussion

Taking the calculations for the DOS, work-functions and adsorption energies together, it is possible to gain some insights into the relationship between electronic structure and catalytic activity. It is clearly evident that doping, and the changes it induces in the electronic structure, have a profound effect on adsorption energies. The formation of electronic defects localised on surface metal atoms can greatly alter the adsorption energy on that site; in the system examined in this study, adsorption of O, Cl and Br are all significantly more exothermic at defective Ti^{3+} and Ru^{3+} sites than at non-defective Ti^{4+} sites. It is possible to rationalise the effect of defects on adsorption in terms of the relative energies of the Fermi level and the atomic and molecular orbitals associated with the adsorbates. Firstly, one can rationalise the stark differences in O dissociative adsorption for the stoichiometric and doped TiO$_2$ systems. The calculated adsorption energies show that for the doped systems, O dissociative adsorption is moderately exothermic, whilst for the stoichiometric system, the process is strongly endothermic. This can be attributed to the fact that for stoichiometric TiO$_2$, the O$_2$ π^* orbitals lie at a much higher energy than the Fermi level (located at the top of the O 2p valence band), making electronic injection from the Fermi level into into the π^* orbitals (thus facilitating dissociation) highly exothermic. In contast, doping the system causes the appearance of occupied defect states in the fundamental band gap, thus raising the Fermi level to an energy above that of the O$_2$ π^* orbitals, making such electronic injection to the antibonding states facile. A similar reasoning can be employed to explain the observed variations in halogen adsorption energies. The stronger bonding of Br to the doped systems can be attributed to the smaller bond dissociation energy for Br$_2$ compared to Cl$_2$, and the higher lying Br 3p orbitals which lie closer to the Fermi level of the material and thus afford stronger bonding to the surface of the catalyst.

The more exothermic adsorption observed at Ru sites compared to Ti sites in Ru- and Br-doped TiO$_2$ requires a more in-depth analysis. The Br dopant introduces one defect state at the surface, as evidenced by the narrow states

appearing in the band gap in the DOS for Br-only doped TiO_2. In Ru- and Br-doped TiO_2, the defect state can be localised on either Ru or Ti, and in both cases, adsorption is more exothermic than for stoichiometric TiO_2. Hence, the more exothermic adsorption energy for adsorption on Ru cannot be explained only in terms of the mere presence of defect states, but by also considering the inherent differences between the Ru and Ti sites and the resulting defect states when Br doping is applied. Essentially, whilst defect state formation in doped TiO_2 shifts the Fermi level from the top of the O 2p valence band to the partially filled Ti 3d defect band associated with Ti^{3+}, in Ru-doped TiO_2, co-doping with Br shifts the Fermi level from the partially filled Ru^{4+} impurity band to that of Ru^{3+}. It happens that this Fermi level shift means that the Fermi level lies at an energy that facilitates bonding with the relevant species to a greater extent for Ru- and Br-doped TiO_2 than Br-doping alone. Whilst Br doping of TiO_2 greatly enhances adsorption by the formation of highly active Ti^{3+} defect states, stoichiometric RuO_2 already shows a highly exothermic O adsorption energy (-1.01 eV for atomic O), hence combining the formation of a defect state with the inherent activity of Ru towards oxygen adsorption leads to an adsorption energy which is more exothermic than either case. Given the inherent differences between Ru and Ti, with Ru^{4+} having a partially occupied 4d band, and Ti^{4+} having an empty 3d band, the addition of an extra electron resulting from defect formation and consequent reduction of the metal site has a much greater effect on Ti than on Ru. For Ti, defect formation radically alters the local electronic structure by causing the occupation of a formerly empty band, whereas for Ru, reduction of Ru^{4+} to Ru^{3+} can be seen as merely a small modification in its electronic structure, since both Ru^{4+} and Ru^{3+} ultimately have a partially filled d band. This can clearly be seen by comparing the calculated DOS for Ru-doped TiO_2 and Ru- and Br-doped TiO_2, with the Ru impurity states merely being slightly shifted after Br co-doping.

The investigation of B-doped TiO_2 reflects another aspect of doping, which is the number of defect states induced by a dopant atom. In the case of substitutional anionic doping of Br for O in TiO_2, Br adopts its most stable -1 oxidation state. Since O^{2-} is being displaced by Br, this induces the formation of one Ti^{3+} defect per Br dopant; essentially atomic Br donates its valence electron to a Ti^{4+} atom in the lattice. For interstitial B doping, a similar phenomenon occurs, but since atomic B has three valence electrons, this induces the formation of three Ti^{3+} defect states. These defect states are clearly present in the band gap of the computed DOS for B-doped TiO_2. As can be seen from the calculated spin density plots, two of the defects are located at adjacent surface Ti sites, confirmed by the spin polarisation

of the defect states appearing in the DOS. This feature is responsible for the highly exothermic dissociative adsorption of O_2 for the B-doped TiO_2 system. The presence two highly active M^{3+} sites on the surface of B-doped TiO_2, compared to only one for Ru- and Br-doped TiO_2, allows both O atoms after dissociation can be accommodated on the highly active defect sites. In contrast, for the Ru- and Br-doped TiO_2 system, there necessarily is only one such additional electron from Br to permit defect formation. Hence, it can be seen that the number and relative position of electronic defects at the surface plays a key role in controlling activity.
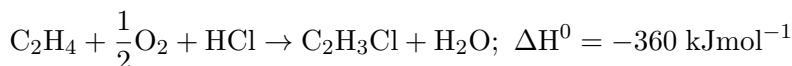
4.5 Conclusions

In this chapter, several TiO_2-based doped systems were examined, exploring the differences in electronic structure and activity induced by different dopants. It is clear that the presence of defect states arising from doping in TiO_2 have major consequences for the adsorption behaviour (and consequently the catalytic activity) of the system, as has been established in previous works on the subject.[45, 194] This study demonstrates that activity can be further modified by considering the nature of the surface atom at which a defect is localised, the number of defects formed per dopant atom, and the relative configuration of defect states. For the adsorption of atomic species, it is only really the first factor that is of great importance, given that atomic species tend to occupy only one active site by definition, however for larger adsorbates consisting of more than one atom, the number and configuration of defect states becomes crucial to the adsorption of the species. The choice of dopant can radically alter the electronic structure of the same host material, meaning that many options exist for controlling catalytic activity. By considering the mechanism of a given reaction on the atomic and electronic level, it is possible to make a judicious selection of dopant to modify the host material in a manner conductive to catalysis. It is intended that future developments will allow for rational catalyst design, with multiple doping strategies allowing for optimal catalytic activity to be achieved.

Chapter 5

Mechanism of Ethylene Oxychlorination over Ruthenium Oxide

In Chapter 3, RuO_2 was investigated as a potential catalyst for HBr oxidation, having already been well-established for the superficially similar HCl oxidation. In this chapter, chlorination processes over RuO_2 are revisited, but this time considering the utility of RuO_2 as a catalyst for ethylene oxychlorination. The inclusion of an additional reactant in the input gas feed affords an additional dimension of selectivity, compared to the much simpler HCl oxidation. The two main products of industrial interest are ethylene dichloride (EDC) and vinyl chloride monomer (VCM). Ethylene oxychlorination to these products occurs according to the following chemical equations:

$$C_2H_4 + \frac{1}{2}O_2 + 2HCl \rightarrow C_2H_4Cl_2 + H_2O; \ \Delta H^0 = -483 \ \mathrm{kJmol}^{-1}$$

$$C_2H_4 + \frac{1}{2}O_2 + HCl \rightarrow C_2H_3Cl + H_2O; \ \Delta H^0 = -360 \ \mathrm{kJmol}^{-1}$$
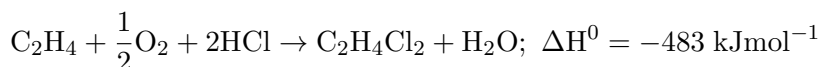
Whilst VCM can be directly polymerised to obtain the industrially valuable PVC, most ethylene oxychlorination processes yield EDC as the major product. VCM can be obtained from EDC by thermal cracking, with excess HCl being produced as a byproduct. In this chapter, calculations are performed to obtain a complete perspective on the various competing processes taking place on $RuO_2(110)$ under ethylene oxychlorination conditions. Supported by experimental studies, the calculations shed light on the origin of selectivity and allow for a detailed analysis of the catalyst behaviour. By comparing with other catalysts, one can identify the essential requirements for a good oxychlorination catalyst.

111

5.1 Previous Work

5.1.1 RuO$_2$ as a C$_2$H$_4$ oxidation catalyst

As the experimental studies discussed in Chapter 1 demonstrated, the composition of CuCl$_2$ based oxychlorination catalysts is extremely sensitive to the reaction conditions, with multiple factors influencing activity. The addition of dopant atoms can affect activity in two main ways, firstly by increasing the fraction of Cu present in the active phase, and secondly by changing the reducibility of the Cu(II) sites through the formation of a new mixed chloride active phase. Clearly, with so many variables affecting catalytic behaviour, modelling these systems computationally is extremely challenging, and as hence few such studies exist, making the firm establishment of structure-activity relationships difficult. Combined with the tendancy of this type of catalyst to undergo volatisation under the intense reaction conditions, other researchers have taken interest in alternatives, with RuO$_2$-based catalysts showing some of the most promising experimental and theoretical results.

Computational studies investigated the selectivity of RuO$_2$ as an ethylene oxidation catalyst, complementing the experimental works discussed in Chapter 1.[151] As it has already been established that O$_{cus}$ plays a key role in the reaction mechanism, DFT calculations were performed and applied to *ab initio* thermodynamics studies to determine the relationship between the extent of oxygen coverage on the surface and the O$_2$ partial pressure. The results suggested that over a wide range of O$_2$ partial pressures, O$_{cus}$ coverages range from between 0.25 ML to 0.75 ML, which is broadly commensurate with the experimental studies.[150] In light of the high O$_{cus}$ coverage, further calculations examined the adsorption energy of relevant species, both reactants and products, as a function of coverage. Generally, it was observed that higher coverages tend to result in weaker adsorption, due to destabilisation caused by crowding on the catalyst surface. The exceptions to this are species which can either form hydrogen bonds or react with adjacent O$_{cus}$, hence for adsorbates such as H$_2$O and the epoxide C$_2$H$_4$O, adsorption is more exothermic at higher O$_{cus}$ coverages. For the whole range of O$_{cus}$ coverages, H$_2$O is strongly adsorbed, whilst the proposed oxidation products, acetaldehyde and ethylene epoxide, as well as oxygen (both molecular and atomic O) are more weakly adsorbed. Ethylene and formaldehyde are adsorbed yet more weakly, with adsorption energies less exothermic than -0.45 eV across the whole range of O$_{cus}$ coverages.

Turning now to ethylene oxidation, the calculated adsorption energy for C$_2$H$_4$ was found to be only -0.25 eV, supporting the experimental results which suggest that adsorption is weak and the C-C double bond is preserved.

Formation of the OMME intermediate was found to be facile, with an activation barrier of 0.47 eV and being exothermic by 0.57 eV. The calculated C-O bond lengths are consistent with the change from a C-C π bond to a σ bond proposed by the experimental studies.[150] A proposed mechanism for the formation of partially oxidised products from the OMME intermediate involved either a ring closure to form the epoxide, or a 1,2-H shift to form acetaldehyde. The calculations for these processes suggest that acetaldehyde formation is the preferred option, since this process is strongly exothermic at -1.01 eV, whilst the epoxide formation is practically thermoneutral at -0.03 eV, and the activation barrier is slightly lower, at 1.25 eV compared to 1.36 eV. The strength of adsorption of these compounds is comparable to that of O_2, and considerably larger than that of C_2H_4, suggesting that acetaldehyde and ethylene epoxide would be retained on the surface to the exclusion of ethylene, hindering the reaction, in contrast to the relative adsorption energies of methanol and formaldehyde in methanol oxidation. The calculations support the experimental conclusions that epoxide formation does not occur, with both thermodynamic and kinetic factors acting against its production.

The previous works show that the highly oxidative character of RuO_2 limits its utility as a catalyst for ethylene oxidation. The results show, however, that the oxidation behaviour is strongly dependent on the presence of coadsorbed O_{cus}, and selectivity is at least partially controlled by the ability of O_{cus} to move on the surface in order to react with adjacent species. Relating this to ethylene oxychlorination, clearly the overly oxidative behaviour could be a potential pitfall for RuO_2 as an oxychlorination. However, it is also important to consider the competitive adsorption between O and Cl on the surface and the impact this will have on the selectivity of the catalyst, thus warranting a detailed theoretical investigation of the oxychlorination reaction over RuO_2.

5.2 Experimental evidence

Experimental studies were conducted by collaborators from the Pérez-Ramírez group at ETH Zürich, examining the utility of a variety of metal oxide systems as ethylene oxychlorination catalysts.[222] The systems investigated, IrO_2, RuO_2 and CeO_2, were selected as they satisfy the prerequiste of being able to facilitate HCl dissociative adsorption necessary for any oxychlorination catalyst.[152] The gas-phase HCl oxidation and ethylene oxychlorination were investigated at ambient pressure in a continuous-flow fixed-bed reactor, providing valuable information on the conversion rate of ethylene, and the product distributions obtained.

The experimental set up consisted of mass flow controllers for each of the three reactants, C_2H_4, HCl and O_2, as well as He to act as a carrier gas and Ar to act as an internal standard. The input gases were fed into a quartz microreactor, containing the catalyst sample, where the reaction takes place and the products are formed. Downstream heat tracing was employed to prevent premature condensation of the products, and finally the products were fed into a combined gas chromatograph and mass spectrometer to analyse the composition of the output feed as it arrives from the reactor. Hence, by this method it is possible to gain insights into selectivity by varying the reaction conditions (e.g. temperature, input feed composition, etc.) and taking on-line measurements of the product distributions. Tests were conducted to examine the catalysts for both the Deacon reaction and for ethylene oxychlorination in order to establish if there is any clear relationship between Deacon activity and oxychlorination activity of the materials. The input gas feed composition was set to reflect the stoichiometry of the reactions being tested, with low concentrations of reactants in order to limit damage to the equipment due to the corrosive environment of the reaction mixture; for HCl oxidation, the input gas contained 3% HCl and 6% O_2 by volume, and for ethylene oxychlorination the input gas contained 3% C_2H_4, 3% HCl and 1.5% O_2.

In order to fairly compare the three catalysts, the product composition was obtained for a temperature T_{20}, which is defined as the temperature at which $20 \pm 1\%$ C_2H_4 conversion is obtained. The results show that RuO_2 is clearly the most active catalyst for HCl oxidation, in line with its well-known utility as a Deacon catalyst, achieving 20% selectivity at only 462 K, compared to 652 K for IrO_2 and 673 K for CeO_2 (Figure 5.1). However, for ethylene oxychlorination, whilst RuO_2 is still the most active with a T_{20} of 623 K, the trend for oxidation is reversed as CeO_2 has a T_{20} of 646 K for oxychlorination, compared to 698 K for IrO_2. Turning now to the product compositions, IrO_2 does not appear to facilitate the formation of any chlorinated carbon products, with only combustion products (CO_2 and CO) being observed. RuO_2 and CeO_2, on the other hand, yield a mixture of products, with EDC and VCM being formed in addition to the combustion products. CeO_2 shows a much greater selectivity for EDC formation than RuO_2, with 88% of the product obtained being accounted for by EDC for CeO_2, compared to 18% for RuO_2. RuO_2 shows a slightly higher selectivity for VCM formation, with 9% VCM compared to just 3% for CeO_2. Hence, in total chlorinated products account for 27% of the products obtained over RuO_2 and 91% for CeO_2. In contrast to their activity as Deacon catalysts, none of the materials exhibited Cl_2 formation under oxychlorination conditions; for IrO_2 and RuO_2, the significant extent

5.2. EXPERIMENTAL EVIDENCE   115

of combustion means that oxygen is mostly consumed to fuel this process, meaning that virtually none is available for Deacon-type HCl oxidation. Similarly, the strong selectivity of CeO_2 towards oxychlorination means that most of the HCl present in the input gas feed is consumed in the formation of EDC and VCM, rather than through oxidation.

The results clearly show that the relationship between a good Deacon catalyst and a good oxychlorination catalyst is complex. Whilst all of the catalysts tested satisfy the basic requirement of being able to facilitate HCl dissociative adsorption, the product composition demonstrates that good Deacon activity does not necessarily correlate to good selectivity towards the desired oxychlorination products.[151, 152] Whilst RuO_2, IrO_2 and CeO_2 show moderate or good Deacon activity, with RuO_2 clearly being the most active, for oxychlorination IrO_2 fails entirely to produce EDC or VCM in any quantity, with RuO_2 affording only modest production and CeO_2 demonstrating very good selectivity to these products. Evidently, multiple factors are relevant in controlling the selectivity of oxychlorination catalysts. As previous works have already identified, some oxide catalysts can result in excessive oxidation compared to traditional $CuCl_2$-based oxychlorination catalysts, and in many cases oxychlorination selectivity is reduced at elevated temperatures. Additionally, it is also evident that both RuO_2 and CeO_2 are capable of producing both VCM and EDC, and studies suggest that EDC formation results from subsequent reaction of VCM in the presence of acidic sites. Therefore, in light of these multiple observed factors, it was decided that all further experimental and the theoretical studies will focus on RuO_2, as its behaviour as a good Deacon catalyst, but modest oxychlorination catalyst, will permit the identification of both strengths and limitations of Deacon catalysts for oxychlorination.

Further experimental tests on RuO_2 investigated the effect of variation in the reaction temperature (Figure 5.2). Decreasing the temperature from 683 K to 473 K, the C_2H_4 conversion rate remained steady at ~20% until 623 K, when a sharp drop to around 7% occurs. It was also observed that whilst at high temperatures combustion products dominate (with CO only being produced at the very highest temperatures), for lower temperatures (523 K), only EDC was observed. Only moderate VCM formation is observed between 523 K and 653 K, with a maximum at 573 K. Evidently, the temperature of operation plays a key role in controlling selectivity between oxidation and chlorination processes.

Turning now to examine the effect of varying the proportion of HCl in the input gas feed, measurements were taken in the range from 1% to 9% (Figure 5.2). This corresponds to the extent of Cl coverage induced over the temperature range employed in Figure 5.1. C_2H_4 conversion remains
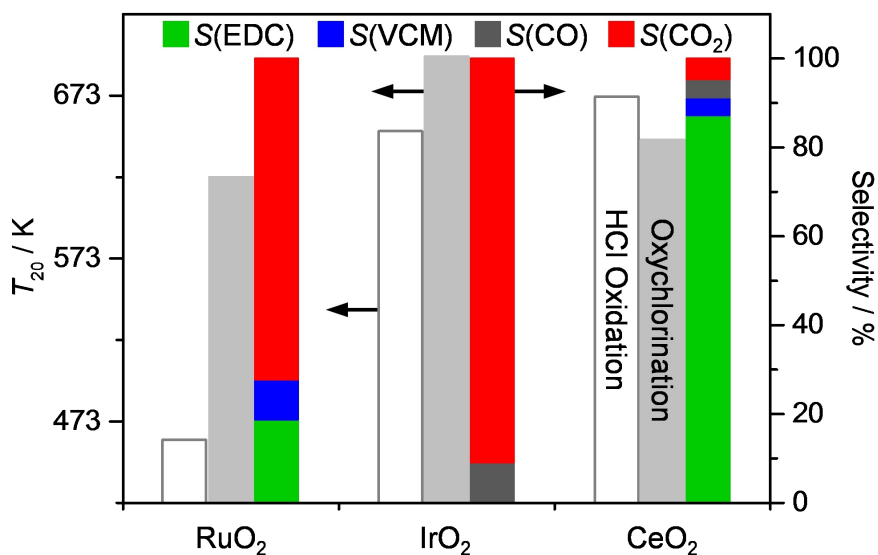
Figure 5.1: T_{20} for HCl oxidation (white bar) and ethylene oxychlorination (grey bar) with corresponding product compositions for ethylene oxychlorination over RuO_2, IrO_2, and CeO_2.

roughy constant across the HCl feed content range at about 27%, with a small minimum of 24% conversion at 3% HCl by volume. Increasing the HCl feed content beyond 3% results in a steady increase in conversion up to 33% at 9% HCl vol. Increasing the HCl feed content results in a virtually linear decrease in the proportion of CO_2 in the product distribution, and likewise causes a first-order increase in EDC production. A first order increase in VCM production is also observed with increasing HCl feed content, but at a smaller gradient than that of EDC.

The experimental results show that both temperature and HCl feed content have a profound effect on selectivity. Therefore, theoretical investigations conducted in this study aim to elucidate the key mechanistic processes involved in ethylene oxychlorination. By calculating reaction energies and activation barriers, insights into the interplay between kinetic and thermodynamic control can be obtained, potentially offering an explanation for the temperature dependence of the selectivity. Furthermore, an atomic-scale understanding of the elementary steps of the reaction can allow one to draw conclusions on the mechanism and the role of coadsorbed species on the selectivity.
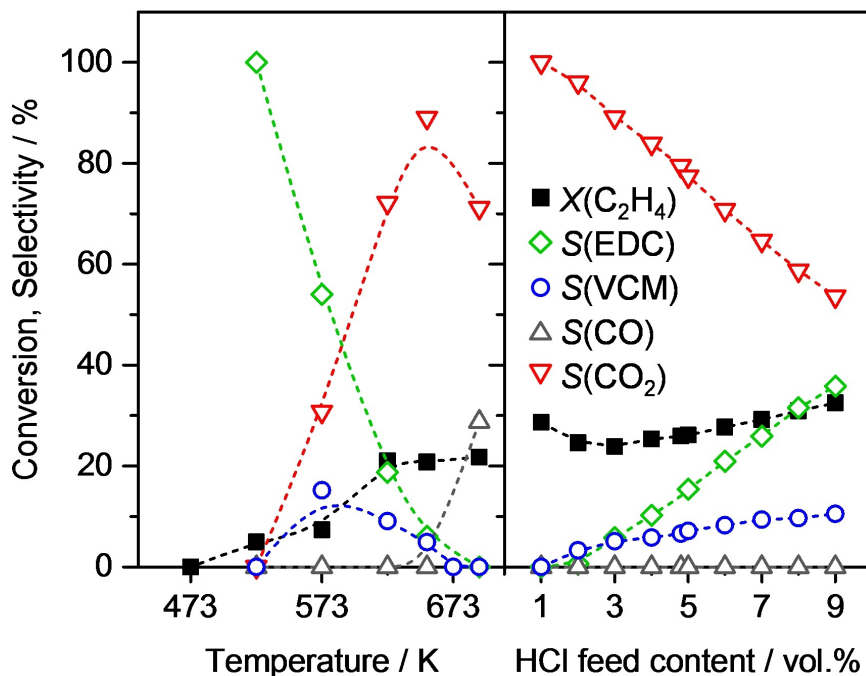
Figure 5.2: Left: conversion and selectivity versus temperature. Right: conversion and selectivity versus volumetric HCl feed content ($T = 623$ K)

5.3 Computational Details

Density Functional Theory (DFT) as implemented in the Vienna Ab initio Simulation Package (VASP), version 5.3.3, was applied to bulk RuO_2.[195, 196] The ionic positions and cell volume were optimised for a cell containing two formula units, using a plane-wave cut-off of 600 eV and a k-point sampling mesh of 9×9×13, using the Monkhorst and Pack scheme.[178] The optimised bulk lattice parameters obtained ($a = b =$4.52 Å, $c =$3.118 Å) are in good agreement with experimental values obtained from single-crystal X-ray diffraction; the difference between calculated lattice parameters and the experimental values is less than 0.7%.[223] From the optimised bulk structure, slabs representing the lowest energy rutile (110) facet of RuO_2 were constructed. A p(4×1) supercell was employed, with a k-point sampling of 2×4×1. A slab consisting of five layers, interleaved by 15 Å of vacuum, was used. The top two layers of the slab were optimised, while the remaining bottom three were fixed. Forces were converged to within 0.015 eVÅ^{-1}. In order to eliminate the spurious electrostatic interactions associated with asymmetric relaxation of the slab, a dipole correction was applied to the

vacuum. The exchange-correlation functional PBE was employed through-out.[167] Inner electrons were replaced with PAW,[176] and the valence states were expanded in plane-waves with a cut-off energy of 450 eV. The chosen functionals provide a reasonable reproduction of experimental results.[151, 224] Transition states were identified by CI-NEB,[182] and vibrational analyses performed numerically with a step of 0.015 Å.

5.4   Computational Results

Extensive computational studies probe the reaction network and examine all of the possible outcomes for the reaction of ethylene, with either oxidation or chlorination, or a mixture of the two processes taking place. The calculated reaction energies and activation barriers provide insights into the likely product distributions. The effect of dimensional confinement and adsorption coverage is investigating by calculating the adsorption energies for relevant chlorinated products as a function of O and Cl surface coverage. Further studies also consider the effect of high coverages on the reaction profile for EDC formation, the key process of industrial relevance taking place in the reaction.

5.4.1   Reaction Network

DFT calculations were performed simulating the surface under low Cl coverage conditions to probe the reactivity and selectivity of the system.[222] A large reaction network was studied (Figure 5.3), considering processes involving both chlorination and oxidation of ethylene, separately and in conjunction. Deacon-type processes take place under the reaction conditions, with HCl and O_2 dissociative adsorption being prerequisites for further reaction with C_2H_4, as well as HCl being oxidised by O_2 to Cl_2 and H_2O as in the standard Deacon process.

Firstly, the processes that are common to both the Deacon and oxychlorination reactions are summarised in Table 5.1 and denoted by Roman numerals. Adsorption of O_2 is exothermic by -1.20 eV (process I, Table 5.1), with subsequent dissociation to $2O^{**}$ also being exothermic by an additional -0.74 eV with an activation barrier of 0.28 eV (process II, Table 5.1). Dissociative adsorption of HCl is exothermic by -1.79 eV (process III, Table 5.1), with H being abstracted by bridging O atoms (O_b) present on the catalyst surface. In the Deacon process, Cl recombination yields the product Cl_2 which subsequently desorbs from the surface (process IV, Table 5.1). Surface H arising from HCl dissociative adsorption leaves the surface in the form of water, with H transferring from O_b to coadsorbed O (O_{cus}) to generate

$O_{cus}H$ (process V, Table 5.1), followed by a second H transfer to yield H_2O (process VI, Table 5.1) which then desorbs from the surface (process VII, Table 5.1). Both H transfer processes have mildly exothermic reaction energies (-0.02 eV and -0.11 eV for processes V and VI, Table 5.1, respectively) and comparable, low activation energies (0.35 eV and 0.18 eV for processes V and VI, Table 5.1, respectively). Desorption of H_2O is endothermic by 1.12 eV (process VII, Table 5.1). Our results are thus in line with previous calculations.[147,149,151,225–228] Some recent theoretical work identifies that water evolution is a key process in HCl oxidation, acting as an energetic bottleneck for the overall reaction.[229] However, with regards to ethylene oxychlorination, eventual evolution of water is a common process to all of the possible reactions, and hence will not have any appreciable impact on selectivity of the chlorinated products.

The addition of ethylene further expands the list of competitive reactions. Physisorption of C_2H_4 on the $RuO_2(110)$ slab was determined to be exothermic by -0.66 eV (process A1, Table 5.1). Subsequently, addition across the C-C double bond can occur with either coadsorbed Cl or O occupying adjacent adsorption sites to C_2H_4, yielding intermediates bound to the surface. The chlorination route (process 1, Table 5.1) is endothermic whilst the oxidation route (process 5, Table 5.1) is exothermic, ($\Delta E(Cl)= 0.14$ eV, compared to $\Delta E(O)= -0.55$ eV). On the other hand, chlorination has a slightly lower activation barrier than oxidation ($E_a(Cl)= 0.26$ eV, compared to $E_a(O)= 0.35$eV). Hence, competition exists between the two processes, and the product distribution will vary depending on whether the system is under kinetic or thermodynamic control.

The chlorination pathway begins with the formation of a $ClCH_2CH_2^*$ intermediate (process 1, Table 5.1). From here, a number of processes can take place. Firstly, direct protonation of the $ClCH_2CH_2^*$ intermediate from O_bH can take place (process 2, Table 5.1), yielding ethyl chloride (C_2H_5Cl); this process was found to possess a feasible activation barrier (E_a=0.96 eV) but was also calculated to be slightly endothermic (ΔE=0.26 eV). Desorption of C_2H_5Cl is endothermic by 0.61 eV (process A2, Table 5.1). A second alternative is vinyl chloride monomer (VCM) generation by H abstraction from the $ClCH_2CH_2^*$ intermediate (process 3, Table 5.1); this process is both exothermic and kinetically feasible (ΔE=-0.21 eV, E_a=1.07 eV). Desorption of VCM from the surface is endothermic by 0.88 eV (process A3, Table 5.1). Finally, direct chlorination of the $ClCH_2CH_2^*$ intermediate yields the product EDC; the process was found to be slightly endothermic (ΔE=0.17 eV) but with a high activation barrier (E_a=1.85 eV) (process 4a, Table 5.1).

Coverage effects are crucial in the Deacon chemistry and thus are likely to be important also under oxychlorination conditions.[187] Under high Cl cov-

erage conditions, EDC formation from direct chlorination of $ClCH_2CH_2^*$ (process 4b†, Table 5.1), yielded results more consistent with experimental observation; no activation barrier was observed for this process (thus it would be controlled by the Cl diffusion energy on the surface), and an exothermic reaction energy was determined (ΔE=-0.87 eV). It was calculated that the $ClCH_2CH_2^*$ intermediate is destabilised by 1.42 eV, which can be easily offset by the dissociative adsorption of HCl (-1.79 eV). In other words, the high coverage responsible for the induced destabilisation is a direct consequence of a high degree of HCl dissociative adsorption. Hence, HCl dissociation and the induced distortion are directly coupled with a net exothermic energy balance. Desorption of EDC is endothermic by 0.71 eV (process 15, Table 5.1).

The competing oxidation route, the oxametallocycle intermediate (OMME) formed by the addition of coadsorbed O to C_2H_4 (process 5, Table 5.1) can undergo a variety of processes. Formation of acetaldehyde (by 1,2-H shift, process 6, Table 5.1) is a possibility, as discussed in previous works.[189] Acetaldehyde formation is exothermic by -0.88 eV and has an activation barrier of E_a=1.22 eV; desorption of acetaldehyde is endothermic by 0.90 eV (process A5, Table 5.1). Under thermodynamic control, it is likely that this species will ultimately undergo combustion to CO_2 and H_2O. It is found that cleavage of the C-C bond in OMME, resulting in fragmentation, has a lower activation barrier of 1.06 eV, making this the more feasible route (process 7, Table 5.1). The fragmentation yields formaldehyde and a CH_2^* species bound to the surface. The CH_2^* fragment can then react with coadsorbed O to generate a second equivalent of formaldehyde (process 8, Table 5.1); this process is highly exothermic (ΔE=-1.30 eV) and has a negligible activation barrier (E_a=0.02 eV) owing to the instability of the CH_2^* fragment. Subsequently, formaldehyde can re-adsorb to the surface, forming an intermediate bridging the coordinately unsaturated Ru site (Ru_{cus}) and another O_{cus}, adding across the CO carbonyl bond in the process (process 9, Table 5.1). The formation of the bridging intermediate is exothermic (ΔE=-0.89 eV) and was determined to have a negligible activation barrier. CO_2 is then generated by two consecutive H abstractions from the intermediate. The first H abstraction (process 10, Table 5.1) is highly exothermic (ΔE=-2.30 eV) and has a low activation barrier (E_a=0.54 eV). The second H abstraction (process 11a, Table 5.1), on the other hand, was determined to have a high activation barrier of 1.70 eV and was found to be thermoneutral (ΔE=-0.04 eV) under the low coverage model applied. Further calculations using a high Cl coverage model (process 11b†, Table 5.1) yielded a much more exothermic reaction energy (ΔE=-2.09 eV), and a negligible activation barrier. The intermediate was calculated to have been destabilised by

1.66 eV, again this energy can be compensated for by the exothermicity of HCl dissociative adsorption. Desorption of CO_2 is endothermic by 0.20 eV (process A6, Table 5.1). Finally, the H abstracted from the intermediates by vicinal O_b will ultimately be transferred to coadsorbed O_{cus}, thus evolving water and preserving the O_b surface atoms, as in the case of the standard Deacon reaction (processes V, VI and VII, Table 5.1).

Since VCM, like C_2H_4, possesses a C-C double bond, the same processes (both chlorination and oxidation) that apply to C_2H_4 may also apply to VCM, at least in theory, resulting potentially in products containing both O and Cl. Several pathways were investigated. Addition of either Cl or O across the C-C double bond results in two possible intermediates, since there are two approach trajectories (as opposed to only one for C_2H_4, owing to the fact that in the latter molecules, the two C atoms are equivalent). Considering first VCM chlorination, it is noted that there are two possibilities arising from Cl addition to VCM; either a vicinal dichloride ($ClCH_2ClCH^*$) or a geminal dichloride ($Cl_2CHCH_2^*$). Formation of the geminal dichloride (process 16, Table 5.1) is endothermic by 0.72 eV and has an activation barrier of 0.99 eV. The $Cl_2CHCH_2^*$ intermediate can then either gain H from O_bH, originating from HCl dissociative adsorption, yielding CH_3CHCl_2 (ΔE=0.25 eV, E_a=0.99 eV, process 17, Table 5.1), or alternatively O_b can abstract H from the intermediate to give an unsaturated product, CH_2CCl_2 (ΔE=-0.25 eV, E_a=1.39 eV, process 18, Table 5.1). Both CH_3CHCl_2 and CH_2CCl_2 have similar adsorption energies (-0.53 eV and -0.54 eV, processes A9 and A10 respectively, Table 5.1). Formation of the vicinal dichloride is endothermic by 0.56 eV and has an activation barrier of 1.09 eV (process 12, Table 5.1). As with the geminal dichloride intermediate, potential products can be evolved by either gaining H from O_bH, or by H abstraction by O_b. Addition of H leads to an alternative route to obtain EDC (ΔE=0.47 eV, E_a=1.18 eV, process 13, Table 5.1). H abstraction can yield two unsaturated products, Z-$C_2H_2Cl_2$ and E-$C_2H_2Cl_2$, which form a pair of geometrical isomers depending on the conformation of the intermediate. The reaction energies for the two processes are very similar (ΔE=-0.16 eV, ΔE=-0.15 eV, for Z-$C_2H_2Cl_2$ and E-$C_2H_2Cl_2$ respectively, processes 14 and 15, Table 5.1). However the activation barrier for the formation of Z-$C_2H_2Cl_2$ is significantly higher than that of E-$C_2H_2Cl_2$ (E_a=1.37 eV, c.f. E_a=0.97 eV), likely due to steric repulsion between Cl on the same side of the molecule in the case of Z-$C_2H_2Cl_2$. Additionally, the E-$C_2H_2Cl_2$ desorption energy is more endothermic at 0.53 eV (process A8, Table 5.1) compared to 0.32 eV for Z-$C_2H_2Cl_2$ (process A7, Table 5.1). Indeed, it is possible that the unsaturated products from VCM chlorination could in turn undergo further reaction in an analogous manner. However, since all of the reaction energies

for the formation of the products of VCM chlorination are endothermic, and all of these processes have high activation barriers, further reactions beyond this point have not been examined.

Turning now to VCM oxidation, similarly two distinct intermediates can be formed, CH_2CHClO^{**} (ΔE=-0.27 eV, E_a=0.73 eV, process 21, Table 5.1), and OCH_2CHCl^{**} (ΔE=-0.04 eV, E_a=0.98 eV, process 19, Table 5.1), depending on the side of the VCM molecule from which O approaches. As with OMME, H transfer can yield an aldehyde, CH_2ClCHO, from OCH_2CHCl^{**} (ΔE=-1.05 eV, E_a=1.10 eV, process 20, Table 5.1), and in the case of CH_2CHCl^{**} an acid chloride, CH_3COCl is formed (ΔE=-1.23 eV, E_a=1.19 eV, process 22, Table 5.1). Desorption of the aldehyde is considerably more endothermic at 1.13 eV (process A11, Table 5.1), compared to 0.72 for the acid chloride (process A12, Table 5.1).

5.4. COMPUTATIONAL RESULTS 123

Table 5.1: Reaction and activation energies for various processes and imaginary frequencies of the corresponding transition states. †: high coverage.

Nº	Reaction	ΔE / eV	E_a / eV	ν_i / cm^{-1}
	Deacon Chemistry			
I	$O_2 + 2^* \rightarrow O_2^{**}$	-1.20	-	-
II	$O_2^{**} \rightarrow 2O^*$	-0.74	0.28	538
III	$HCl + O_b +^* \rightarrow Cl^* + O_bH$	-1.79	-	-
IV	$2Cl^* \rightarrow Cl_2 + 2^*$	+2.23	-	-
V	$O^* + O_bH \rightarrow OH^* + O_b$	-0.02	0.35	1073
VI	$OH^* + O_bH \rightarrow H_2O^* + O_b$	-0.11	0.18	845
VII	$H_2O^* \rightarrow H_2O +^*$	+1.12	-	-
	C$_2$H$_4$ Chlorination			
A1	$C_2H_4 +^* \rightarrow C_2H_4^*$	-0.66	-	-
1	$C_2H_4^* + Cl^* \rightarrow C_2H_4Cl^* +^*$	+0.14	0.26	201
2	$C_2H_4Cl^* + O_bH \rightarrow C_2H_5Cl^* + O_b$	+0.23	0.96	1345
A2	$C_2H_5Cl^* \rightarrow C_2H_5Cl +^*$	+0.61	-	-
3	$C_2H_4Cl^* + O_b \rightarrow VCM^* + O_bH$	-0.21	1.07	1555
A3	$VCM^* \rightarrow VCM +^*$	+0.88	-	-
4a	$C_2H_4Cl^* + Cl^* \rightarrow EDC^* +^*$	+0.17	1.85	193
4b†	$C_2H_4Cl^* + Cl^* \rightarrow EDC^* +^*$	-0.87	0.00	-
A4	$EDC^* \rightarrow EDC +^*$	+0.71	-	-
	C$_2$H$_4$ Oxidation			
5	$C_2H_4^* + O^* \rightarrow OMME^{**}$	-0.55	0.35	261
6	$OMME^{**} \rightarrow CH_3CHO^* +^*$	-0.88	1.22	990
A5	$CH_3CHO^* \rightarrow CH_3CHO +^*$	+0.90	-	-
7	$OMME^{**} \rightarrow CH_2^* + H_2CO^*$	+0.96	1.06	71
8	$CH_2^* + O^* \rightarrow H_2CO^* +^*$	-1.30	0.02	71
9	$H_2CO^* + O^* \rightarrow OCH_2O^{**}$	-0.89	0.00	-
10	$OCH_2O^{**} + O_b \rightarrow OCHO^* + O_bH +^*$	-2.30	0.54	1358
11a	$OCHO^* + O_b \rightarrow CO_2^* + O_bH$	-0.04	1.70	1169
11b†	$OCHO^* + O_b \rightarrow CO_2^* + O_bH$	-2.09	0.00	-
A6	$CO_2^* \rightarrow CO_2 +^*$	0.20	-	-
	VCM Chlorination			
12	$VCM^* + Cl^* \rightarrow ClCHCH_2Cl^* +^*$	+0.56	1.09	248
13	$ClCHCH_2Cl^* + O_bH \rightarrow EDC^* + O_b$	+0.47	1.18	1307
14	$ClCHCH_2Cl^* + O_b \rightarrow Z-C_2H_2Cl_2^* + O_bH$	-0.16	1.37	892
A7	$Z-C_2H_2Cl_2^* \rightarrow Z-C_2H_2Cl_2 +^*$	+0.32	-	-
15	$ClCHCH_2Cl^* + O_b \rightarrow E-C_2H_2Cl_2^* + O_bH$	-0.15	0.97	1429
A8	$E-C_2H_4Cl_2^* \rightarrow E-C_2H_2Cl_2 +^*$	+0.53	-	-
16	$VCM^* + Cl^* \rightarrow CH_2CHCl_2^* +^*$	+0.72	0.99	207
17	$CH_2CHCl_2^* + O_bH \rightarrow CH_3CHCl_2^* + O_b$	+0.25	0.99	1314
A9	$CH_3CHCl_2^* \rightarrow CH_3CHCl_2 +^*$	+0.53	-	-
18	$CH_2CHCl_2^* + O_b \rightarrow CH_2CCl_2^* + O_bH$	-0.25	1.39	1407
A10	$CH_2CCl_2^* \rightarrow CH_2CCl_2 +^*$	+0.54	-	-
	VCM Oxidation			
19	$VCM^* + O^* \rightarrow OCH_2CHCl^{**}$	-0.04	0.98	323
20	$OCH_2CHCl^{**} \rightarrow CH_2ClCHO^* +^*$	-1.05	1.10	946
A11	$CH_2ClCHO^* \rightarrow CH_2ClCHO +^*$	+1.13	-	-
21	$VCM^* + O^* \rightarrow CH_2CHClO^{**}$	-0.27	0.73	272
22	$CH_2CHClO^{**} \rightarrow CH_3COCl^* +^*$	-1.23	1.19	1118
A12	$CH_3COCl^* \rightarrow CH_3COCl +^*$	+0.72	-	-
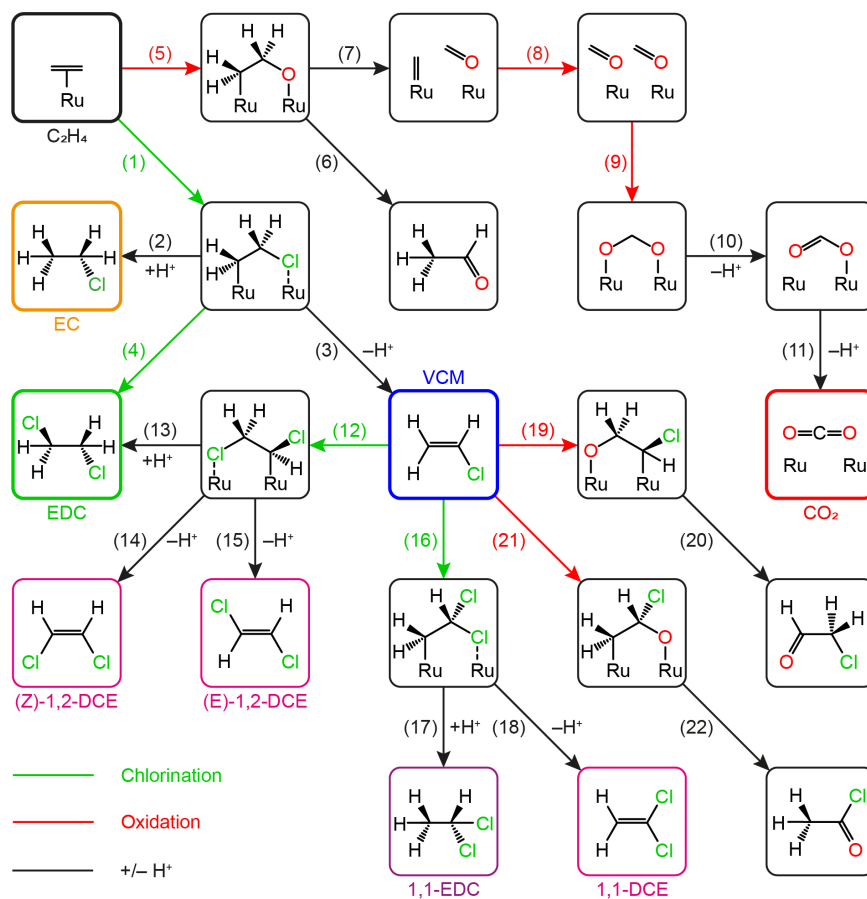
Figure 5.3: Reaction network for the processes investigated. Deacon-type processes, which are common to all of the reaction pathways, are omitted for clarity. Adsorption and desorption processes are omitted for similar reasons. Numbers refer to processes in Table 5.1. The starting point ($C_2H_4{}^*$) and the possible chlorinated products are indicated with bold, colour-coded boxes.

5.4.2 Effect of surface coverage on adsorption

The effect of both Cl and O coverage of the $RuO_2(110)$ surface on the adsorption of C_2H_4 and the relevant products was investigated by calculating the adsorption energy as a function of surface coverage. In the 4×1 surface cell, there are four surface Ru active sites, hence the adsorption energy for each of the carbon-containing species was determined for increasing amounts of coadsorbed O or Cl (i.e. up to 3 Cl or O atoms per 4×1 surface cell, with the remaining active site occupied by the carbon-containing species). Since previous work confirmed that substitution of surface O_b for Cl occurs under

5.4. COMPUTATIONAL RESULTS   125

typical Deacon reaction conditions,[149] further calculations also examined the adsorption energy as a function of Cl coverage with 50% of the O_b replaced by Cl (i.e. two of the four O_b present in the 4×1 surface cell replaced by Cl). The results show that, in general, higher surface coverages
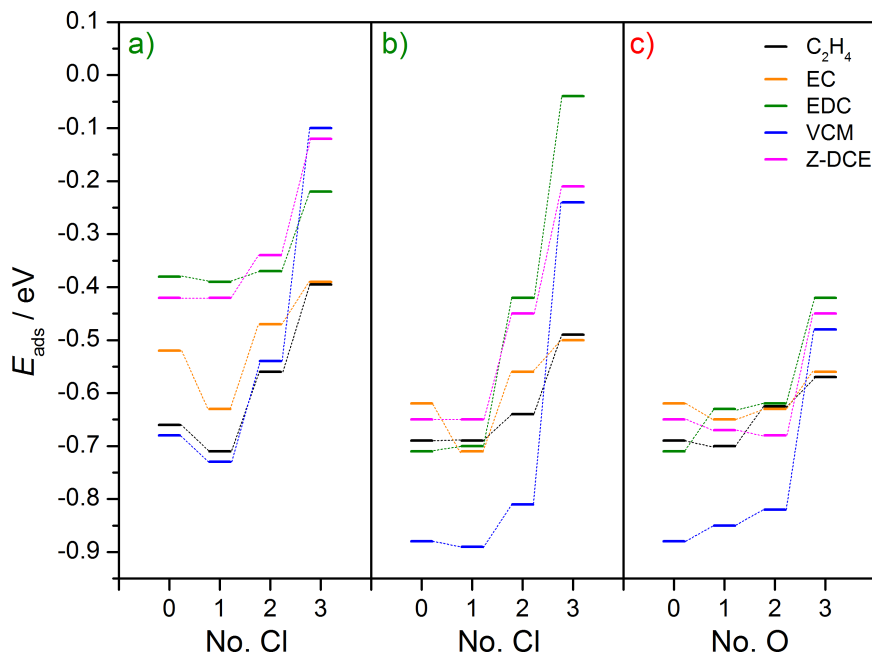
Figure 5.4: Adsorption energies of ethylene, ethylene chloride (EC), ethylene dichloride (EDC), vinyl chloride monomer (VCM) and Z-dichloroethylene (Z-DCE) for a variety of surface compositions. a) Adsorption energy as a function of Cl coverage on the RuO_2 surface, where half of the bridging oxygen atoms were replaced with Cl. b) Adsorption energy as a function of Cl coverage. c) Adsorption energy as a function of O coverage.

result in less exothermic adsorption energies, as higher coverages destabilise adsorbates through steric repulsions. Higher O coverages destabilise the adsorbates less than higher Cl coverages, owing to the smaller size of O adsorbates and hence the more limited steric repulsion, hence less exothermic adsorption energies are observed for lower Cl coverages, whereas adsorption energies are generally stable for lower O coverages whilst becoming more endothermic for the very highest O coverages. Generally speaking, when 50% of the O_b substituted is by Cl, adsorption energies are shifted to be more endothermic compared to the values obtained with no O_b substitution. In every case, VCM adsorption is the most strongly exothermic at lower coverages, but is considerably less so at the highest of coverages. The

adsorption energies for EDC and Z-DCE follow a similar trend, being fairly stable over a range of lower coverages but becoming much less exothermic for higher coverages. The adsorption energies for EC and C_2H_4 appear to be most stable over the full range of coverages, in every case having the most exothermic adsorption when all three remaining active Ru sites are occupied by either Cl or O. It is also observed that in many cases, the adsorption energy for the carbon-containing species is slightly more exothermic for low Cl and O coverages compared to the clean surface. This can be attributed to inductive effects arising from the high electronegativity of O, and to a lesser extent Cl, thus there is an interplay between stabilising inductive effects and destabilising steric repulsions associated with Cl or O coverage.

5.5 Discussion

The experimental studies show that selectivity can be controlled by a number of factors, whilst the theoretical studies reveal some mechanistic and energetic insights into the elementary processes of the reaction. By using the theoretical results to rationalise the experimental observations, one can gain a detailed understanding of the origins of the observed selectivity from an atomic-scale perspective of the surface chemistry. Understanding the underlying principles governing the selectivity assists in identifying the most important properties of a good oxychlorination catalyst for industrial purposes.

5.5.1 Origin of Selectivity

The experimental evidence suggests that the selectivity of RuO_2 as an oxychlorination catalyst depends strongly on the reaction temperature and the HCl feed content. The theoretical results provide insights into the precise nature of each of the elementary steps for the possible reactions and indicate the origin of the observed selectivity. Selectivity between oxidation and chlorination of C2H4 is gov- erned by the interplay between thermodynamic and kinetic fac- tors. Thermodynamic selectivity can originate from differing adsorption energies between species. Products with highly exothermic adsorption energies are more likely to undergo further reaction than to be desorbed as an observed product, thus dictating selectivity.[75]

The temperature dependence of the selectivity is such that oxidation, and ultimately combustion, is favoured at higher temperatures, whilst oxychlorination is favoured at lower temperatures. This implies that oxidation is the thermodynamically favoured option, whilst chlorination prevails as the kinetic product, and hence variation in temperatures determines the inter-

play between kinetic and thermodynamic control. The theoretical results show that the first step in the reaction is crucial in determining the overall selectivity, i.e. whether chlorination (process 1, Table 5.1) or oxidation (process 5, Table 5.1) of C_2H_4 takes place. The activation barrier for addition of Cl to C_2H_4 is lower than for the addition of O, however the chlorination process is endothermic compared to the exothermic oxidation route. At lower temperatures, the system is more prone to kinetic control. Whilst it is very likely that the initial and final states for Cl addition to C_2H_4 exist in equilibrium, the higher activation barrier for oxidation cannot be breached. Hence, only chlorination products are observed, as the intermediate $C_2H_4Cl^*$ is consumed to form chlorination products over time. On the other hand, at higher temperatures, thermodynamic control prevails, and since the oxidation process is much more exothermic, it is more likely that the formation of OMME is irreversible, and hence at higher temperatures more combustion products are observed to the exclusion of chlorination products.

The experimental results also show that higher a HCl feed content directs the selectivity towards oxychlorination and away from combustion, with a mixture of products being obtained at higher HCl feed contents. The theoretical results offer a rational explanation for this based on the effect of coadorbed Cl on key elementary steps in the reaction. From the calculations performed simulating low coverage conditions, it can clearly be seen that under such conditions, the activation barrier for EDC formation (process 4, Table 5.1) is prohibitively high. Under high coverage conditions, however, It was calculated that the $ClCH_2CH_2^*$ intermediate is destabilised by 1.42 eV, which can be easily offset by the dissociative adsorption of HCl (-1.74 eV). In this case, the destabilisation of adsorbed species by the coadsorbed chlorine atoms diminishes the activation barrier of the processes as the energetic gap is closed between the initial and transition states of each process (Figure 5.5). This is reflected in differences in the atomic distances at high Cl coverage compared to low Cl coverage. At low Cl coverage, the distance between a Cl atom and the C atom of a coadsorbed $C_2H_5Cl^*$ intermediate is 3.53 Å. However, at high coverage, the corresponding distance is only 3.08 Å, reflecting the crowding on the surface responsible for the destabilisation of the $C_2H_5Cl^*$ intermediate. It is also notable that whilst the activation barrier for C_2H_4 chlorination is lower than that of oxidation under low coverage conditions, at high coverages the pattern is reversed and the activation barriers are comparable. This implies that under high coverage, the competition between oxidation and chlorination of C_2H_4 is enhanced, leading to reduced selectivity. This is observed in the experimental results which show that whilst the reaction is highly selective towards oxidation at lower HCl

feed contents, with combustion products dominating the product distribution, when a higher proportion of HCl is included in the input gas, both combustion and oxychlorination products are observed.
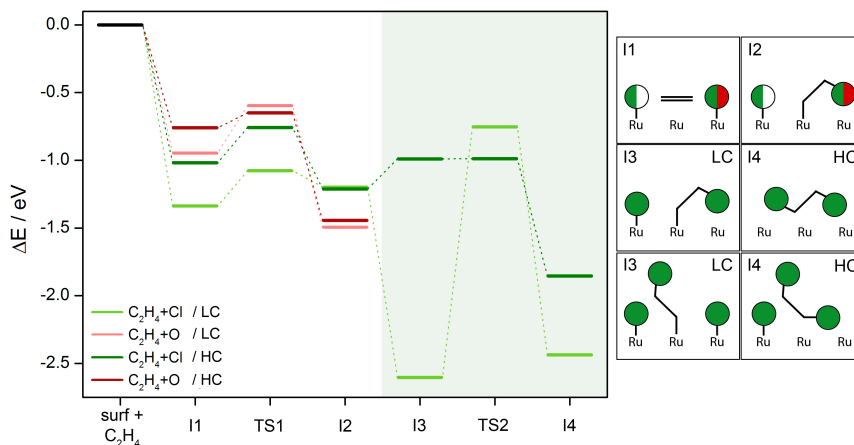
Figure 5.5: Left: Reaction profiles for oxidation and chlorination of C_2H_4 at low and high Cl surface coverages. The chlorination route depicts the eventual formation of EDC. The white background region indicates where the oxidation and chlorination processes compete at the specific coverage. LC and HC stand for low and high coverage, respectively. Right: Diagrams depicting the configuration of the surface species for each step in the reaction profile, where green circles indicate chlorine atoms, green/white circles indicate either chlorine or no atom, and green/red circles indicate either chlorine or oxygen atom.

The effect of coverage can also offer insights into why EDC is the preferred kinetic product, rather than any other chlorinated product such as VCM or EC. As discussed, the presence of coadsorbed Cl destabilises the $C_2H_5Cl^*$ intermediate, nullifying the high activation barrier observed under low coverage conditions. However, when this intermediate undergoes reaction with an adjacent coadsorbed Cl to form EDC, the confinement of the species is relieved and consequently the process is energetically favourable. For products such as EC and VCM, on the other hand, the reaction involves gaining (losing) H from (to) O_bH (O_b) to generate EC (VCM). These processes do not involve any of the coadsorbed Cl responsible for the destabilisation, and hence there is no way that these processes can relieve the carbon-containing intermediates of their confinement, hence it is likely that the thermodynamics and kinetics of these processes at high coverage would be largely unchanged from their low coverage values. Hence, under kinetic control, of all of the chlorinated products, formation of EDC would be most thermodynamically feasible.

A further important aspect regarding the preference of EDC over other chlorinated products originates from the fact that it is well-known that under HCl oxidation conditions, substitution of surface O atoms in $RuO_2(110)$ for Cl takes place.[149] The loss of O_b sites would clearly have an impact on VCM and EC production, as both of these products rely on H transfer processes to or from O_b or O_bH.[189] The only alternative would be the fortuitous presence of coadsorbed O adjacent to the intermediates to fulfil the role of O_b in the stoichiometric system, which at high Cl coverages would be unlikely. The reaction profile for EDC production, on the other hand, does not depend in any way on the presence of O_b, since the reaction essentially consists of two sequential coadsorbed Cl addition processes across the C_2H_4 double bond. Hence, under higher HCl partial pressures, where replacement of O_b is likely to occur, EDC would be favoured over EC and VCM as the dominant chlorinated product.

The theoretical results also provide insights into the preference for combustion under thermodynamic control, rather than more limited forms of oxidation. Upon addition of O to C_2H_4 (process 5, Table 5.1), the resulting OMME intermediate can either fragment (process 7, Table 5.1), yielding H_2CO^* and CH_2^*, or undergo intramolecular H transfer to give CH_3CHO (process 6, Table 5.1). From the calculations, it can be seen that the fragmentation has a considerably lower activation barrier, hence this option is preferred, eventually progressing to total combustion as the products of the fragmentation undergo further reaction with coadsorbed O. Whilst under low coverage conditions the final abstraction to yield CO_2 has a high activation barrier (process 11a, Table 5.1), under high coverage conditions the process is both highly exothermic and has no activation barrier, and can be explained in terms of destabilisation caused by coadsorbed species, analogous to the observed low activation barrier for EDC formation under high coverage conditions.

Another important consequence of high coverage of Cl and the induced destabilisation of other adsorbates is the effect on competitive adsorption of reactants and products. The number of active sites on the catalyst surface is limited and thus the species which adsorb more strongly will dominate. Likewise, products that are adsorbed less strongly than reactants will be displaced in favour of the more strongly adsorbed species, preventing such products from undergoing further reactions.[75] Hence, competitive adsorption represents another aspect of thermodynamic selectivity relevant to ethylene oxychlorination. As the calculations examining the adsorption energy of a variety of species as a function of Cl or O coverage show, different adsorbed species are affected by the presence of a high concentration of coadsorbates in different ways. Especially important is the effect of cover-
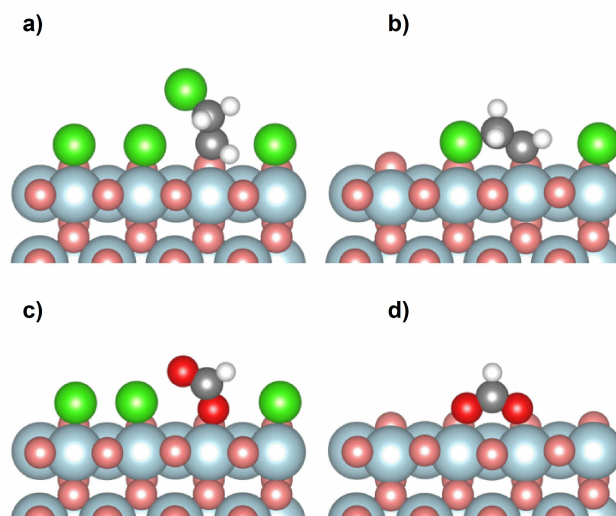
Figure 5.6: a) Surface conformation for Ru-C_2H_4Cl under high Cl coverage. b) Ru-C_2H_4Cl under low Cl coverage. c) Surface conformation for Ru-OCHO under high Cl coverage. d) Ru-OCHO under low coverage. Legend: blue: Ru; pale red: bulk O; bright red: adsorbed O; green: Cl; dark grey: C; light grey: H.

age on VCM adsorption. At low coverages, VCM is more strongly adsorbed than other species, owing to its compact size and its ability to interact with Ru active sites through either Cl or the C-C double bond, or indeed both (occupying two active sites). Therefore, under such circumstances VCM would be likely to stay on the surface and undergo further reactions as it is the most stable product at low coverages. It is also important to note that the C_2H_4 adsorption energy remains relatively unchanged at high O coverage, compared to the adsorption energy for a clean surface. Since C_2H_4 is the precursor for combustion products, the stronger C_2H_4 adsorption further supports oxidation to CO_2 and H_2O. However, at high coverages, VCM shows a lower adsorption energy than C_2H_4, thus favouring the thermodynamic selectivity. This phenomena has been reported for the gold-catalysed selective hydrogenation of C-C triple bonds in alkynes, to the exclusion of hydrogenation of C-C double bonds in the resulting alkenes, since competitive adsorption between the reac- tants and products ensure that the products do not undergo further reaction, being displaced in favour of the adsorption of the reactant.[230] The lower adsorption energy for VCM compared to C_2H_4 means that under high coverage conditions, the two species

compete for the remaining adsorption sites, with C_2H_4 being preferentially adsorbed. Consequently, VCM desorbs from the catalyst surface once it is generated in favour of adsorption of C_2H_4, rather than undergoing further reaction and thus leading to an enhanced selectivity. This would also explain the appearance of some amount of VCM in the product distribution, but no significant amounts of chlorinated products such as DCE.

5.5.2 Requirements for an ideal catalyst for VCM production

Having conducted a detailed analysis of the utility of $RuO_2(110)$ as an oxychlorination catalyst, examining the product distribution and the origin of the observed selectivity, it is possible to identify some key features of $RuO_2(110)$, their role in selectivity, and how this knowledge may be applied to develop new catalysts that afford high yields of the most industrially valuable product, VCM. The clearest limitation of $RuO_2(110)$ as a catalyst for VCM production is the lack of basic sites on the surface needed to abstract H from intermediates to yield VCM. The basicity of the bridging O_b positions needs to be strong enough to allow effective H abstraction. On the RuO_2 surface, $HCl:O_2$ mixtures produce surfaces where O_b are partially replaced by Cl atoms (about 50% replacement). While this limit is crucial to ensure the stability of the catalyst under Deacon conditions, it impedes an effective dehydrogenation of the intermediates, most likely leading to enhanced EDC production. Therefore, a successful VCM catalyst needs to maintain effective O centres able to strip hydrogen from the intermediates. The role of O_{cus} in facilitating combustion means that O_{cus} cannot be relied upon to provide basic sites for H abstraction, and furthermore, under high Cl coverage conditions it is likely that very few O_{cus} would be geometrically accessible to intermediates for H abstraction. Hence, RuO_2 has only limited utility in this repect as a catalyst for VCM production.

Previous work has established[152] that it is also possible to produce VCM sequentially from EDC by dehydrochlorination, rather than forming it directly, providing an alternative route to generate VCM. This, however, requires the presence of acidic surface sites, which are not present in RuO_2 under oxychlorination condtions for the same reason that basic sites are not present. Potentially, hydroxyl groups arising from H abstraction from HCl by O_b atoms or adsorbed O_{cus} could serve as acidic sites, but as has been established, a large proportion of the O_b atoms is replaced by Cl under Deacon-type conditions, and under high Cl coverage expected for typical ethylene oxychlorination conditions, relatively few O_bH groups would be present on the surface and the probability of these species being adjacent to adsorbed EDC on the surface in order to react is low.

Another key point for a good catalyst for VCM production relates to the competitive adsorption. In this respect, the competitive adsorption between C_2H_4 and VCM over $RuO_2(110)$ is a positive feature for VCM production; under high coverage conditions, C_2H_4 has a more exothermic adsorption energy than VCM, hence C_2H_4 will be preferentially adsorbed over VCM, limiting the extent to which VCM can undergo further oxidation or chlorination in a manner analogous to C_2H_4. On the other hand, competitive adsorption between the reactants can be problematic for oxychlorination. The adsorption energy for O_2 is within the same range as that of C_2H_4, meaning that the two reactants compete for active Ru sites on the surface. The persistent presence of O_{cus} on the surface threatens VCM production by promoting oxidation of ethylene, rather than oxychlorination. The C-O bond is much stronger than the C-Cl bond (358 compared to 327 kJmol^{-1}), meaning that whilst chlorination processes tend to be reversible, oxidation is much more exothermic and thus irreversible, resulting in an inevitable degree of oxidation. Due to the highly active nature of O_{cus}, it can be anticipated that any situation where C_2H_4 and O_{cus} are present adsorbed on adjacent sites will result in irreversible oxidation of the alkene.

A further aspect worthy of discussion is the dimensional confinement of adsorbates on the catalyst surface. In common with other the low-index facets of RuO_2, the (110) surface features rows of active Ru sites defined by rows of bridging oxygen atoms. These rows of atoms on the surface provide a barrier to diffusion, which on the 110 surface is limited to being exclusively along the [001] direction. Hence, reactants adsorbed on the surface are limited to only being able to react with coadsorbed species located adjacent and in the same row. This confinement limits selectivity as adsorbed species necessarily react with whatever species happens to be nearby, rather than preferentially reacting with one nearby species over another, as would be the case for a catalytic surface not exhibiting such dimensional confinement. Relating back the to irreversible, thermodynamically-driven oxidation of C_2H_4, this confinement means that the presence of a single O_{cus} can result in the full combustion of ethylene to CO_2, forgoing any possibility of obtaining chlorinated products once it has occurred. Hence, this one-dimensional confinement is detrimental to the formation of VCM, or indeed any chlorinated products of oxychlorination.

5.6   Conclusions

Under the conditions required for catalytic oxychlorination of ethylene over $RuO_2(110)$, a variety of chemical reactions are possible, with competing oxidation and chlorination processes. Whilst oxidation, and ultimately com-

5.6. CONCLUSIONS 133

bustion to CO_2 and H_2O, is favoured thermodynamically, conversion to the desired oxychlorination products is possible at lower temperatures through kinetic control. The coverage and composition of the surface is crucial to the behaviour of the system. Under high Cl coverages, competitive adsorption between C_2H_4 and VCM ensures that VCM is displaced by C_2H4, owing to its less exothermic adsorption energy, preventing the excessive formation of products derived from VCM. The effect of dimensional confinement of C_2H_4 means that coadsorbed species react on a "first-come, first-served" basis, thus resulting in a potentially considerable degree of combustion where coadsorbed O is involved. The effect of substitution of bridging O sites by Cl, is key to understanding the prevalence of EDC over VCM under kinetic control, since the O_b sites required to abstract H from intermediates are essential to VCM formation. Therefore, the surface composition of the catalyst has a major impact on activity and selectivity and is an important consideration in the development of new catalysts. It is intended that this study will inform future work in developing highly selective, robust and active catalysts for ethylene oxychlorination, defining the basic requirements for a good catalyst by offering mechanistic insights at the molecular level.

Part III

Conclusions

UNIVERSITAT ROVIRA I VIRGILI
THEORETICAL STUDIES OF HETEROGENEOUS CATALYSIS FOR HALOGEN CHEMISTRY
Michael David Higham

Conclusions

The preceding chapters have demonstrated that catalytic activity and selectivity is highly dependent on the surface structure and compositions under typical reaction conditions. Through theoretical investigations, supported by experimental evidence, the results present a comprehensive perspective on the nature of rutile transition metal oxides as heterogeneous catalysts for halogen chemistry. In the following sections, the main point are thus summarised.

Interplay between surface chemistry and performance of rutile-type catalysts for halogen production

- DFT calculations showed that the stability of rutile-type transition metal oxides is dependent upon the extent of halogen uptake into the surface and subsurface layers of the catalyst.

- Chlorine uptake was significantly less than bromine uptake, under hydrogen chloride and hydrogen bromine oxidation conditions, respectively.

- For RuO_2, whilst the modest observed Cl uptake was associated with improved activity, owing to a greater degree of stability afforded, under HBr oxidation conditions, Br uptake was significantly greater, with experimental PGAA evidence suggesting that Br uptakes greatly exceeds monolayer substitution.

- DFT calculations showed that high Br uptake is associated with surface amorphisation, explaining the observed HRTEM images of RuO_2 after HBr exposure.

- DFT calculations also showed that in every case, halogen evolution is the most energy-demanding step.

137

138

- High Br uptake in RuO_2 does not appear to be significantly detrimental to Br_2 production, despite the active Ru sites needed for the the Langmuir-Hinshelwood type mechanism proposed for HCl oxidation over RuO_2 being occluded.

- High Br uptakes were identified as causing a shift in reaction mechanism, proposed to resemble a Mars-van-Krevelen type mechanism, relying on vacancies in the Br saturated RuO_2 surface.

- Cl uptake is negigible for TiO_2, whilst Br uptake is limited and plays a key role in providing active defect sites on the surface.

Doping Strategies for Rutile Transition Metal Oxides in Hydrogen Halide Oxidation

- Catalytic activty of TiO_2 is strongly dependent on electronic structure defects induced by impurities and dopants.

- Dopant species activate surface Ti sites towards oxygen adsorption by donating electrons to the Ti 3d conduction band, providing electrons at a suitable energy level to interact with O_2 π^* orbitals, thus facilitating dissociative adsorption.

- Whilst self-doping of TiO_2 with Br under HBr oxidation conditions renders the catalyst active through the formation of reactive surface Ti defect states, the energy levels associated with the defect states can be further modified by substitional doping of the defective Ti for Ru.

- Adsorption behaviour can be controlled by considering the number of dopant atoms introduced, the number of defects introduced per dopant atom, and the distribution of electrons originating from dopants amongst surface Ti atoms.

- Interstitial doping of B in TiO_2 induces the formation of two adjacent Ti defect sites, rendering the surface extremely active towards O_2 dissociative adsorption.

Mechanism of Ethylene Oxychlorination over Ruthenium Oxide

- Interplay between either ethylene oxychlorination or combustion is due to kinetic or thermodynamic control, respectively.

- The first elementary step in the reaction, after the adsorption of reactants, is key to overall selectivity, since ethylene oxidation to OMME is strongly exothermic and thus irreversible.

- Surface coverage is key in both oxychlorination and combustion processes in determining the selectivity observed.

- High coverages of either Cl or O can induce destabilisation of key intermediates, directing selectivity by ultimately lowering activation barriers associated with some of the most important elementary processes.

- Dimensional confinement on the 1-D RuO_2 (110) surface further affects selectivity by limiting the number of neighbouring active sites available to any given adsorbate.

- Competitive adsorption between reactants (ethylene) and products (VCM) means that under high coverage conditions, VCM adsorption is less exothermic than ethylene adsorption, preventing the formation of over-chlorinated products from further reaction of VCM.

- Ideal VCM production catalysts require suitable basic sites present under reaction conditions to abstract hydrogen from chlorinated intermediates, leading to VCM formation.

The thesis as a whole demonstrates the importance of surface composition and the lateral interactions between adsorbates when considering the utility of materials as catalysts under real reaction conditions. The fluxional and dynamic nature of the active phase is emphasised, and it is intended that the results presented herein will contribute to a more rational approach to catalyst design which considers the aforementioned factors.

140

Part IV

List of Publications

UNIVERSITAT ROVIRA I VIRGILI
THEORETICAL STUDIES OF HETEROGENEOUS CATALYSIS FOR HALOGEN CHEMISTRY
Michael David Higham

List of Publications

1. M. Moser, V. Paunović, Z. Guo, L. Szentmiklósi, M. G. Hevia, M. Higham, N. López, D. Teschner, and J. Pérez-Ramírez, "Interplay between surface chemistry and performance of rutile-type catalysts for halogen production," *Chem. Sci.*, vol. 7, pp. 2996–3005, 2016.

2. M. Higham, M. Scharfe, M. Capdevila-Cortada, J. Pérez-Ramírez, and N. López, "Mechanism of ethylene oxychlorination over ruthenium oxide," *Journal of Catalysis*, vol. 353, pp. 171–180, 2017.

The author has made the following contributions to the above publications listed: in publication 1, the author performed all of the calculations relating to the uptake of Br and Cl by RuO_2 and TiO_2, determining all of the energies associated with the replacement of surface (and subsurface) O atoms for halogen atoms, using the VASP code. The author also performed the necessary numerical work to obtain the *ab initio* thermodynamics plots, using the appropriate DFT results and experimental data obtained from the NIST webbook. The author contributed to writing the article, in particular the sections concerning the computational results, theoretical methodology, and related portions of the introduction, results and conclusion sections. In publication 2, the author performed all of the calculations to determine the reaction energy and activation barriers for all of the elementary processes involved in the oxychlorination and combustion of ethylene. The author also performed the calculations to determine the adsorption energies of relevant species as a function of catalyst surface coverage. The author also served as the primary contributor to the writing of the article text, especially the sections concerning the computational results.

144

Bibliography

[1] J. J. Berzelius, *Årsberättelsen om framsteg i fysik och kemi.* Stockholm, Sweden: Royal Swedish Academy of Sciences, 1836.

[2] S. J. Green, *Industrial Catalysis.* London, UK: E. Benn Limited, 1928.

[3] J. Wisniak, "The History of Catalysis. From the Beginning to Nobel Prizes," *Educ. Quim.*, vol. 21, no. 1, pp. 60–69, 2010.

[4] H. Davy, "Some New Experiments and Observations on the Combustion of Gaseous Mixtures, with an Account of a Method of Preserving a Continued Light in Mixtures of Inflammable Gases and Air without Flame," *Philos. T. R. Soc.*, 1817.

[5] L.-J. Thenard, "Observations sur des Combinaisons nouvelles entre l'oxigène et divers acides," *Ann. Chim. Phys.*, 1818.

[6] E. Davy, "On Some Combinations of Platinum," *Philos. T. R. Soc.*, vol. 110, no. January, pp. 108–125, 1820.

[7] J. W. Döbereiner, "Neu entdeckte merkwürdige Eigensschaften des Sub-oxyds des Platins, des oxydirten Schwefel-Platins und des metallisschen Platin-Staubes," *Ann. Phys. Berlin*, 1823.

[8] W. Prandtl, "Johann Wolfgang Döbereiner, Goethe's chemical adviser," *J. Chem. Educ.*, vol. 27, no. 4, p. 176, 1950.

[9] G. B. Kauffman, "Johann Wolfgang Döbereiner's Feuerzeug: On the sesquicentennial anniversary of his death," *Platin. Met. Rev.*, vol. 43, no. 3, pp. 122–128, 1999.

[10] H. Davy, *On the Safety Lamp for Preventing Explosives in Mines, Houses Lighted by Gas, Spirit Warehouses or Magazines on Ships etc. with Some Researches on Flame.* London, UK: R. Hunter, 1825.

[11] A. Fusinieri, *Memorie Sperimentali di Mecanica Molecolare.* Padova, Italy: Angelo Sicca, 1844.

[12] M. Faraday, "Experimental Researches in Electricity. Sixth Series," *Philos. T. R. Soc.*, vol. 124, no. January, pp. 55–76, 1834.

[13] H. Knözinger and K. Kochloefl, "Heterogeneous catalysis and solid catalysts," *Ullmann's Encyclopedia of Industrial Chemistry*, vol. 1, pp. 2–110, 2009.

[14] L. Wilhelmy, "Ueber das Gesetz, nach welchem die Einwirkung der Säuren auf den Rohrzucker stattfindet," *Ann. Phys. Berlin*, 1850.

[15] B. Lindström and L. J. Pettersson, "A brief history of catalysis," *Cattech*, vol. 7, no. 4, pp. 130–138, 2003.

[16] R. Clausius, *The Mechanical Theory of Heat: with its Applications to the Steam Engine and to Physical Properties of Bodies*. London, UK: John van Voorst, 1865.

[17] J. W. Gibbs, "On the Equilibrium of Heterogeneous Substances," *Transactions of the Connecticut Academy*, 1876.

[18] H. von Helmholtz, "On the Thermodynamics of Chemical Processes," *Physical Memoirs Selected and Translated from Foreign Sources*, vol. 1, pp. 43–97, 1876.

[19] G. Lemoine, "Équilibres chimiques entre l'hydrogène et la vapeur d'iode," *Ann. Chim. Phys.*, vol. 12, p. 145, 1877.

[20] W. Ostwald, "Abstracts," *Z. Phys. Chem.*, vol. 15, pp. 705–706, 1894.

[21] P. Sabatier, "Action du nickel sur l'éthylène," *C. R. Acad. Sci.*, vol. 124, pp. 616–618, 1897.

[22] P. Sabatier, "Action du nickel sur l'éthylène. Synthèse de l'éthane," *Compt. Rendus*, vol. 124, pp. 1358–1361, 1897.

[23] P. Sabatier, "La catalyse en chimie organique," *Encyclopédie de Sciences Chimique Appliquée*, vol. III, 1920.

[24] F. Haber and G. van Oordt, "Über die bildung von ammoniak den elementen," *Z. Anorg. Chem.*, vol. 44, no. 1, pp. 341–378, 1905.

[25] W. Nernst, "Über das ammoniakgleichgewicht," *Z. Elektrochem. Angew. P.*, vol. 13, no. 32, pp. 521–524, 1907.

[26] F. Haber and R. Le Rossignol, "Bestimmung des ammoniakgleichgewichtes unter druck," *Z. Elektrochem. Angew. P.*, vol. 14, no. 15, pp. 181–196, 1908.

[27] I. Langmuir, "Chemical reactions at low pressures," *J. Am. Chem. Soc.*, vol. 37, no. 5, pp. 1139–1167, 1915.

[28] I. Langmuir, "Part ii - heterogeneous reactions - chemical reactions on surfaces," *Trans. Faraday Soc.*, vol. 17, pp. 607–620, 1922.

[29] Z. Wang, *Fischer-Tropsch-Synthesis.* John Wiley & Sons Inc., 2010.

[30] M. Boudart, B. H. Davis, and H. Heinemann, *Handbook of Heterogeneous Catalysis*, pp. 1–48. Wiley-VCH Verlag GmbH, 2008.

[31] N. Chen, "Industrial application of shape selective catalysis," *Stud. Surf. Sci. Catal.*, vol. 38, pp. 153 – 163, 1988. Catalysis 1987.

[32] H. Topsøe, B. S. Clausen, and F. E. Massoth, *Hydrotreating Catalysis*, pp. 1–269. Berlin, Heidelberg: Springer Berlin Heidelberg, 1996.

[33] A. C. Byrns, W. E. Bradley, and M. W. Lee, "Catalytic desulfurization of gasolines by cobalt molybdate process," *Ind. Eng. Chem.*, vol. 35, no. 11, pp. 1160–1167, 1943.

[34] J. Wisniak, "The history of bromine from discovery to commodity," *Indian J. Chem. Techn.*, vol. 9, no. May, pp. 263–271, 2002.

[35] R. M. Heck, R. J. Farrauto, and S. T. Gulati, *Automotive Catalyst*, pp. 101–175. John Wiley & Sons Inc., 2009.

[36] J. N. Armor, "A history of industrial catalysis," *Catal. Today*, vol. 163, no. 1, pp. 3–9, 2011.

[37] I. Fechete, Y. Wang, and J. Védrine, "The past, present and future of heterogeneous catalysis," *Catal. Today*, vol. 189, no. 1, pp. 2–27, 2012.

[38] W. Ostwald, "Catalysis," *Nature*, vol. 65, no. 1692, pp. 522–526, 1902.

[39] P. Sabatier and J.-B. Senderens, "Nouvelle synthèses du méthane," *C. R. Hebd. Acad. Sci.*, vol. 134, pp. 514–516, 1902.

[40] A. Balandin, "Modern state of the multiplet theory of heterogeneous catalysis," *Adv. Catal.*, vol. 19, pp. 1 – 210, 1969.

[41] M. Boudart, A. Aldag, L. Ptak, and J. Benson, "On the selectivity of platinum catalysts," *J. Catal.*, vol. 11, no. 1, pp. 35 – 45, 1968.

[42] H. S. Taylor, "A theory of the catalytic surface," *P. Roy. Soc. Lond. A Mat.*, vol. 108, no. 745, pp. 105–111, 1925.

[43] G. A. Somorjai, "Surface reconstruction and catalysis," *Annu. Rev. Phys. Chem.*, vol. 45, no. 1, pp. 721–751, 1994.

[44] G. Novell-Leruth, G. Carchini, and N. Lopez, "On the properties of binary rutile MO_2 compounds, M = Ir, Ru, Sn, and Ti: A DFT study," *J. Chem. Phys.*, vol. 138, no. 19, p. 194706, 2013.

[45] M. Moser, I. Czekaj, N. López, and J. Pérez-Ramírez, "The virtue of defects: Stable bromine production by catalytic oxidation of hydrogen bromide on titanium oxide," *Angew. Chem. Int. Edit.*, vol. 53, no. 33, pp. 8628–8633, 2014.

[46] R. P. Eischens, W. A. Pliskin, and S. A. Francis, "Infrared spectra of chemisorbed carbon monoxide," *J. Chem. Phys.*, vol. 22, no. 10, pp. 1786–1787, 1954.

[47] D. W. Turner and M. I. A. Jobory, "Determination of ionization potentials by photoelectron energy measurement," *J. Chem. Phys.*, vol. 37, no. 12, pp. 3007–3008, 1962.

[48] P. Redhead, "Thermal desorption of gases," *Vacuum*, vol. 12, no. 4, pp. 203 – 211, 1962.

[49] J. Niemantsverdriet, K. Markert, and K. Wandelt, "The compensation effect and the manifestation of lateral interactions in thermal desorption spectroscopy," *Appl. Surf. Sci.*, vol. 31, no. 2, pp. 211 – 219, 1988.

[50] R. F. de Farias, "Estimation of some physical properties for tennessine and tennessine hydride (TsH)," *Chem. Phys. Lett.*, vol. 667, pp. 1–3, 2017.

[51] R. Lin, A. P. Amrute, and J. Pérez-Ramírez, "Halogen-Mediated Conversion of Hydrocarbons to Commodities," *Chem. Rev.*, vol. 117, no. 5, pp. 4182–4247, 2017.

[52] P. Schmittinger, T. Florkiewicz, L. C. Curlin, B. Lüke, R. Scannell, T. Navin, E. Zelfel, R. Bartsch, M. Rossberg, W. Lendle, G. Pfleiderer, A. Tögel, T. R. Torkelson, and K. K. Beutel, "Chlorine," *Ullmann's Encyclopedia of Industrial Chemistry*, vol. 8, pp. 531–621, 2012.

[53] J. R. Partington, *A text-book of inorganic chemistry for university students.* London, UK: Macmillan, 1921.

[54] A. J. Balard, "Sur une Substance particulière contenu dans l'eau de la mere," *Ann. Chim. Phys.*, vol. 32, pp. 337–384, 1826.

[55] J. F. Mills, R. Frim, S. D. Ukeles, and D. Yoffe, *Bromine.* Wiley-VCH Verlag GmbH Co. KGaA, 2000.

[56] Webelements, https://www.webelements.com/, accessed 19/09/2017.

[57] PlasticsToday, https://www.plasticstoday.com/content/study-global-pvc-demand-grow-32-annually-through-2021/17670326321043, accessed 19/09/2017.

[58] F. Z. Eram Sharmin, *Polyurethane: An Introduction.* InTech, 2012.

[59] G. Abts, T. Eckel, and R. Wehrmann, *Polycarbonates.* Wiley-VCH Verlag GmbH Co. KGaA, 2000.

[60] S. Boldyryev and P. Varbanov, "Process integration for bromine plant," *Chem, Engineer. Trans.*, vol. 39, pp. 1423–1428, 2014.

[61] E. McFarland, "Unconventional Chemistry for Unconventional Natural Gas," *Science*, vol. 338, no. 6105, pp. 340–342, 2012.

[62] H. Deacon, "Manufacture of chlorine," Dec. 29 1868. US Patent 85,370.

[63] H. Deacon, "Improvement in the manufacture of chlorine," July 29 1873. US Patent 141,333.

[64] C. Thieme, "Sodium Carbonates," *Ullmann's Encyclopedia of Industrial Chemistry*, vol. 33, 2012.

[65] Great Britain Local Government Board, *Alkali Act, 1863 (Alkali &c. Works Regulation Act, 1906). Ninth (-Fifty-First) Annual Report by the Inspector (Chief Inspector) of His Proceedings During the Year 1872(-1914), Etc.* Parliamentary Papers. House of Commons. Session 1873. vol. 19. C. 815-Session 1914-16. vol. 7. no. 253., 1873.

[66] R. M. MacLeod, "The alkali acts administration, 1863-84: The emergence of the civil scientist," *Victorian Stud.*, vol. 9, no. 2, pp. 85–112, 1965.

[67] H. Over and R. Schomäcker, "What makes a good catalyst for the Deacon process?," *ACS Catal.*, vol. 3, no. 5, pp. 1034–1046, 2013.

[68] C. J and J. J, "Chlorine production," Feb. 20 1951. US Patent 2,542,961.

[69] F. Wattimena and W. M. H. Sachtler, *Catalyst Research for the Shell Chlorine Process*, vol. 7. Kodansha Ltd., 1981.

[70] H. Itoh, Y. Kono, M. Ajioka, S. Takenaka, and M. Kataita, "Production process of chlorine," Feb. 7 1989. US Patent 4,803,065.

[71] T. Kiyoura, Y. Kogure, T. Nagayama, and K. Kanaya, "Manufacturing process of chlorine," Apr. 18 1989. US Patent 4,822,589.

[72] H. Over, "Atomic scale insights into electrochemical versus gas phase oxidation of HCl over RuO_2-based catalysts: A comparative review," *Electrochim. Acta*, vol. 93, pp. 314–333, 2013.

[73] J. Pérez-Ramírez, C. Mondelli, T. Schmidt, O. F.-K. Schlüter, A. Wolf, L. Mleczko, and T. Dreier, "Sustainable chlorine recycling via catalysed HCl oxidation: from fundamentals to implementation," *Energ. Environ. Sci.*, vol. 4, no. 12, pp. 4786–4799, 2011.

[74] T. Hibi, H. Nishida, and H. Abekawa, "Process for producing chlorine," Feb. 16 1999. US Patent 5,871,707.

[75] D. Crihan, M. Knapp, S. Zweidinger, E. Lundgren, C. J. Weststrate, J. N. Andersen, A. P. Seitsonen, and H. Over, "Stable deacon process for HCl oxidation over RuO_2," *Angew. Chem. Int. Edit.*, vol. 47, no. 11, pp. 2131–2134, 2008.

[76] J. P. Hofmann, S. Zweidinger, M. Knapp, A. P. Seitsonen, K. Schulte, J. N. Andersen, E. Lundgren, and H. Over, "Hydrogen-promoted chlorination of $RuO_2(110)$," *J. Phys. Chem. C*, vol. 114, no. 24, pp. 10901–10909, 2010.

[77] Eurochlor website, www.eurochlor.org, accessed 19/09/2017.

[78] S. Trasatti, "Electrocatalysis: understanding the success of DSA®," *Electrochim. Acta*, vol. 45, no. 15-16, pp. 2377–2385, 2000.

[79] P. Hayfield, "Development of the Noble Metal / Oxide Coated Titanium Electrode. Part 1: The Beginning of the Story," *Platin. Met. Rev.*, vol. 42, no. 1, pp. 27–33, 1998.

[80] H. B. Beer, "The Invention and Industrial Development of Metal Anodes," *J. Electrochem. Soc.*, vol. 127, no. 8, p. 303C, 1980.

[81] P. Hayfield, "Development of the Noble Metal / Oxide Coated Titanium Electrode. Part 2: The Move from Platinum / Iridium to Ruthenium Oxide Electrocatalysts," *Platin. Met. Rev.*, vol. 42, no. 3, pp. 46–55, 1998.

[82] H. Beer, "Improvements in or relating to electrodes for electrolysis," May 12 1965. British Patent 1,147,442.

[83] H. Beer, "Improvements in or relating to electrodes," Feb. 10 1967. British Patent 1,195,871.

[84] G. A. Vlasov, N. D. Bushina, G. I. Buravtseva, and L. V. Mukhamet-shina, "Improvement of the iodine and bromine production processes," *Russ. J. Appl. Chem.*, vol. 74, pp. 1093–1097, Jul 2001.

[85] J. B. A. Dumas, "Éloge de M. Antoine-Jérome Balard ," *Mémoires de l'Académie des sciences de l'Institut de France*, vol. 41.

[86] J. Kogel, *Industrial Minerals & Rocks: Commodities, Markets, and Uses.* Society for Mining, Metallurgy, and Exploration, 2006.

[87] "Process of extracting bromine," Sept. 29 1891. US Patent 460,370.

[88] L. C. Stewart, "Commercial Extraction of Bromine from Sea Water," *Ind. Eng. Chem.*, vol. 26, no. 4, pp. 361–369, 1934.

[89] S. B. Heath, "Process of producing bromine," Jan. 10 1939. US Patent 2,143,223.

[90] G. Hooker, "Halogen extraction," Jan. 10 1939. US Patent 2,143,224.

[91] http://www.essentialchemicalindustry.org/chemicals/bromine.html, accessed 19/09/2017.

[92] A. Toftelund, I. C. Man, H. A. Hansen, F. Abild-Pedersen, T. Bligaard, J. Rossmeisl, and F. Studt, "Volcano Relations for Oxidation of Hydrogen Halides over Rutile Oxide Surfaces," *ChemCatChem*, vol. 4, no. 11, pp. 1856–1861, 2012.

[93] K. Ding, H. Metiu, and G. D. Stucky, "Interplay between bromine and iodine in oxidative dehydrogenation," *ChemCatChem*, vol. 5, no. 7, pp. 1906–1910, 2013.

[94] M. Moser, L. Rodríguez-García, A. P. Amrute, and J. Pérez-Ramírez, "Catalytic Bromine Recovery: An Enabling Technology for Emerging Alkane Functionalization Processes," *ChemCatChem*, vol. 5, no. 12, pp. 3520–3523, 2013.

[95] H. Yalçin, T. Koç, and V. Pamuk, "Hydrogen and Bromine Production From Concentrated Sea-Water," *Int. J. Hydrogen Energ.*, vol. 22, no. 10, pp. 967–970, 1997.

[96] N. Imanaka and Y. Kato, "Novel bromide anion conducting refractory solid electrolytes based on lanthanum oxybromide," *J. Mater. Sci.*, vol. 40, no. 24, pp. 6495–6498, 2005.

[97] C. N. Wauters and J. Winnick, "Electrolytic membrane recovery of bromine from waste hydrogen bromide streams," *AIChE J.*, vol. 44, no. 10, pp. 2144–2148, 1998.

[98] J.-S. Park, C. Chen, N. Wieder, J. Vohs, and R. Gorte, "Electrolysis of HBr using molten, alkali-bromide electrolytes," *Electrochim. Acta*, vol. 56, no. 3, pp. 1581 – 1584, 2011.

[99] A. Ivanovskaya, N. Singh, R.-F. Liu, H. Kreutzer, J. Baltrusaitis, T. Van Nguyen, H. Metiu, and E. McFarland, "Transition metal sulfide hydrogen evolution catalysts for hydrobromic acid electrolysis," *Langmuir*, vol. 29, no. 1, pp. 480–492, 2013.

[100] P. F. Schubert, R. D. Beatty, and S. Mahajan, *Catalytic Bromine Recovery from HBr Waste*, ch. 33, pp. 405–419.

[101] G. R. Lester, "Quantitative recovery of bromine by two stage catalytic oxidation of hydrogen bromide," Nov. 21 1967. US Patent 3,353,916.

[102] X.-P. Zhou, A. Yilmaz, G. A. Yilmaz, I. M. Lorkovic, L. E. Laverman, M. Weiss, J. H. Sherman, E. W. McFarland, G. D. Stucky, and P. C. Ford, "An integrated process for partial oxidation of alkanes," *Chem. Commun.*, pp. 2294–2295, 2003.

[103] A. Breed, M. F. Doherty, S. Gadewar, P. Grosso, I. M. Lorkovic, E. W. McFarland, and M. J. Weiss, "Natural gas conversion to liquid fuels in a zone reactor," *Catal. Today*, vol. 106, no. 1, pp. 301 – 304, 2005.

[104] E.-L. Dreher, K. Beutel, J. Myers, T. Lübbe, S. Krieger, and L. Pottenger, "Chloroethanes and Chloroethylenes," *Ullmann's Encyclopedia of Industrial Chemistry*, p. 2, 2014.

[105] E. Baumann, "Ueber einige vinylverbindungen," *Liebigs Ann. Chem.*, vol. 163, no. 3, pp. 308–322, 1872.

[106] W. L. Semon and G. A. Stahl, "History of Vinyl Chloride Polymers," *J. Macromol. Sci. Chem.*, vol. 6, pp. 1263–1278, 1981.

[107] F. Klatte, "The manufacture and production of new polymerisation products and their employment in the arts.," 3 1913. German Patent 281687.

[108] J. D. Cotman, M. F. Gonzalez, and G. C. Claver, "Studies on poly(vinyl chloride). iii. the role of the precipitated polymer in the kinetics of polymerization of vinyl chloride," *J. Polym. Sci. A1*, vol. 5, no. 6, pp. 1137–1164, 1967.

[109] R. Wolf and B. L. Kaul, *Plastics, Additives*. Wiley-VCH Verlag GmbH Co. KGaA, 2000.

[110] I. Fischer, W. F. Schmitt, H.-C. Porth, M. W. Allsopp, and G. Vianello, "Poly (Vinyl Chloride)," *Ullmann's Encyclopedia of Industrial Chemistry*, p. 1, 2014.

[111] http://www.pvc.org, accessed 19/09/2017.

[112] "R&D Progress of and Feasibility Study Report on Mercury-free Catalyst in China," 2010. Foreign Economic Cooperation Office, Ministry of Environmental Protection of the People's Republic of China.

[113] G. W. Johnson, "Improvements in the manufacture of haloid hydrogen additive products of acetylene," 18 1913. British Patent 21,134.

[114] D. H. R. Barton and M. Mugdan, "The synthesis of vinyl chloride from acetylene and hydrogen chloride," *J. Soc. Chem. Ind.*, vol. 69, no. 3, pp. 75–79, 1950.

[115] J. Mulders, "Process for fabricating mixtures containing vinyl chloride and 1,2-dichloroethane," Apr. 14 1970. US Patent 3,506,727.

[116] B. Pope, "Method for vinyl halides," Feb. 4 1975. US Patent 3,864,409.

[117] United Nations Environment Programme, Minamata Convention on Mercury, www.mercuryconvention.org/, accessed 19/09/2017.

[118] G. Hutchings, "Vapor phase hydrochlorination of acetylene: Correlation of catalytic activity of supported metal chloride catalysts," *J. Catal.*, vol. 96, no. 1, pp. 292 – 295, 1985.

[119] B. Nkosi, N. Coville, and G. Hutchings, "Vapour phase hydrochlorination of acetylene with group viii and ib metal chloride catalysts," *Appl. Catal.*, vol. 43, no. 1, pp. 33 – 39, 1988.

[120] J. Oliver-Meseguer, A. Doménech-Carbó, M. Boronat, A. Leyva-Pérez, and A. Corma, "Partial reduction and selective transfer of hydrogen chloride on catalytic gold nanoparticles," *Angew. Chem. Int. Edit.*, vol. 56, no. 23, pp. 6435–6439, 2017.

[121] G. Malta, S. A. Kondrat, S. J. Freakley, C. J. Davies, L. Lu, S. Dawson, A. Thetford, E. K. Gibson, D. J. Morgan, W. Jones, P. P. Wells, P. Johnston, C. R. A. Catlow, C. J. Kiely, and G. J. Hutchings, "Identification of single-site gold catalysis in acetylene hydrochlorination," *Science*, vol. 355, no. 6332, pp. 1399–1403, 2017.

[122] P. G. Ashmore, J. W. Gardner, A. J. Owen, B. Smith, and P. R. Sutton, "Chlorine-catalysed pyrolysis of 1,2-dichloroethane. part 1.- experimental results and proposed mechanism," *J. Chem. Soc., Faraday Trans. 1*, vol. 78, pp. 657–676, 1982.

[123] M. Malentacchi and C. Rubini, "Catalytic composition for controlling exothermic reactions on a fixed bed," Nov. 21 2001. EP Patent App. EP19,990,126,143.

[124] N. B. Muddada, U. Olsbye, L. Caccialupi, F. Cavani, G. Leofanti, D. Gianolio, S. Bordiga, and C. Lamberti, "Influence of additives in defining the active phase of the ethylene oxychlorination catalyst," *Phys. Chem. Chem. Phys.*, vol. 12, no. 21, p. 5503, 2010.

[125] F. Van Rooijen, A. De Bruijn, and J. Nieuwland, "Catalytic oxychlorination," Feb. 26 2009. US Patent App. 12/064,066.

[126] R. V. Carrubba and J. L. Spencer, "Kinetics of the Oxychlorination of Ethylene," *Ind. Eng. Chem. Proc. D. D.*, vol. 9, no. 3, pp. 414–419, 1970.

[127] A. Baiker and W. L. Holstein, "Impregnation of alumina with copper chloride-modeling of impregnation kinetics and internal copper profiles," *J. Catal.*, vol. 84, no. 1, pp. 178–188, 1983.

[128] E. M. Fortini, C. L. García, and D. E. Resasco, "Stabilization of the active phase by interaction with the support in $CuCl_2$ oxychlorination catalysts," *J. Catal.*, vol. 99, no. 1, pp. 12–18, 1986.

[129] P. S. S. Prasad and P. K. Rao, "Low temperature ethylene chemisorption (LTEC): a novel technique for the characterisation of $CuCl_2$–KCl/γ-Al_2O_3 oxychlorination catalysts," *J. Chem. Soc. Chem. Comm.*, no. 12, pp. 951–953, 1987.

[130] J. Blanco, J. Fayos, J. D. L. Banda, and J. Soria, "Study of supported copper chloride catalysts by electron paramagnetic resonance and x-ray diffraction," *J. Catal.*, vol. 31, no. 2, pp. 257 – 263, 1973.

[131] P. A. Sermon, K. Rollins, P. N. Reyes, S. A. Lawrence, M. A. M. Luengo, and M. J. Davies, "Nature of Oxide-supported Copper (II) Ions and Copper derived from Copper (II) Chloride," *J. Chem. Soc. Faraday Trans.*, no. 83, pp. 1347–1353, 1987.

[132] C. L. García and D. E. Resasco, "High-temperature oxychlorination catalysts: Role of $LaCl_3$ as an inhibitor of the segregation of ac-

tive species during heating/cooling cycles," *J. Catal.*, vol. 122, no. 1, pp. 151–165, 1990.

[133] J. C. Bart and G. Vlaic, "Extended X-Ray Absorption Fine Structure Studies in Catalysis," *Adv. Catal.*, vol. 35, no. 287, pp. 1–138, 1987.

[134] G. Leofanti, A. Marsella, B. Cremaschi, M. Garilli, A. Zecchina, G. Spoto, S. Bordiga, P. Fisicaro, G. Berlier, C. Prestipino, G. Casali, and C. Lamberti, "Alumina-Supported Copper Chloride 1: Characterization of Freshly Prepared Catalyst," *J. Catal.*, vol. 189, pp. 91–104, 2000.

[135] N. B. Muddada, U. Olsbye, G. Leofanti, D. Gianolio, F. Bonino, S. Bordiga, T. Fuglerud, S. Vidotto, A. Marsella, and C. Lamberti, "Quantification of copper phases, their reducibility and dispersion in doped-$CuCl_2/Al_2O_3$ catalysts for ethylene oxychlorination," *Dalton Trans.*, vol. 39, pp. 8437–8449, 2010.

[136] C. Zipelli, J. C. J. Bart, G. Petrini, S. Galvagno, and C. Cimino, "Study of $CuCl_2$ Supported on SiO_2 and Al_2O_3," *Z. Anorg. Allg. Chem.*, vol. 502, pp. 199–208, 1983.

[137] G. Leofanti, A. Marsella, B. Cremaschi, M. Garilli, A. Zecchina, G. Spoto, S. Bordiga, P. Fisicaro, G. Berlier, C. Prestipino, G. Casali, and C. Lamberti, "Alumina-Supported Copper Chloride 2: Effect of Aging and Thermal Treatments," *J. Catal.*, vol. 189, p. 105, 2000.

[138] C. Lamberti, S. Bordiga, M. Salvalaggio, G. Spoto, A. Zecchina, F. Geobaldo, G. Vlaic, and M. Bellatreccia, "XAFS, IR, and UV-Vis Study of the Cu(I) Environment in Cu(I)-ZSM-5," *J. Phys. Chem. B*, vol. 101, no. 3, pp. 344–360, 1997.

[139] D. Scarano, P. Galletto, C. Lamberti, R. De Franceschi, and A. Zecchina, "Morphology and CO adsorptive properties of CuCl polycrystalline films: a SEM and FTIR study," *Surf. Sci.*, vol. 387, no. 1-3, pp. 236–242, 1997.

[140] G. Leofanti, A. Marsella, B. Cremaschi, M. Garilli, A. Zecchina, G. Spoto, S. Bordiga, P. Fisicaro, G. Berlier, C. Prestipino, G. Casali, and C. Lamberti, "Alumina-Supported Copper Chloride 3: Effect of Exposure to Ethylene," *J. Catal.*, vol. 202, p. 279, 2001.

[141] G. Leofanti, A. Marsella, B. Cremaschi, M. Garilli, A. Zecchina, G. Spoto, S. Bordiga, P. Fisicaro, G. Berlier, C. Prestipino, G. Casali, and C. Lamberti, "Alumina-Supported Copper Chloride 4: Effect of Exposure to O_2 and HCl," *J. Catal.*, vol. 205, p. 375, 2002.

[142] C. Lamberti, C. Prestipino, F. Bonino, L. Capello, S. Bordiga, G. Spoto, A. Zecchina, S. D. Moreno, B. Cremaschi, M. Garilli, A. Marsella, D. Carmello, S. Vidotto, and G. Leofanti, "The chemistry of the oxychlorination catalyst: An in situ, time-resolved XANES study," *Angew. Chem. Int. Edit.*, vol. 41, no. 13, pp. 2341–2344, 2002.

[143] P. Sai Prasad, K. Prasad, P. Kanta Rao, and V. Kaushik, "Redistribution of copper in KCl-promoted $CuCl_2$/γ-Al_2O_3 catalyst during oxychlorination of ethylene," *J. Mater. Sci.*, vol. 32, no. 6, pp. 1479–1482, 1997.

[144] D. Gianolio, N. B. Muddada, U. Olsbye, and C. Lamberti, "Doped $CuCl_2$/Al_2O_3 catalysts for ethylene oxychlorination: Influence of additives on the nature of active phase and reducibility," *Nuc. Instrum. Meth. B*, vol. 284, pp. 53–57, 2012.

[145] M. Feijen-Jeurissen, J. Ajorna, B. Nieuwenhuys, G. Sinquin, C. Petit, and J.-P. Hindermann, "Mechanism of catalytic destruction of 1,2-dichloroethane and trichloroethylene over gamma-Al_2O_3 and gamma-Al_2O_3 supported chromium and palladium catalysts," *Catal. Today*, vol. 54, pp. 65–79, 1999.

[146] D. Carmello, E. Finocchio, A. Marsella, B. Cremaschi, G. Leofanti, M. Padovan, and G. Busca, "An FT-IR and Reactor Study of the Dehydrochlorination Activity of $CuCl_2$/γ-Al_2O_3-Based Oxychlorination Catalysts," *J. Catal.*, vol. 191, no. 2, pp. 354–363, 2000.

[147] A. S. Shalygin, L. V. Malysheva, and E. A. Paukshtis, "Mechanism of 1,2-dichloroethane dehydrochlorination on the acid sites of oxide catalysts as studied by IR spectroscopy," *Kinet. Catal.*, vol. 52, no. 2, pp. 305–315, 2011.

[148] N. B. Muddada, T. Fuglerud, C. Lamberti, and U. Olsbye, "Tuning the Activity and Selectivity of $CuCl_2$/γ-Al_2O_3 Ethene Oxychlorination Catalyst by Selective Promotion," *Top. Catal.*, vol. 57, no. 6-9, pp. 741–756, 2014.

[149] N. López, J. Gómez-Segura, R. P. Marín, and J. Pérez-Ramírez, "Mechanism of HCl oxidation (Deacon process) over RuO_2," *J. Catal.*, vol. 255, no. 1, pp. 29–39, 2008.

[150] U. A. Paulus, Y. Wang, H. P. Bonzel, K. Jacobi, and G. Ertl, "Adsorption and interaction of ethylene on RuO_2(110) surfaces," *J. Phys. Chem. B*, vol. 109, no. 6, pp. 2139–2148, 2005.

[151] N. López and G. Novell-Leruth, "Rules for selectivity in oxidation processes on RuO$_2$(110).," *Phys. Chem. Chem. Phys.*, vol. 12, no. 38, pp. 12217–12222, 2010.

[152] M. Scharfe, P. A. Lira-Parada, V. Paunović, M. Moser, A. P. Amrute, and J. Pérez-Ramírez, "Oxychlorination—Dehydrochlorination Chemistry on Bifunctional Ceria Catalysts for Intensified Vinyl Chloride Production," *Angew. Chem. Int. Edit.*, vol. 128, no. 9, pp. 3120–3124, 2016.

[153] A. P. Amrute, C. Mondelli, M. Moser, G. Novell-Leruth, N. López, D. Rosenthal, R. Farra, M. E. Schuster, D. Teschner, T. Schmidt, and J. Pérez-Ramírez, "Performance, structure, and mechanism of CeO$_2$ in HCl oxidation to Cl$_2$," *J. Catal.*, vol. 286, pp. 287 – 297, 2012.

[154] M. Moser, C. Mondelli, T. Schmidt, F. Girgsdies, M. E. Schuster, R. Farra, L. Szentmiklósi, D. Teschner, and J. Pérez-Ramírez, "Supported CeO$_2$ catalysts in technical form for sustainable chlorine production," *Appl. Catal. B Environ.*, vol. 132-133, pp. 123–131, 2013.

[155] M. Moser, A. P. Amrute, and J. Pérez-Ramírez, "Impact of feed impurities on catalysts for chlorine recycling," *Appl. Catal. B Environ.*, vol. 162, pp. 602–609, 2015.

[156] M. Scharfe, P. A. Lira-Parada, A. P. Amrute, S. Mitchell, and J. Pérez-Ramírez, "Lanthanide compounds as catalysts for the one-step synthesis of vinyl chloride from ethylene," *J. Catal.*, vol. 344, pp. 524–534, 2016.

[157] M. L. Hallensleben, R. Fuss, and F. Mummy, *Polyvinyl Compounds, Others.* Wiley-VCH Verlag GmbH Co. KGaA, 2000.

[158] N. Fischer, "Morphology of mass PVC," *J. Vinyl Addit. Techn.*, vol. 6, no. 1, pp. 35–49, 1984.

[159] P. Hohenberg and W. Kohn, "Inhomogeneous electron gas," *Phys. Rev.*, vol. 136, pp. B864–B871, 1964.

[160] L. H. Thomas, "The calculation of atomic fields," *Proc. Cambridge Phil. Soc.*, vol. 23, pp. 542–548, 1927.

[161] E. Fermi, "Un Metodo Statistico per la Determinazione di alcune Prioprietà dell'Atomo," *Rend. Accad. Naz. Lincei.*, vol. 6, pp. 602–607, 1927.

[162] P. A. M. Dirac, "Note on Exchange Phenomena in the Thomas Atom," *Proc. Cambridge Phil. Soc.*, vol. 26, pp. 376–385, 1930.

[163] W. Kohn and L. J. Sham, "Self-consistent equations including exchange and correlation effects," *Phys. Rev.*, vol. 140, no. 4A, 1965.

[164] J. P. Perdew and A. Zunger, "Self-interaction correction to density-functional approximations for many-electron systems," *Phys. Rev. B*, vol. 23, no. 10, pp. 5048–5079, 1981.

[165] Y. Wang and J. P. Perdew, "Spin scaling of the electron-gas correlation energy in the high-density limit," *Phys. Rev. B*, vol. 43, no. 11, pp. 8911–8916, 1991.

[166] Y. Wang and J. P. Perdew, "Correlation hole of the spin-polarized electron gas, with exact small-wave-vector and high-density scaling," *Phys. Rev. B*, vol. 44, no. 24, pp. 13298–13307, 1991.

[167] J. P. Perdew, K. Burke, and M. Ernzerhof, "Generalized Gradient Approximation Made Simple," *Phys. Rev. Lett.*, vol. 77, no. 18, pp. 3865–3868, 1996.

[168] J. Tao, J. P. Perdew, V. N. Staroverov, and G. E. Scuseria, "Climbing the Density Functional Ladder: Non-Empirical Meta-Generalized Gradient Approximation Designed for Molecules and Solids," *Phys. Rev. Lett.*, vol. 91, no. 14, p. 146401, 2003.

[169] D. Rappoport, N. Crawford, F. Furche, and K. Burke, "Approximate Density Functionals: Which Should I Choose?," *Encyclopedia of Inorganic Chemistry*, 2009.

[170] M. Cococcioni and S. de Gironcoli, "Linear response approach to the calculation of the effective interaction parameters in the LDA+U method," *Phys. Rev. B*, vol. 71, no. 3, p. 035105, 2005.

[171] H. J. Kulik, M. Cococcioni, D. A. Scherlis, and N. Marzari, "Density Functional Theory in Transition-Metal Chemistry: A Self-Consistent Hubbard U Approach," *Phys. Rev. Lett.*, vol. 97, no. 10, p. 103001, 2006.

[172] S. L. Dudarev, G. A. Botton, S. Y. Savrasov, C. J. Humphreys, and A. P. Sutton, "Electron-energy-loss spectra and the structural stability of nickel oxide: An LSDA+U study," *Phys. Rev. B*, vol. 57, no. 3, pp. 1505–1509, 1998.

[173] S. Grimme, "Semiempirical GGA-type density functional constructed with a long-range dispersion correction," *Journal of computational chemistry*, vol. 16, pp. 1787–1799, 2006.

[174] N. W. Ashcroft and N. Mermin, *Solid State Physics*. Philadelphia, Pennsylvania, USA: Saunders College Publishing, 1976.

[175] D. Vanderbilt, "Soft self-consistent pseudopotentials in a generalized eigenvalue formalism," *Phys. Rev. B*, vol. 41, no. 11, pp. 7892–7895, 1990.

[176] P. E. Blöchl, "Projector augmented-wave method," *Phys. Rev. B*, vol. 50, no. 24, pp. 17953–17979, 1994.

[177] G. Kresse and D. Joubert, "From ultrasoft pseudopotentials to the projector augmented-wave method," *Phys. Rev. B*, vol. 59, pp. 1758–1775, 1999.

[178] H. Monkhorst and J. Pack, "Special points for Brillouin-zone integrations," *Phys. Rev. B*, vol. 13, no. 12, pp. 5188–5192, 1976.

[179] B. Berne, G. Ciccotti, and D. Coker, *Classical and Quantum Dynamics in Condensed Phase Simulations*. 1998.

[180] G. Mills and H. Jónsson, "Quantum and thermal effects in H_2 dissociative adsorption: Evaluation of free energy barriers in multidimensional quantum systems," *Phys. Rev. Lett.*, vol. 72, no. 7, pp. 1124–1127, 1994.

[181] G. Mills, H. Jónsson, and G. Schenter, "Reversible work transition state theory: application to dissociative adsorption of hydrogen," *Surf. Sci.*, vol. 324, pp. 305–337, 1995.

[182] G. Henkelman and H. Jónsson, "Improved tangent estimate in the nudged elastic band method for finding minimum energy paths and saddle points," *J. Chem. Phys.*, vol. 113, no. 22, p. 9978, 2000.

[183] J. Rogal and K. Reuter, "Ab Initio Atomistic Thermodynamics for Surfaces : A Primer," *Experiment, Modeling and Simulation of Gas-Surface Interactions for Reactive Flows in Hypersonic Flights*, pp. 2–1 – 2–18, 2007.

[184] M. Bollinger, K. Jacobsen, and J. Nørskov, "Atomic and electronic structure of MoS_2 nanoparticles," *Phys. Rev. B*, vol. 67, no. 8, pp. 1–17, 2003.

[185] J. T. Gleaves, G. Yablonsky, X. Zheng, R. Fushimi, and P. L. Mills, "Temporal analysis of products (TAP)-Recent advances in technology for kinetic analysis of multi-component catalysts," *J. Mol. Catal. A Chem.*, vol. 315, no. 2, pp. 108–134, 2010.

[186] K. Morgan, N. Maguire, R. Fushimi, J. T. Gleaves, A. Goguet, M. P. Harold, E. V. Kondratenko, U. Menon, Y. Schuurman, and G. S. Yablonsky, "Forty years of temporal analysis of products," *Catal. Sci. Technol.*, vol. 7, pp. 2416–2439, 2017.

[187] D. Teschner, R. Farra, L. Yao, and R. Schlögl, "An integrated approach to Deacon chemistry on RuO_2-based catalysts," *J. Catal.*, vol. 285, no. 1, pp. 273–284, 2012.

[188] D. Teschner and G. Novell-Leruth, "In situ surface coverage analysis of RuO_2-catalysed HCl oxidation reveals the entropic origin of compensation in heterogeneous catalysis," *Nature Chemistry*, vol. 4, pp. 739–745, sep 2012.

[189] S. Zweidinger, D. Crihan, M. Knapp, J. P. Hofmann, A. P. Seitsonen, C. J. Weststrate, E. Lundgren, J. N. Andersen, and H. Over, "Reaction mechanism of the oxidation of HCl over $RuO_2(110)$," *J. Phys. Chem. C*, vol. 112, no. 27, pp. 9966–9969, 2008.

[190] F. Studt, F. Abild-Pedersen, H. A. Hansen, I. C. Man, J. Rossmeisl, and T. Bligaard, "Volcano relation for the deacon process over transition-metal oxides," *ChemCatChem*, vol. 2, no. 1, pp. 98–102, 2010.

[191] M. D. Rasmussen, L. M. Molina, and B. Hammer, "Adsorption, diffusion, and dissociation of molecular oxygen at defected $TiO_2(110)$: A density functional theory study," *J. Chem. Phys.*, vol. 120, no. 2, pp. 988–997, 2004.

[192] H. Metiu, S. Chrétien, Z. Hu, B. Li, and X. Sun, "Chemistry of Lewis acid-base pairs on oxide surfaces," *J. Phys. Chem. C*, vol. 116, no. 19, pp. 10439–10450, 2012.

[193] S. Wendt, R. Schaub, J. Matthiesen, E. K. Vestergaard, E. Wahlström, M. D. Rasmussen, P. Thostrup, L. M. Molina, E. Lægsgaard, I. Stensgaard, B. Hammer, and F. Besenbacher, "Oxygen vacancies on $TiO_2(110)$ and their interaction with H_2O and O_2: A combined high-resolution STM and DFT study," *Surf. Sci.*, vol. 598, no. 1-3, pp. 226–245, 2005.

[194] S. Chrétien and H. Metiu, "Enhanced adsorption energy of Au_1 and O_2 on the stoichiometric $TiO_2(110)$ surface by coadsorption with other molecules," *J. Chem. Phys.*, vol. 128, no. 4, pp. 1–13, 2008.

[195] G. Kresse and J. Furthmüller, "Efficiency of ab-initio total energy calculations for metals and semiconductors using a plane-wave basis set," *Comput. Mater. Sci.*, vol. 6, pp. 15–50, 1996.

[196] G. Kresse and J. Furthmüller, "Efficient iterative schemes for ab initio total-energy calculations using a plane-wave basis set," *Phys. Rev. B*, vol. 54, no. 16, pp. 11169–11186, 1996.

[197] G. Wulff, "Zur Frage der Geschwindigkeit des Wachstums und der Auflösung der Krystallflagen," *Z. Krystallogr. Minera.*, vol. 34, pp. 449–530, 1901.

[198] NIST WebBook, http://webbook.nist.gov/chemistry, accessed 08/06/2015.

[199] M. Moser, C. Mondelli, and A. P. Amrute, "HCl Oxidation on IrO_2-Based Catalysts: From Fundamentals to Scale-Up," *ACS Catal.*, vol. 3, pp. 2813–2822, 2013.

[200] M. Moser, V. Paunović, Z. Guo, L. Szentmiklósi, M. G. Hevia, M. Higham, N. López, D. Teschner, and J. Pérez-Ramírez, "Interplay between surface chemistry and performance of rutile-type catalysts for halogen production," *Chem. Sci.*, vol. 7, pp. 2996–3005, 2016.

[201] S. Trasatti, "Progress in the understanding of the mechanism of chlorine evolution at oxide electrodes," *Electrochimica Acta*, vol. 32, no. 3, pp. 369–382, 1987.

[202] H. Over, "Surface chemistry of ruthenium dioxide in heterogeneous catalysis and electrocatalysis: From fundamental to applied research," *Chem. Rev.*, vol. 112, no. 6, pp. 3356–3426, 2012.

[203] P. Triggs and F. Lévy, "Optical and Electrical Properties of of Ruthenium-Doped TiO_2," *Phys. Status Solidi (B)*, vol. 129, no. 1, pp. 363–374, 1985.

[204] J. Glassford, J. Chelikovsky, "Electronic structure of TiO_2:Ru," *Phys. Rev. B*, vol. 47, no. 19, pp. 12550–12553, 1993.

[205] P. Triggs, F. Lévy, and F. E. Wagner, "Mossbauer evidence for Ru(IV) and Ru(II) in TiO_2," *Mat. Res. Bull.*, vol. 19, no. IV, pp. 197–200, 1984.

[206] C. Gutierrez and P. Salvador, "The effect of the substitution of Ru for Ti on the electro- and photoelectrochemical properties of TiO_2 crystals," *J. Electroanal. Chem.*, vol. 187, pp. 139–150, 1985.

[207] P. Atkins and J. de Paula, *Physical Chemistry.* Oxford, UK: Oxford University Press, 2006.

[208] R. K. Karlsson, H. A. Hansen, T. Bligaard, A. Cornell, and L. G. Pettersson, "Ti atoms in $Ru_{0.3}Ti_{0.7}O_2$ mixed oxides form active and selective sites for electrochemical chlorine evolution," *Electrochim. Acta*, vol. 146, pp. 733 – 740, 2014.

[209] H. A. Hansen, I. C. Man, F. Studt, F. Abild-Pedersen, T. Bligaard, and J. Rossmeisl, "Electrochemical chlorine evolution at rutile oxide (110) surfaces," *Phys. Chem. Chem. Phys.*, vol. 12, pp. 283–290, 2010.

[210] I. C. Man, H. Y. Su, F. Calle-Vallejo, H. A. Hansen, J. I. Martínez, N. G. Inoglu, J. Kitchin, T. F. Jaramillo, J. K. Nørskov, and J. Rossmeisl, "Universality in Oxygen Evolution Electrocatalysis on Oxide Surfaces," *ChemCatChem*, vol. 3, no. 7, pp. 1159–1165, 2011.

[211] U. Balachandran and N. G. Eror, "Self-compensation in tantalum-doped TiO_2," *J. Mater. Sci.*, vol. 17, no. 4, pp. 1207–1212, 1982.

[212] E. Finazzi, C. Di Valentin, and G. Pacchioni, "Boron-Doped Anatase TiO_2: Pure and Hybrid DFT Calculations," *J. Phys. Chem. C*, vol. 113, no. 1, pp. 220–228, 2009.

[213] W. Zhao, W. Ma, C. Chen, J. Zhao, and Z. Shuai, "Efficient Degradation of Toxic Organic Pollutants with $Ni_2O_3/TiO_{2-x}B_x$ under Visible Irradiation," *J. Am. Chem. Soc.*, vol. 126, no. 15, pp. 4782–4783, 2004.

[214] D. Chen, D. Yang, Q. Wang, and Z. Jiang, "Effects of boron doping on photocatalytic activity and microstructure of titanium dioxide nanoparticles," *Ind. Eng. Chem. Res.*, vol. 45, no. 12, pp. 4110–4116, 2006.

[215] W.-K. Wang, J.-J. Chen, M. Gao, Y.-X. Huang, X. Zhang, and H.-Q. Yu, "Photocatalytic degradation of atrazine by boron-doped TiO_2 with a tunable rutile/anatase ratio," *Appl. Catal. B Environ.*, vol. 195, pp. 69–76, 2016.

[216] L. Artiglia, D. Lazzari, S. Agnoli, G. A. Rizzi, and G. Granozzi, "Searching for the Formation of Ti–B Bonds in B-Doped TiO_2–Rutile," *J. Phys. Chem. C*, vol. 117, no. 25, pp. 13163–13172, 2013.

[217] H. Geng, S. Yin, X. Yang, Z. Shuai, and B. Liu, "Geometric and electronic structures of the boron-doped photocatalyst TiO$_2$," *J. Phys. Condens. Mat.*, vol. 18, no. 1, p. 87, 2006.

[218] V. Gombac, L. De Rogatis, A. Gasparotto, G. Vicario, T. Montini, D. Barreca, G. Balducci, P. Fornasiero, E. Tondello, and M. Graziani, "TiO$_2$ nanopowders doped with boron and nitrogen for photocatalytic applications," *Chem. Phys.*, vol. 339, no. 1-3, pp. 111–123, 2007.

[219] K. Yang, Y. Dai, and B. Huang, "Origin of the photoactivity in boron-doped anatase and rutile TiO$_2$ calculated from first principles," *Phys. Rev. B*, vol. 76, no. 19, p. 195201, 2007.

[220] H. Jin, Y. Dai, W. Wei, and B. Huang, "Density functional characterization of B doping at rutile TiO$_2$(110) surface," *J. Phys. D Appl. Phys.*, vol. 41, no. 19, p. 195411, 2008.

[221] J. S. Dalton, P. A. Janes, N. G. Jones, J. A. Nicholson, K. R. Hallam, and G. C. Allen, "Photocatalytic oxidation of NO$_x$ gases using TiO$_2$: A surface spectroscopic approach," *Environ. Pollut.*, vol. 120, no. 2, pp. 415–422, 2002.

[222] M. Higham, M. Scharfe, M. Capdevila-Cortada, J. Pérez-Ramírez, and N. López, "Mechanism of ethylene oxychlorination over ruthenium oxide," *J. Catal.*, vol. 353, pp. 171 – 180, 2017.

[223] C.-E. Boman, J. Danielsen, A. Haaland, B. Jerslev, C. E. Schäffer, E. Sunde, and N. A. Sørensen, "Refinement of the Crystal Structure of Ruthenium Dioxide.," *Acta Chem. Scand.*, vol. 24, pp. 116–122, 1970.

[224] S. Pogodin and N. López, "A more accurate kinetic monte carlo approach to a monodimensional surface reaction: The interaction of oxygen with the RuO$_2$(110) surface," *ACS Catal.*, vol. 4, no. 7, pp. 2328–2332, 2014.

[225] H. Over, "Atomic-scale understanding of the HCl oxidation over RuO$_2$, a novel deacon process," *J. Phys. Chem. C*, vol. 116, no. 12, pp. 6779–6792, 2012.

[226] A. P. Seitsonen and H. Over, "Oxidation of HCl over TiO$_2$-Supported RuO$_2$: A Density Functional Theory Study," *J. Phys. Chem. C*, vol. 114, no. 51, pp. 22624–22629, 2010.

[227] H. Over, "Atomic-Scale Structure and Catalytic Reactivity of the RuO$_2$(110) Surface," *Science*, vol. 287, no. 5457, pp. 1474–1476, 2000.

[228] H. Over, "Ruthenium dioxide, a fascinating material for atomic scale surface chemistry," *Appl. Phys. A Mater.*, vol. 75, no. 1, pp. 37–44, 2002.

[229] F. Hess and H. Over, "Rate-Determining Step or Rate-Determining Configuration? The Deacon Reaction over $RuO_2(110)$ Studied by DFT-Based KMC Simulations," *ACS Catal.*, vol. 7, no. 1, pp. 128–138, 2017.

[230] Y. Segura, N. López, and J. Pérez-Ramírez, "Origin of the superior hydrogenation selectivity of gold nanoparticles in alkyne + alkene mixtures: Triple- versus double-bond activation," *J. Catal.*, vol. 247, no. 2, pp. 383–386, 2007.

UNIVERSITAT ROVIRA I VIRGILI
THEORETICAL STUDIES OF HETEROGENEOUS CATALYSIS FOR HALOGEN CHEMISTRY
Michael David Higham

UNIVERSITAT ROVIRA I VIRGILI
THEORETICAL STUDIES OF HETEROGENEOUS CATALYSIS FOR HALOGEN CHEMISTRY
Michael David Higham

UNIVERSITAT ROVIRA I VIRGILI
THEORETICAL STUDIES OF HETEROGENEOUS CATALYSIS FOR HALOGEN CHEMISTRY
Michael David Higham

UNIVERSITAT ROVIRA I VIRGILI
THEORETICAL STUDIES OF HETEROGENEOUS CATALYSIS FOR HALOGEN CHEMISTRY
Michael David Higham

UNIVERSITAT
ROVIRA i VIRGILI